Heat Transfer in Boiling Dilute Emulsion with Strong Buoyancy

A THESIS
SUBMITTED TO THE FACULTY OF
UNIVERSITY OF MINNESOTA

BY

Eric Thomas Freeburg

IN PARTIAL FULFILLMENT OF THE REQUIREMENTS
FOR THE DEGREE OF
MASTER OF SCIENCE IN MECHANICAL ENGINEERING

Francis A. Kulacki

August 2015

Acknowledgements

I would like to thank my adviser, Professor Frank Kulacki, for his support and invaluable guidance throughout my graduate career. His enthusiasm for this research and his experience have been crucial throughout my graduate studies.

Thank you to Professor Jiarong Hong, Mostafa Toloui, and Santosh Sankar for generously allowing me to use their optical equipment and for helping in the setup and calibration of the optical equipment.

I would also like to thank Mike Jensen for his advice and guidance in the design and manufacturing of my apparatus.

It has been a pleasure to become friends with my fellow lab members, Everett Wenzel, Brandon Shadakofsky, Yang Liu, Danimae Janssen, and Brian McClintock.

And finally, I would like to thank my parents Jim and Kris, my brother Max, and my extended family, especially Ilse and Todd, for their love and unwavering support throughout the pursuit of my education. Without them, none of this would have been possible.

Dedication

This thesis is dedicated to my parents, Jim and Kris.

Abstract

Little attention has been given to the boiling of emulsions compared to that of boiling in pure liquids. The advantages of using emulsions as a heat transfer agent were first discovered in the 1970s and several interesting features have since been studied by few researchers. Early research focuses primarily on pool and flow boiling and looks to determine a mechanism by which the boiling process occurs. This thesis looks at the boiling of dilute emulsions in fluids with strong buoyant forces.

The boiling of dilute emulsions presents many favorable characteristics that make it an ideal agent for heat transfer. High heat flux electronics, such as those seen in avionics equipment, produce high heat fluxes of 100 W/cm^2 or more, but must be maintained at low temperatures. So far, research on single phase convection and flow boiling in small diameter channels have yet to provide an adequate solution. Emulsions allow the engineer to tailor the solution to the specific problem. The fluid can be customized to retain the high thermal conductivity and specific heat capacity of the continuous phase while enhancing the heat transfer coefficient through boiling of the dispersed phase component.

Heat transfer experiments were carried out with FC-72 in water emulsions. FC-72 has a saturation temperature of 56 °C, far below that of water. The parameters were varied as follows: $0\% \leq \varepsilon \leq 1\%$ and $1.82 \times 10^{12} \leq Ra_H \leq 4.42 \times 10^{12}$. Surface temperatures along the heated surface reached temperature that were 20 °C in excess of the dispersed phase saturation temperature. An increase of ~20% was seen in the average Nusselt numbers at the highest Rayleigh numbers.

Holography was used to obtain images of individual and multiple FC-72 droplets in the boundary layer next to the heated surface. The droplet diameters ranged from 0.5 mm to 1.3 mm. The Magnus effect was observed when larger individual droplets were injected into the boundary layer, causing the droplets to be pushed outside the boundary layer. Vaporization of FC-72 droplets in the boundary layer next to the heated surface was not observed.

Table of Contents

List of Tables

List of Figures

Nomenclature

A	heater area [m^2]
C_p	constant pressure specific heat [$J \cdot kg^{-1}\ K^{-1}$]
D	thermocouple well depth [mm]
d	thermocouple well diameter [mm]
d_d	FC-72 droplet diameter [mm]
F	force [$kg\ m \cdot s^{-1}$]
G	vortex strength [$m^2 \cdot s^{-1}$]
Gr_H	Grashof number based on heater height [$g\ \beta\ q''\ H^4 \cdot \nu^{-2}\ k^{-1}$]
Gr_S	Grashof number based on enclosure width [$g\ \beta\ q''\ S^4 \cdot \nu^{-2}\ k^{-1}$]
H	height of the heater [m]
h	heat transfer coefficient [$W \cdot m^{-2} K^{-1}$]
k	thermal conductivity [$W \cdot m^{-1} K^{-1}$]
l	length of cartridge heater [m]
L	thickness of the heater [m]
L_V	Latent heat of vaporization [$J \cdot g^{-1}$]
m	mass [g]
Nu	Nusselt number [$h\ H \cdot k^{-1}$]
$\overline{Nu}_H$	Average Nusselt number [$\bar{h}\ H \cdot k^{-1}$]
P	Power produced by cartridge heater [W]
Pr	Prandtl number [$\nu \cdot \alpha^{-1}$]
q''	heat flux [$W \cdot m^{-2}$]
Q	heat transfer rate [W]
R	droplet radius [mm]
R_h	heater electrical resistance [Ω]
Ra_H	Rayleigh number based on heater height [$g\ \beta\ q''\ H^4 \cdot \nu^{-1}\ k^{-1}\ \alpha^{-1}$]
Ra_S	Rayleigh number based on enclosure width [$g\ \beta\ q''\ S^4 \cdot \nu^{-1}\ k^{-1}\ \alpha^{-1}$]
Ra_y	Local Rayleigh number [$g\ \beta\ q''\ y^4 \cdot \nu^{-1}\ k^{-1}\ \alpha^{-1}$]

S	width of test enclosure [m]
T	temperature [°C or K]
ΔT	temperature difference [°C or K]
t	time [s]
U	uncertainty [-]
u	velocity [$m \cdot s^{-1}$]
V	volume [m^3]
Δv	voltage drop [V]
W	width of the heater [m]
x	horizontal position [mm]
y	vertical position [mm]

Greek Symbols

α	thermal diffusivity [$m^2 \cdot s^{-1}$]
β	coefficient of thermal expansion [K^{-1}]
γ	fraction of heat flow through copper plate [-]
δ	boundary layer thickness [mm]
ε	volume fraction of dispersed component [-]
θ	shifted temperature $T(x) - T_b$ [°C or K]
λ	Eigenvalue
μ	dynamic viscosity [$kg \cdot m^{-1} s^{-1}$]
ν	kinematic viscosity [$m^2 \cdot s^{-1}$]
ρ	density [$kg \cdot m^{-3}$]
Ψ	stream function [s^{-1}]
ω	angular velocity [$rad \cdot s^{-1}$]

Subscripts

0	initial property
acr	acrylic property

amb	ambient property
avg	averaged property
b	bulk property
c	continuous phase property
d	dispersed phase property
f	fluid property
H	homogenous solution
h	heater property
ins	insulation property
max	maximum
n	eigenvalue index
ss	steady state solution
TC	thermocouple
total	sum of property
wall	wall property

1. Introduction

Boiling as an effective mode of heat transfer has been studied extensively to date. However not much attention has been given to boiling of emulsions in the literature. An emulsion is a mixture of two immiscible fluids such that the dispersed component consists of many small droplets suspended in the continuous component. Generally, the dispersed component has a boiling point that is significantly lower than that of the continuous component. A dilute emulsion is an emulsion in which the dispersed component makes up less than ~5% of the mixture by volume. Previous studies dating back to as early as the 1970s have looked at pool boiling and flow boiling heat transfer in emulsions and have attempted to develop models for the situations studied. This study looks at the effect of strong buoyancy on the convective heat transfer coefficient, as well as the mechanism by which the droplets boil in the thermal boundary layer.

Boiling of dilute emulsions displays many favorable characteristics that make it a topic of interest for certain applications where high heat fluxes are involved. The cooling of high heat flux electronics, for example, requires that the electronic device operate at temperatures below ~ 95 °C to avoid overheating. Military avionics is constantly pushing the thermal limits in terms of watt densities while maintaining temperatures as low as ~100 °C.

Recent research has and continues to look at single phase convection and flow boiling in microchannels for solutions to the problems described in the applications above. The literature shows that there are typically too many tradeoffs with these methods. Design engineers must choose between small temperature rises in the fluid, low pressure drops, and low temperature differences between the surface and fluid. An emulsion in which water is the continuous phase is highly desirable because the emulsion retains the high heat capacity and thermal conductivity of water, while boiling of the dispersed component increases the convective heat transfer coefficient.

The difficulties in boiling of dilute emulsions arise from the fact that little is understood about the boiling process and the mechanisms that are in play when boiling of the dispersed component occurs. Bulanov and co-workers (2001) have developed a

model for the boiling of dilute emulsions. However the simplifying assumptions made in the development of the model contradict each other, and thus, lead to a misrepresentation of the physics (Roesle and Kulacki 2013). Mechanisms for boiling of the dispersed component include spontaneous nucleation and chain boiling. The ways in which these mechanisms work in boiling of a dilute emulsion differ between the different models. A lot of research has been done previously to look at the effects of certain parameters on the heat transfer coefficients in dilute emulsions. These studies, if nothing else, have shown that the heat transfer in a boiling dilute emulsions is dependent upon many factors. It is suspected that in the future, more and more work will be done to develop an adequate model for the boiling of dilute emulsions.

Previous studies in the boiling of dilute emulsions primarily examine the boiling mechanisms and effects in pool boiling situations. This study examines the effect of strong buoyancy on the boiling of the dispersed component in a dilute emulsion and how that will affect the overall heat transfer. A number of questions arise when this situation is considered: Where will the droplet boil in the boundary layer in both the vertical and horizontal directions? The temperature difference between the surface and the bulk of the emulsion is rather large (~60°C). What kind of increase, if any, will be seen in the convective heat transfer coefficient when boiling is initiated?

Previous experiments on boiling of dilute emulsions have investigated pool boiling. These studies show the many favorable and unfavorable characteristics of boiling of dilute emulsions. More often than not, the working fluid is enclosed in a container where the heat transfer causing a circulation effect, or the fluid is forced through a container so as to remove the heat being generated. In either of these cases, one must consider the fluid dynamics that are present and how that can affect the heat transfer process.

In Roesle's experiments (2013), a horizontal wire was immersed in a dilute emulsion. Lunde (2011) took Roesle's experiments a step further by looking at pool boiling in dilute emulsion with a narrow strip suspended horizontally in a dilute emulsion. In both cases, the wire diameter and strip were not large to observe effects caused by the boundary layer. In both Roesle's and Lunde's experiments, significant

increases were seen in the heat transfer coefficient when the dispersed component began to boil.

One of the questions this study seeks to answer is whether or not a similar increase in the heat transfer coefficient will be observed in the boundary layer with strong buoyancy. It is suspected that at a minimum, an equivalent increase in the heat transfer coefficient will be seen. The boiling of the dispersed phase has already proven to be an efficient mechanism for heat transfer. The addition of the buoyancy effects are expected to aid in the transport of heat away from the surface of the heater.

An additional aspect of this study is to examine a single droplet as it moves through the boundary layer. The dispersed component in dilute emulsions are often opaque, making them difficult to observe without advanced equipment. How individual droplets boil has been a topic of interest in this field for quite some time. Roesle and Kulacki (2013) and Bulanov (2001) have both proposed mechanisms by which individual droplets boil. This study uses holography to observe the droplet at different heights within the boundary layers. It is suspected that the individual droplet will need to come very close to or in contact with the heated surface to initiate the boiling process. The temperature profile in the boundary layer exhibits very steep gradients near the wall, indicating that the temperature quickly falls to a value close to that of bulk. It is possible for the droplet to be in a portion of the boundary layer where the temperature is not above the droplet's boiling point.

1.1 Boiling of Dilute Emulsions

Boiling in emulsions is not as well understood as other topics in the field of heat transfer. This can be attributed to the fact that boiling in emulsions is a rather complex phenomenon that has a wide range of behaviors and mechanisms.

Observation of the boiling process in emulsions is generally impossible due to the emulsions being opaque (Roesle and Kulacki 2013). Early studies performed by Mori et al. (1978) investigate pool boiling heat transfer in oil in water and water in oil emulsions. The term oil in water indicates that water makes up more than 50% of the mixture. Therefore the structure of the emulsion is considered to be droplets of oil dispersed in water. The experiments cover a wide range of mass fractions for water, 10 to 90% and

show that the heat transfer coefficient for the emulsion is always greater than that of the pure fluid. Because the mass fractions of water are between 10 and 90%, the emulsions are not considered dilute in these studies. Mori et al. found that the heat transfer coefficient may be smaller or larger than that of water depending on the emulsifier.

Roesle and Kulacki (2013) were able to obtain images during the experiments using a high-speed video camera. One of the main problems encountered at high heat flux is that the number of bubbles became too large to observe the boiling process. They observed boiling of the accumulated droplet liquid on the heated surface and that of droplets near the heated surface simultaneously. Observing the behavior of boiling droplets in emulsions near the heated surface is important for developing models and determining the exact processes that are occurring.

Several favorable characteristics have been observed in the boiling in dilute emulsions. In studies performed by Bulanov et al. (1993), the low boiling point liquid is water and the continuous phase is oil. They observed that in both pool and flow boiling, it is found that the heat transfer coefficient is always higher for the emulsion than for the pure oil. In flow boiling experiments, the improvement in heat transfer is found to increase by up to 33% with increasing mass fractions of water. Bulanov and co-workers also looked at different mass fractions of water, and found that up to 1%, the heat transfer coefficient is dependent on mass fraction. However from 1% to 8 %, the heat transfer coefficient is independent of mass fraction (Bulanov et al. 1996).

An unfavorable characteristic that has been observed in the boiling in dilute emulsions is the relatively high degree of superheat required to initiate boiling of the dispersed phase (Figure 1). For the water in oil emulsion shown in Figure 1, the heat transfer coefficient does not begin to increase until the wall temperature reaches almost 160 °C, 60 °C above that of the boiling point of water. One theory behind this phenomenon is that because the droplets are never in direct contact with the heated surface, they must undergo spontaneous nucleation (Roesle and Kulacki 2013).

Bulanov and co-workers have also studied other aspects of boiling in dilute emulsions, including the effect of droplet size and the addition of surfactants and

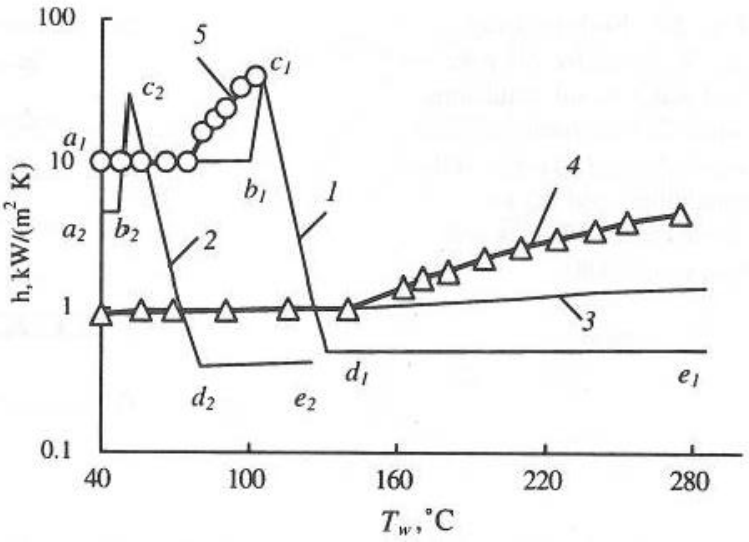

Figure 1. Pool boiling heat transfer coefficients for (1) water, (2) R-113, (3) transformer oil, (4) water in oil emulsion, and (5) R-113 in water emulsion (Bulanov and Gasanov 2008)

suspended particles. In one of the their studies, it was found that increasing droplet size led to a decrease in the amount of superheat required to initiate boiling. However, the heat transfer coefficient has little dependence on droplet size once boiling has been initiated (Bulanov and Gasanov 2007). One study suggests recommendations on altering the emulsion to obtain certain desired characteristics. If one wishes to increase the heat transfer coefficient and decrease the delay in the initiation of boiling, they should add a gas absorbent. However, if one wishes to increase the heat transfer coefficient only, then a surfactant should be added (Bulanov and Gasanov 2006). Combinations of these additives have not been studied in the literature.

Recent studies by Bulanov et al. (2001) and Roesle and Kulacki (2013) have aimed at trying to develop a model suitable for boiling in dilute emulsions. Bulanov's model assumes that each droplet boils randomly and only while inside the thermal boundary layer next the heated surface. However, he states that boiling does depend on contact with the heated surface itself. One of the problems with Bulanov's model is the contradicting boundary conditions he uses to derive his equations. Bulanov assumes that the probability of a droplet boiling is dependent on the nucleation rate. In order to calculate this nucleation rate, he assumes the temperature in the thermal boundary is

uniform and equal to that of the heated surface. However, to determine the thickness of the thermal boundary layer, he assumes a linear temperature profile. While these results can be fitted to experimental data, the contradicting boundary conditions limit the ability to provide insight into the boiling process. Roesle suggests a model of boiling in dilute emulsions based on the Euler-Euler model of multiphase flows. His model contains three phases that represent the continuous component, the liquid phase of the dispersed component, and the vapor phase of the dispersed component (Roesle and Kulacki 2013). Three phases are required instead of the usual two-phase Euler-Euler method because phase change in the dispersed phase does not occur at a single known temperature (Roesle 2010).

Roesle and Kulacki (2010) suggest that two mechanisms exist by which boiling in an emulsion can occur. The first mechanism occurs when the droplets come into direct contact with the heated surface. Whether the droplets will contact the surface and how many will contact the surface depends on the flow geometry and other conditions (Roesle and Kulacki 2010). The second mechanism by which droplets boil is through collisions between droplets and bubbles. This mechanism has led to a quantity known as the collision efficiency. Roesle and Kulacki (2010) state that collision efficiency has not been studied with respect to droplets suspended in a liquid. Therefore, they make use of the literature available on collision efficiency of raindrops in cloud formations, along with some other assumptions to make use of an approximation for the collision efficiency.

Chain boiling is another aspect of boiling in emulsions that has been suggested by Bulanov and Gasanov (2005). They propose that chain boiling occurs through a shockwave that forms when droplets boil. This shockwave then comes into contact with other droplets, thus causing them to boil and release a shockwave of their own. Roesle and Kulacki (2010) argue that the thermal diffusion to the droplet from the surrounding fluid does not move quickly enough to form a shockwave. They state that another, more likely mechanism for chain boiling is simple contact between a boiling droplet and adjacent droplets.

Boiling of dilute emulsions has many characteristics that make it a very desirable medium for heat transfer applications where high heat fluxes are concerned. However, it also brings with it its difficulties and problems. The thermal designer has the option to customize the properties of the emulsion through the addition of surfactants and suspended particles, and through control of the droplet size. Boiling of the dispersed component gives an increase in heat transfer without the presence of a significant amount of vapor, which is often not desirable in heat transfer fluids. The problems include the large amount of superheat required to initiate boiling of the dispersed phase and the difficulty in modeling the boiling mechanism and process. Previous studies have shown that temperature overshoots of as much as 60 °C above the saturation temperature of the dispersed phase are required to initiate boiling. Modeling the boiling of dilute emulsions is extremely difficult because of the many behaviors and mechanisms observed.

1.2 Free Convection in Rectangular Enclosures

Free convection in enclosures has been studied extensively, and there is an abundance of literature available on the subject. Owing to the length of time for which the subject has been studied, there are many different boundary conditions, geometric configurations, and other situations that have been studied.

Engineers have come up with many designs that deal with this type of problem. For example, situations can range from double-glazed windows in buildings to nuclear reactor cores. A common situation often seen in everyday life is the movement of air within a building. During the day, the sun heats the air by the window, causing a density change, which causes the air to flow upwards. When this air hits the ceiling, it is forced towards the inner, cooler part of the building, where it cools and sinks to the floor. Once the air makes its way back to the window, the whole process starts over again.

Despite the length of time that has been spent studying the subject, the problem still is yet to be solved completely. Engineers today still rely on correlations developed by fitting curves to data. The problem with these correlations is that they are often only applicable to specific ranges and situations. Even numerical simulations are difficult because the mathematical description of the problem involves a set of partial differential equations that are difficult to solve (De Vahl Davis 1968). Some issues with the

numerical solutions to date are the errors involved with these calculations and the boundary conditions that are being studied. It is much easier said than done to achieve in practice a truly isothermal or isoflux surface. The numerical calculations must also account for the density change caused by heating. Not all of the regions within the volume of interest include buoyancy, and Ostrach (1988) states,

> "There are, however, regions in which there is no buoyancy, such as the core for boundary layer flows, but a very small numerical error in the buoyancy term can cause it improperly to contribute to the solution there and, thus, misrepresent the true physics."

Another issue with numerical calculations is the trade-off between accuracy and computing time. A finer mesh will lead to more accurate results, but at the cost of increased computing time. The corners in enclosure flows are of particular interest. The researcher must make sure to use a fine enough mesh to resolve the flow around the corners, where the flow must turn. In an engineering sense, we can get away with a less than perfect mesh because the corner effects on overall heat transfer rates are expected to be small (De Vahl Davis 1968).

Analytical solutions are even more difficult than numerical solutions. The simplifying assumptions used in external flows do not apply to internal problems. This is because the core flow is dependent on the boundary layers, which are dependent on the boundary conditions and the core flow. The dependence of the boundary layer flow and core flow on each other makes things rather complicated. Ostrach (1988) also points out that the vertical boundary layer theory does not appear to be useful for prediction or correlation of the computed results.

Ostrach's review article (1988) on natural convection in enclosures provided a thorough review of the literature prior to his article. In his article, he gives three points of emphasis that show the complexity of the problem and part of the reason that a true solution is yet to be presented. The first point of emphasis is that it is ill-advised to make ad hoc physical assumptions for complex problems. Many researchers, such as Batchelor, incorrectly guessed the configuration of the core, which delayed proper

description of the problem and misled many researchers who used the information. Batchelor's (1954) initial theory was that the core region was isothermal. He also concluded that at sufficiently high Rayleigh number, the flow would consist of a core of constant temperature and vorticity (De Vahl Davis 1968). In many publications, the core flow is often assumed or estimated based on seemingly similar problems. Ostrach points out that natural convection is very sensitive to changes in the geometric configuration and boundary conditions. This often makes it unwise to use results from problems that seem to be similar in nature.

Ostrach's second point is that despite clear and explicit rules on how to go about normalizing the equations for natural convection problems, there are many different, inappropriate ways in which the process is done. This can lead to errors, and thus, a misrepresentation of the physics. Many researchers prior to Ostrach were guilty of this. Only once the proper scaling analyses were performed with formal mathematical procedures, did researchers gain a deeper insight into the physics and obtain meaningful results.

Finally, Ostrach points out that the modified Oseen linearization proved to only give incorrect results. This linearization proved extremely helpful in simplifying the equations of other problems such as external flows. However, the buoyancy characteristics in natural convection in enclosures and the coupling of the boundary layer and core do not permit the use of this linearization.

An important part of natural convection in enclosures is the relationship between the boundary layer flow near the walls and the core flow in the center of the enclosure. At high Rayleigh numbers, classical boundary layer theory yields simplifications that are very helpful for other fluid flow problems. However, for internal flows, the core flow is affected by the boundary layer flow rather than the boundary conditions because it is enclosed by the boundary layers. In addition, the boundary layer flow is affected by the core flow. This coupling of the boundary layer flow and core flow doesn't allow the same simplifications as in other fluid-flow problems. To make things even more complicated, Ostrach points out that the core can contain more than one global core flow, and flow sub-regions, such as cells and layers. De Vahl Davis (1968) noticed reverse

flow near the center of the cavity for high Rayleigh number flows. He suggests that at high enough Rayleigh numbers, the vorticity near the wall is so strong that it is able to reverse the direction of the core flow.

In many of the simulations and solutions presented in the literature, the Boussinesq approximation is used to handle the buoyancy variation within the domain. This approximation neglects density variation in the inertial terms of motion, but retains it in the buoyancy term of the vertical equation. The key to this approximation is that the density variations due to inertial effects are extremely small compared to gravity. Gravity is strong enough to make a large enough difference in the specific weight of the fluid.

Natural convection in enclosures has many different geometric configurations and boundary conditions. There are many different situations and parameters that come into play with these types of problems. Chu et al. (1976) investigated the effect of heater location, heater size, aspect ratio, and boundary conditions on two-dimensional laminar natural convection in rectangular enclosures. Their range of parameters included Pr = 0.7, $0 \leq \text{Ra} \leq 10^5$, a complete range of heater widths and locations, and a wide range of aspect ratios. They looked at an isothermal heater with an isothermal cooler wall opposite the heater with two different boundary conditions for the horizontal walls. The adiabatic boundary condition refers to the situation where the horizontal walls of the enclosure are adiabatic. The isothermal condition refers to the situation where the horizontal walls are isothermal and kept at the same temperature as the cooler wall. Figure 2 shows the boundary conditions that Chu et al. used in their study.

The effect of the heater location on the Nusselt number and stream function was tested for $\ell/H = 0.2$ at various Rayleigh numbers, S/H values, and for isothermal and adiabatic horizontal walls. They found that the values of Ψ_{max} do not differ greatly for

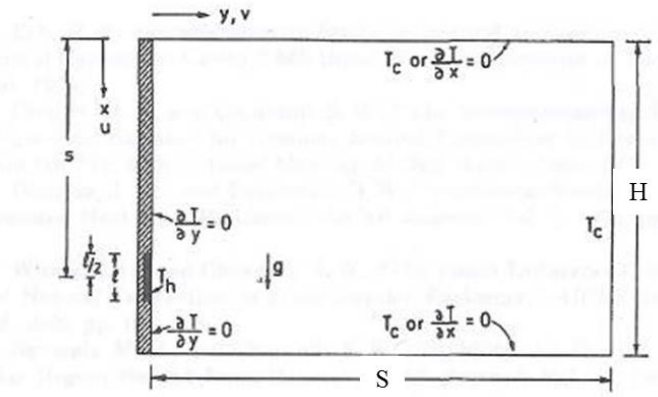

Figure 2. Coordinate system and thermal boundary conditions used by Chu et al. (1976).

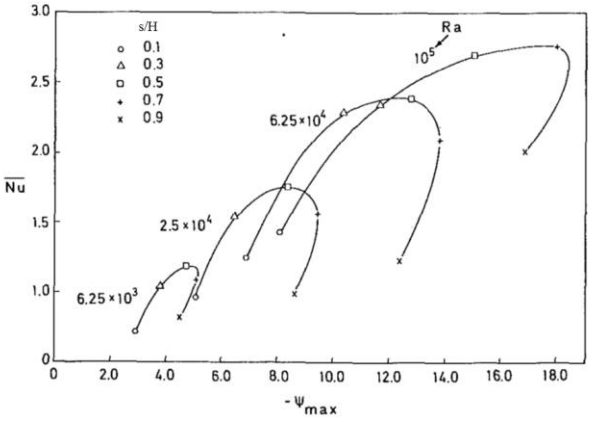

Figure 3. Rates of heat transfer and circulation in a square channel with insulated horizontal walls. ℓ/h = 0.2 (Chu et al. 1976)

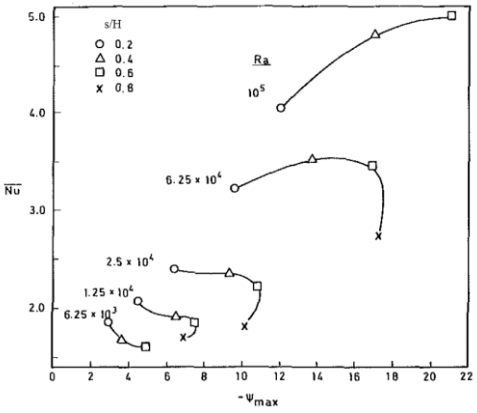

Figure 4. Rates of heat transfer and circulation in a square channel with cooled horizontal walls. ℓ/h = 0.2 (Chu et al. 1976).

the two boundary conditions. However, the rates of heat transfer were significantly higher for the isothermal condition.

When the Nusselt number and Ψ_{max} are plotted against each other, they show a complicated relationship. An important observation is that for the adiabatic condition, the same heat transfer rate can be attained at either a low or high rate of circulation just by adjusting the heater location. The same can be said for the same rate of circulation: "This multiplicity also occurs for the isothermal case but the range is more restricted…" (Chu et al. 1976).

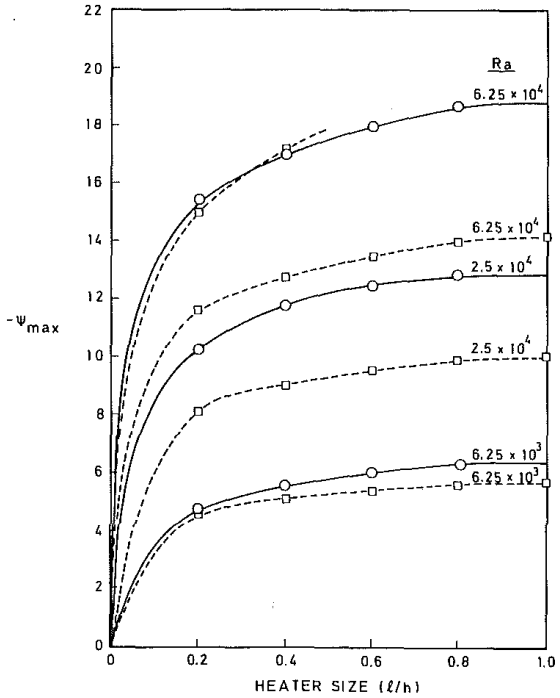

Figure 5. Effect of heater size and Rayleigh number on rate of circulation in a square channel. s/H = 0.5 (Chu et al. 1976).

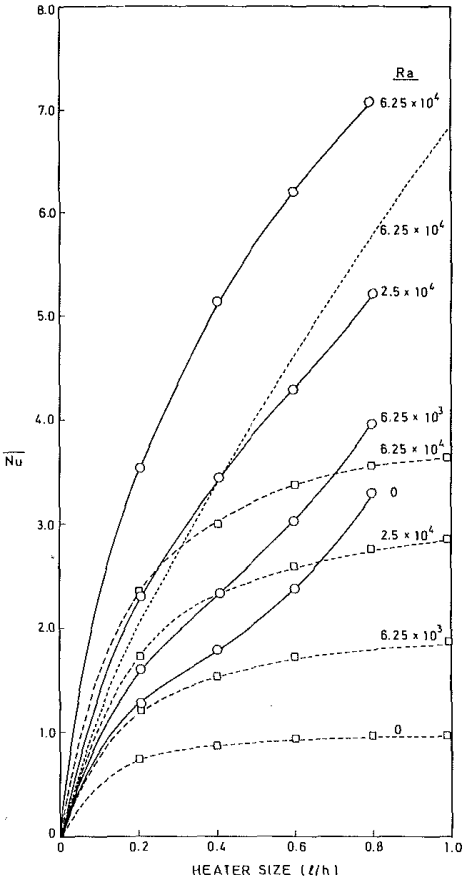

Figure 6. Effect of heater size Rayleigh number on rate of heat transfer in a square channel. s/H = 0.5 (Chu et al. 1976).

—O— isothermal horizontal walls
- - - □ - - - adiabatic horizontal walls
. . . . . boundary layer theory

—O— isothermal horizontal walls
- - - □ - - - adiabatic horizontal walls
. . . . . boundary layer theory

The effect of the heater size is examined with a centrally located heater, s/H = 0.5, at various Rayleigh numbers, ℓ/h values, and for both horizontal boundary conditions. "As the heater size is increased above 20 percent of the wall height the circulation is seen to increase only slightly. The rate of heat transfer behaves similarly for the adiabatic case but approaches infinity" (Chu et al. 1976).

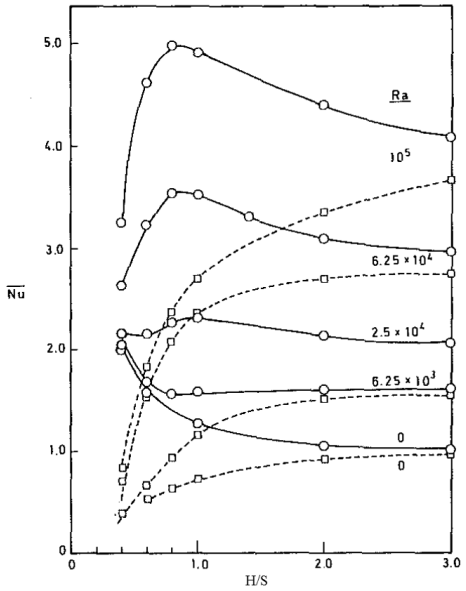

Figure 7. Effect of cavity height and Rayleigh number on rate of heat transfer. ℓ/S = 0.2, S/H = 0.5 (Chu et al. 1976).

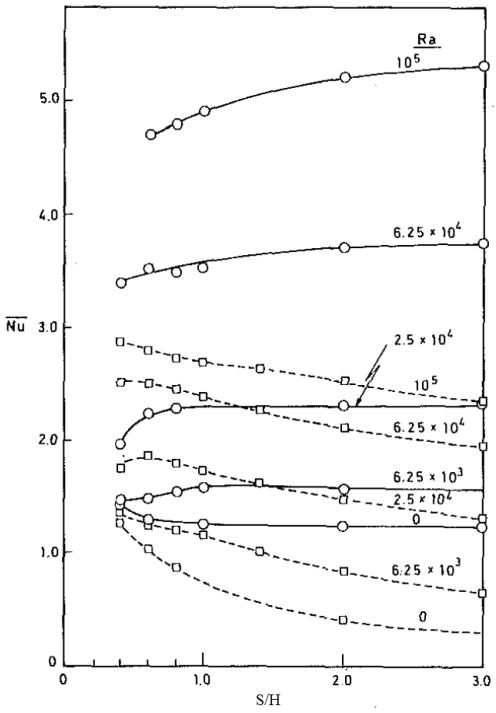

Figure 8. Effect of cavity width and Rayleigh number on rate of heat transfer. ℓ/H = 0.2, s/H = 0.5 (Chu et al. 1976)

—O— isothermal horizontal walls
- - - □ - - - adiabatic horizontal walls
. . . . . boundary layer theory

—O— isothermal horizontal walls
- - - □ - - - adiabatic horizontal walls
. . . . . boundary layer theory

Another important parameter is the aspect ratio. Chu et al. look at the effect of varying both the height and width of the enclosure. Chu et al. used the width of the enclosure to define the modified Rayleigh number, Ra_S, when they varied the height of the enclosure. The aspect ratio, H/S, is varied from 0.4 to 3 in Figure 7. Whereas, in Figure 8, the S/H value is varied from 0.4 to 3 because this figure shows the effect of increasing width on the average Nusselt number. It can be seen in Figure 7 that for large values of Ra_S, the rate of heat transfer increases due to increased circulation and decreases due to greater width (Chu et al. 1976). The heat transfer rate for both horizontal boundary conditions is observed to approach the same value as the aspect ratio increases.

When the width is varied, the height of the enclosure is used as the characteristic length in the Rayleigh number. The maximum value of the stream function increases for all Rayleigh numbers for the isothermal case. It is observed that the rate of heat transfer typically decreases as the width of the enclosure increases. Again, the rate of heat transfer for both boundary conditions approach the same value as the width is decreased.

2. Apparatus and Procedure

2.1 Apparatus

The experimental apparatus used in this study consists of a rectangular enclosure with inner dimensions 203 mm × 203 mm × 25.4 mm. The top of the enclosure is open to the ambient environment and the base and walls are made out of 5 mm acrylic. This gives a total volume of approximately one liter. The base has four slots for mounting the enclosure to a vibration resistant optical table and to allow for easy horizontal adjustment. A FIREROD® cartridge heater (Watlow #G8A45) is placed in a rectangular, aluminum block and is attached to the back of the copper plate with a thermal adhesive. The cartridge heater has a maximum power of 1000 W. Figure 9 shows the apparatus with the enclosure, the aluminum, and the copper plate. The figure also shows the placement of the holes in the base. Detailed drawings of all parts of the enclosure are in Appendix B. The aluminum block is 203 mm tall × 19.05 mm wide × 19.05 mm thick.

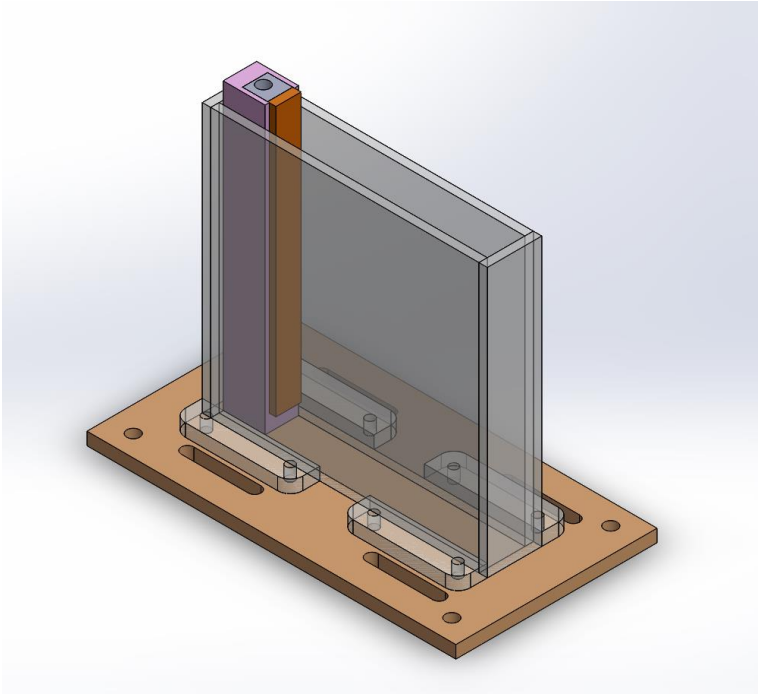

Figure 9. Acrylic enclosure and heater configuration.

The copper plate (copper 110) is 203 mm tall × 19.05 mm wide × 6.35 thick. The copper plate has an unpolished finish that meets the specifications set by the ASTM B187 standard. No additional work was done to alter the surface characteristics. Along the backside of the copper plate are twelve 1.5 mm DIA holes along the centerline for embedded thermocouples. Each hole is drilled 5.35 mm deep and to within 1 mm of the surface. At each hole location, a rectangular slot is cut into the copper from the edge to the center. This slot is for the thermocouple wires to be fed out of the heater configuration and each slot has dimensions 1.5 mm tall × 0.75 mm deep. The heater configuration (the aluminum and copper plate) is then insulated on all sides except the face that interacts with the emulsion. A voltage regulator is used to vary the voltage being supplied to the cartridge heater.

In the middle of the enclosure are three thermocouples at 7.6, 10.2, and 12.7 cm from the bottom. These thermocouples are used to measure the bulk temperature of the emulsion away from the surface of the heater. A copper coil with 6.35 mm DIA is used as a cooling coil on the side of the enclosure opposite the heater. Cold water is fed directly from the laboratory supply through the coil, and then into the laboratory sink.

An Agilent 34970A data acquisition unit is used to record the temperature and voltage data throughout each experimental run. Each run is 10 min in duration and data is collected at 0.57 Hz.

Optical holography is used to capture images of the emulsion near the surface of the heater throughout each experimental run. Because the FC-72 droplets are transparent, simple photographs will not suffice. The refractive index of FC-72 is 1.251. Holography uses the diffraction pattern created by the FC-72 droplets to distinguish them from the water. These images are used to observe droplet behavior as they move through the boundary layer and begin to boil. Appendix D contains a picture showing the various components of the optical setup.

2.2 Heat Transfer Formulation

The first portion of the analysis uses a one-dimensional, transient formulation of the heat conduction equation to get an estimate of the necessary heat flux to produce the temperatures required to initiate boiling of the dispersed component in the emulsion and

to determine the amount of time required to reach steady state. With constant thermophysical properties, the governing equation and the boundary conditions are

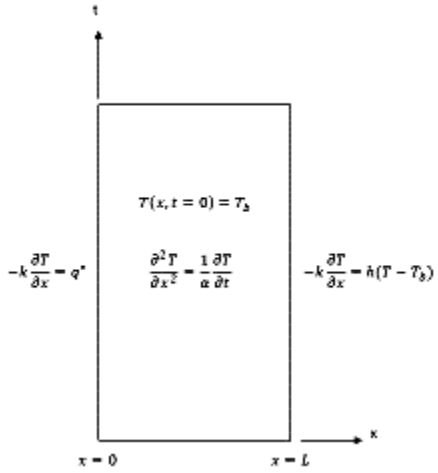

Figure 10. Domain of one-dimensional, transient heat conduction in the copper plate.

$$\frac{\partial^2\theta}{\partial x^2} = \frac{1}{\alpha}\frac{\partial\theta}{\partial t}$$

$$@\ x = 0; \quad -k\frac{\partial\theta}{\partial x} = q'' \tag{1}$$

$$@\ x = L; \quad -k\frac{\partial\theta}{\partial x} = h(\theta)$$

$$\theta(x, t = 0) = 0$$

The solution to this problem is obtained through superposition,

$$\theta(x, t) = \theta_H(x, t) + \theta_{ss}(x) \tag{2}$$

The homogenous problem, $\theta_H(x, t)$, takes the homogenous boundary conditions and the non-homogenous initial condition. The steady-state problem, $\theta_{ss}(x)$, takes the non-homogenous boundary condition. The complete solution is,

$$T(x,t) = \sum_{n=1}^{\infty} C_n \cos(\lambda_n x)\, e^{-\alpha\lambda_n^2 t} + q''\left(\frac{1}{h} + \frac{L-x}{k}\right) + T_b \tag{3}$$

$$C_n = \frac{-\frac{q''L}{k\lambda_n}\sin(\lambda_n L) - \frac{q''}{h\lambda_n}\sin(\lambda_n L) + \frac{q''}{k}\left(\frac{1}{\lambda_n^2}\cos(\lambda_n L) + \frac{L}{\lambda_n}\sin(\lambda_n L)\right) - \frac{q''}{k\lambda_n^2}}{N(\lambda_n)} \tag{4}$$

$$\frac{1}{N(\lambda_n)} = 2\frac{\lambda_n^2 + K^2}{L(\lambda_n^2 + K^2) + K} \tag{5}$$

$$\lambda_n \tan(\lambda_n L) = K\,; \quad K = \frac{h}{k}\ . \tag{6}$$

The details of the solution are given in Appendix A.

The steady-state temperature distribution is used in conjunction with the heat transfer correlation proposed by Bejan (2004) to determine the heat flux and corresponding heat transfer coefficient for a desired wall temperature. These equations must be solved simultaneously. In order to evaluate the heat flux, the heat transfer coefficient is required. However, at the same time, the heat flux is required to evaluate the Rayleigh number, and thus the heat transfer coefficient. Eqn. (7) is an empirical correlation proposed by Bejan (2004) for natural convection in enclosures when one sidewall is heated and the other is cooled with uniform heat flux. The horizontal walls are adiabatic.

$$\overline{Nu}_H = \frac{\bar{h}H}{k_f} = 0.34\, Ra_H^{2/9}\left(\frac{H}{S}\right)^{1/9} \tag{7}$$

The Bejan correlation is valid for fluids for which $Pr \gtrsim 1$. The steady-state temperature distribution is,

$$T_{ss}(x) - T_b = q''\left(\frac{1}{h} + \frac{L-x}{k}\right)\ . \tag{8}$$

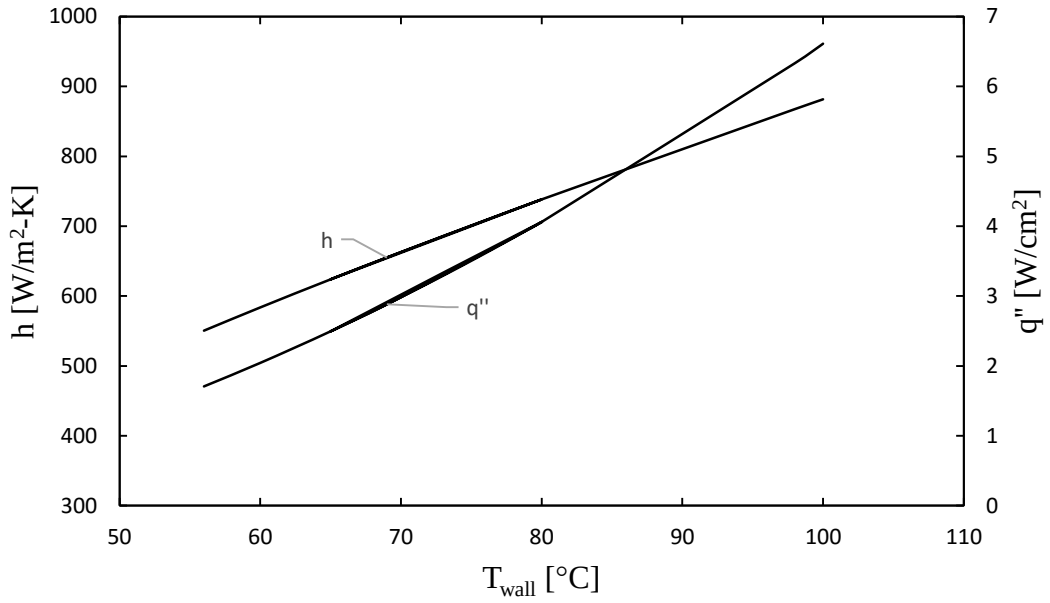

Figure 11. Required heat flux and corresponding heat transfer coefficient for specified wall temperatures.

All thermophysical properties are assumed constant and evaluated at the film temperature. Once the heat flux is known, the heat transfer coefficient is solved for using Eqn. (7). Figure 11 shows the variation in heat flux and heat transfer coefficient as a function of the desired wall temperature.

The temperature of the wall should be high enough to initiate boiling of the dispersed component in the boundary layer, yet low enough so that the water does not boil. FC-72 has a boiling point of 56 °C. Figure 11 above shows that for a desired wall temperature of 80 °C the required heat flux is 4.06 W/cm^2, and the corresponding heat transfer coefficient is 738.3 W/m^2-K. In order to maintain a wall temperature of at least 56 °C, the minimum required heat flux is 1.71 W/cm^2. This value of heat flux yields a heat transfer coefficient of 550.5 W/m^2-K.

In determining the temperature at the wall and the steady-state temperature distribution in the copper plate, the largest error arises from the correlation used to determine the heat transfer coefficient. For this reason, the time-dependent wall temperature is calculated using values of the heat transfer coefficient that are within 10%

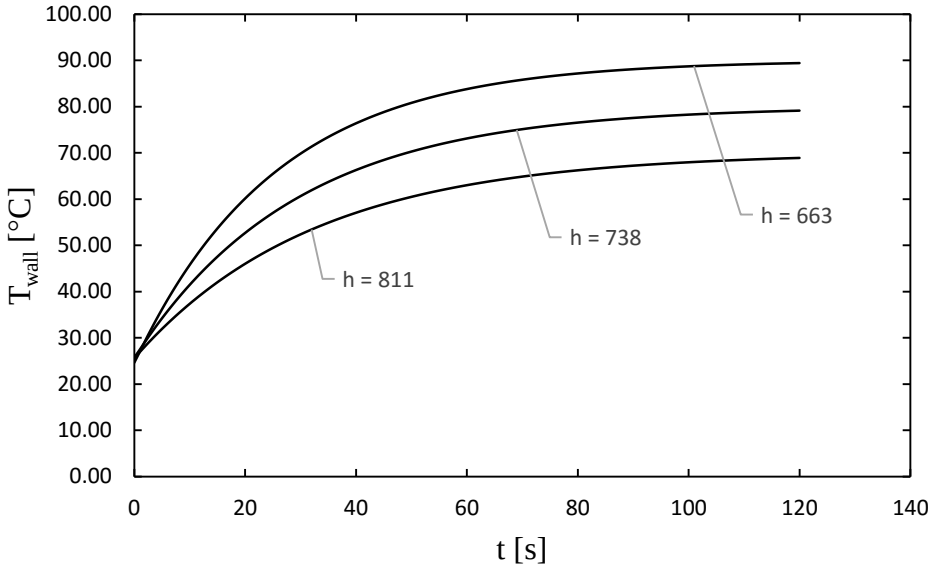

Figure 12. Wall temperature as a function of time for varying heat transfer coefficients.

of the calculated value. This comparison gives a good estimate of the range of temperatures that can be observed in the experiment.

Figure 12 shows the wall temperature as a function of time for varying heat transfer coefficients. The figure shows that an increase in the heat transfer coefficient of 10% will yield a wall temperature of approximately 70 °C, and a decrease of 10% in the heat transfer coefficient will yield a wall temperature of approximately 90 °C. Both of these temperature extremes are acceptable for the experiment as they are both above 56 °C, the boiling point of FC-72, and below the boiling point of water. For all three heat transfer coefficients, the heated surface takes ~2 min to reach steady-state temperature values.

The design considerations for the aluminum and copper plate are: 1) the heat flux must be uniform over the surface that interacts with the emulsion, 2) the heat flux must be great enough to achieve a high enough temperature at the surface that interacts with the emulsion so that boiling of the dispersed component occurs, and 3) the aluminum is thick enough to minimize heat transfer out the sides of the heater configuration. Owing to the complex nature of the geometry between the circular cartridge and the square surfaces between the aluminum and copper plate, ANSYS Workbench 15.0 was used to

Table 1: Analysis plan for heater design.

Alum. Thickness [in.]	Heater Diameter [in.]	No. of heaters
0.75	0.375	1
0.5	0.375	1
0.75	0.25	2
0.5	0.25	2

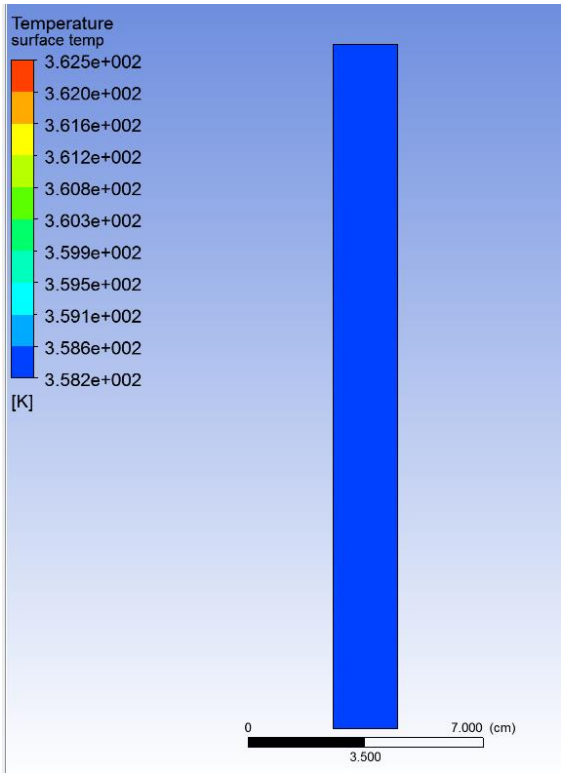

Figure 13. Wall temperature distribution along the copper surface.

calculate heat flux and temperature distributions at desired points and across desired surfaces of the aluminum and copper plate.

The ANSYS workbench 15.0 code was used to analyze the effect of the heater diameter and the thickness of the aluminum on the heat flux and temperature distribution in the heater configuration. Table 1 shows the cases considered.

To ensure that a high enough temperature is reached on the copper surface, a surface contour showing the temperature along this surface was analyzed. The lowest

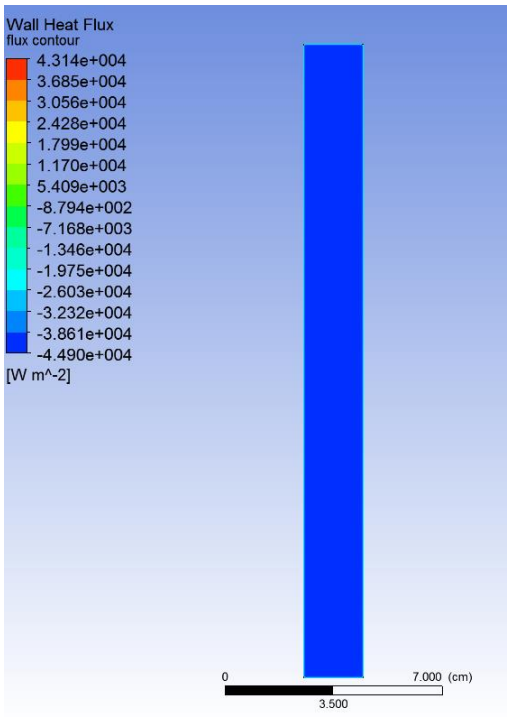

Figure 14. Wall heat flux distribution along the copper surface.

surface temperature is observed is approximately 85 °C, which is well above the boiling point of 56 °C for FC-72.

The other important design consideration was that the heat flux be uniform along the copper surface that interacts with the emulsion. Figure 14 shows that the heat flux is uniform over the entire surface. The only portions that are not uniform are along the edges of the surface. Close to these edges, the heat flux decreases dramatically due to the adiabatic boundary condition used in the calculation. However, a decrease in the wall heat flux is not seen until within 0.06 cm (0.024 in.) from any edge. The width of the heater is 0.75 in., which means that only 6.3% of the width of the heater is at a heat flux less than desired. To determine the overall effect of the decreased heat flux seen along the edges of the heated surface, the heat flux is integrated over the heated surface area to determine the total amount of heat leaving the heated surface. This is then compared to the total amount of heat that would be leaving the surface if the surface had uniform heat flux across the entire area. This was done in ANSYS Workbench 15.0. Theoretically,

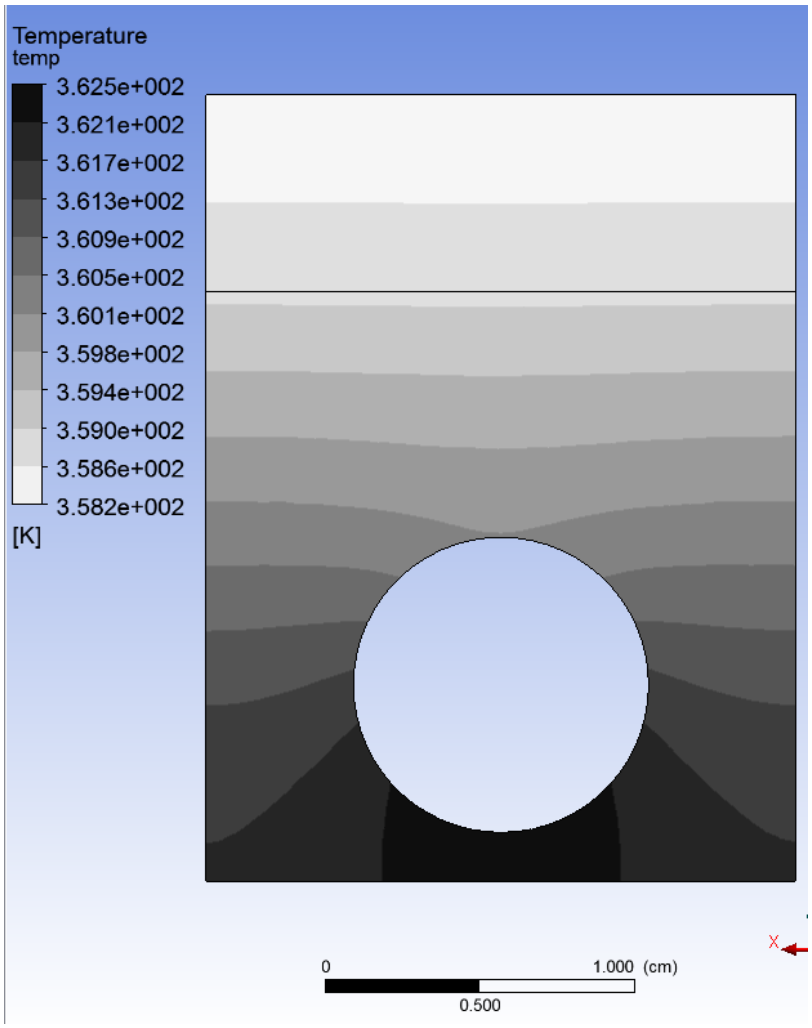

Figure 15. Temperature distribution along horizontal cross section of heater 4 in. from the bottom.

given no edge effect and uniform heat flux, the total heat flow through the area is 173.8 W. The total amount of heat flowing through the area of the heated surface with the edge effect is calculated to be 171.4 W, 1.4% less than the theoretically predicted heat flow.

The temperature distribution shown in Figure 15 is used to ensure that the aluminum is thick enough. When the aluminum is thicker, temperature contours tend to even out in the horizontal direction, thereby eliminating heat transfer in the horizontal direction. This figure shows the temperature contours leveling out before they reach the aluminum-copper interface. It is important to minimize heat transfer to the sides and out

the back of the heater. Ideally, all heat should travel through the aluminum and copper and be expelled into the emulsion via the top edge in Figure 15.

2.3 Heat Loss through Enclosure Wall

The heater used in this study is placed along the side of the enclosure. In order to prevent heat from moving through the wall and to the external surroundings, enough

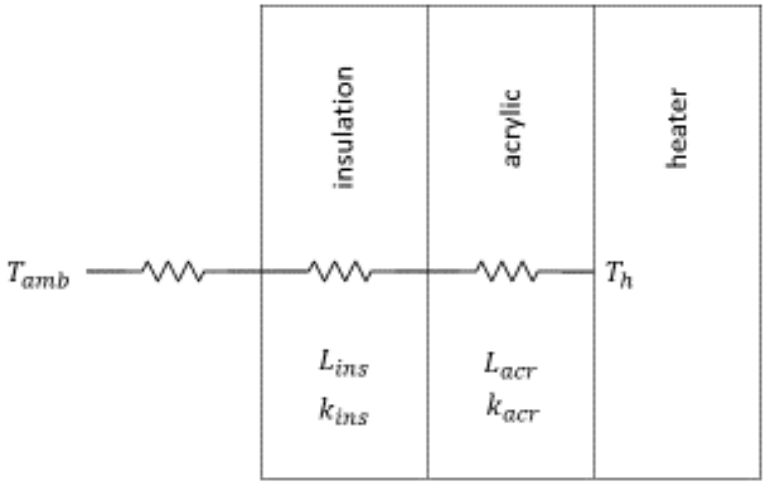

Figure 16. Thermal resistance diagram for copper plate, acrylic wall, and insulation.

insulation must be used so that the majority of the power produced by the heater is transported into the working fluid.

This type of problem is well-suited for the thermal resistance. The structure is composed of the acrylic wall of the enclosure, the Styrofoam insulation, and the outside air at room temperature (Figure 16).

The thermal resistance of a single component in the structure is

$$R = \frac{L}{kA} \tag{9}$$

The heat flow through the structure to the surroundings can be modeled mathematically by,

$$(1-\gamma)Q = \frac{T_h - T_{amb}}{\frac{L_{acr}}{k_{acr}A} + \frac{L_{ins}}{k_{ins}A} + \frac{1}{h_{amb}A}} \quad (10)$$

The total amount of heat flow, temperature, and area of the heater are known. The thermal conductivities for all materials can be found in various heat transfer resources and the heat transfer coefficient is known for still air at ambient conditions. The thickness of the acrylic wall is known and the thickness of the insulation is chosen. For a chosen insulation thickness, the fraction of heat produced by the heater that is transported to the working fluid, γ, is determined using Eqn. (10). With an insulation thickness of 0.5 cm, the fraction of heat transported to the working fluid is 99.67%. Less than 0.5% of the heat generated by the heater is lost to the external surroundings of the enclosure.

2.4 Increase in Bulk Temperature of the Fluid

With the amount of heat being generated by the heater, it is possible that the bulk temperature of the fluid could rise significantly over the course of an experimental run. To determine the amount by which the bulk temperature increases as a function of time, a lumped capacitance model is used,

$$q''A = \rho_f C_p \frac{dT_b}{dt} V \quad . \quad (11)$$

All thermophysical properties are assumed constant in the analysis. Solving the above differential equation for $T_b(t)$ yields,

$$T_b(t) = \frac{q''A}{\rho_f C_p V} t + T_{b,0} \quad . \quad (12)$$

The initial temperature of the bulk, $T_{b,0}$, is 25 °C, and all properties of the fluid are evaluated at the film temperature, which uses the initial temperature of the bulk. The amount of time it takes the bulk to increase by 20 °C is considered the maximum amount

of increase allowable because the boiling point of the dispersed component of the emulsion is 56 °C. An increase of twenty degrees would mean the bulk of the fluid is at 45 °C, which is close to the boiling point of the dispersed component.

Eqn. (12) is re-arranged to solve for the time, t, based on a desired final temperature of the bulk,

$$t = \frac{T_b(t) - T_{b,0}}{\frac{q''A}{\rho_f C_p V}} \quad . \tag{13}$$

At a heat flux of 30 kW/m^2, it takes 10.65 min for the bulk temperature of the fluid to increase by 20 °C. It takes the heater approximately 2 min to reach steady-state temperature values. Therefore, each experimental run must be less than 12 minutes in duration. This is an adequate amount of time to inject droplets into the boundary layer and allow them to travel through the entire boundary layer while still maintaining a low enough bulk temperature. It is important to note that in this analysis, heat loss from the fluid to the surrounding is not accounted for. Therefore, with a cooling coil, it will take longer than the estimated time above for the bulk temperature of the fluid to rise by 20 °C.

2.5 Error between Thermocouple reading and Surface Temperature

In order to measure the wall temperature of the copper plate (i.e. the surface temperature on the fluid side), thermocouples are embedded in wells on the heater side of the copper plate. Each hole is drilled 5.35 mm into the copper plate. Any deeper, and the surface of the copper plate would be damaged during the manufacturing process. The thermocouples are placed in the wells, which are then filled with thermally conductive paste so as to hinder the flow of heat as little as possible. The complex geometry and the combination of different materials make this problem difficult to solve analytically. For this reason, ANSYS CFX 15.0 was used to get an estimate of the difference in temperature between the end of the well and the surface of the plate as well as to gain an understanding of how that difference is influenced by different geometric parameters. A picture of the ANSYS model is shown in Figure 17.

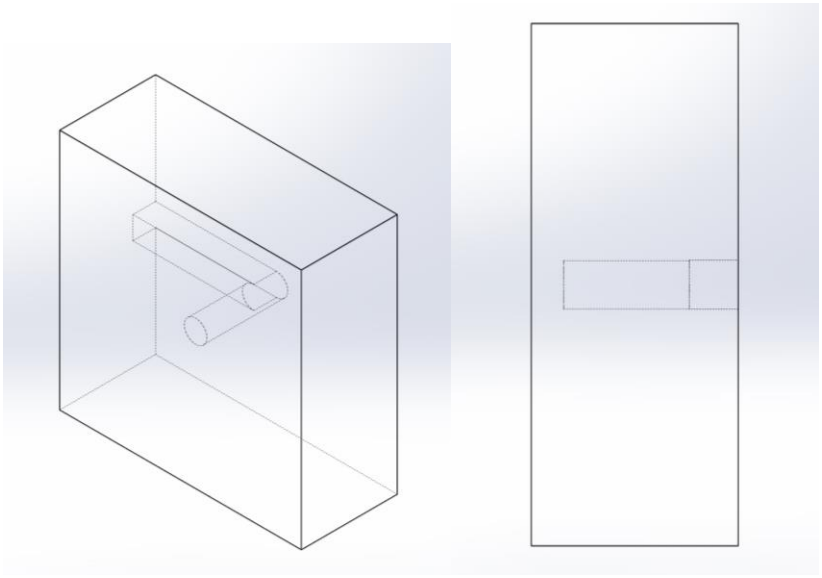

Figure 17. ANSYS model used for determining the difference in temperature between thermocouple reading and wall temperature.

The rectangular slot that goes from the well to the side of the plate is for the thermocouple wires to be fed through and out of the enclosure. Its height is equal to the diameter of the well, and its depth is 1.5 mm. The box shown is 16 mm wide × 16 mm tall × 6.35 mm thick. There are a total of ten thermocouples embedded in the copper plate. Each thermocouple is separated by 16 mm from center to center. Rather than use a model of the entire the geometry, symmetry was used to improve the accuracy of the analysis. With a smaller geometry that is representative of the larger geometry, more nodes can be used in a smaller volume, thus improving the accuracy.

The boundary condition on the front face of the box is convective with a heat transfer coefficient of 738.3 W/m^2-K and a bulk temperature of 25 ℃. The boundary condition on the back face is a constant heat flux of 4.06 W/cm^2. All other faces are set as adiabatic. The top and bottom faces can be set to adiabatic boundary conditions due to symmetry because of the other thermocouples. The adiabatic condition on the sides of the box can be physically realized by placing insulation on the side of the copper plate.

The ANSYS model was ran for various well depths and diameters. For each test, the area averaged temperature was calculated at the end of the thermocouple well and at the convective surface. Table 2 shows the tabulated results.

Table 2. ANSYS results for temperature difference between thermocouple well and convective surface when the well diameter is varied.

d [mm]	D [mm]	d/D	T_{TC} [K]	T_{wall} [K]	ΔT [K]
1	5.35	0.187	353.23	353.162	0.068
1.5	5.35	0.280	353.204	352.154	0.05
2	5.35	0.374	353.175	352.144	0.031
3	5.35	0.561	353.163	352.172	-0.009

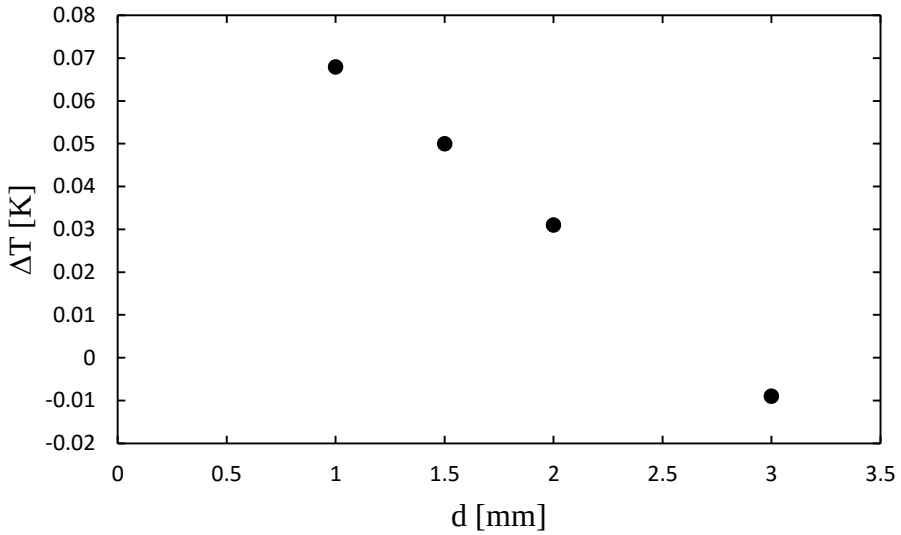

Figure 18. Temperature difference between thermocouple well and convective surface as a function of well diameter.

Figure 18 shows the difference in area-averaged temperatures between the bottom of the thermocouple well and the convective surface. As the diameter of the well is increased, the difference in temperature between the two surfaces decreases. Intuitively, this is as expected, because more and more volume consists of the thermally conductive past in the well. However, the goal of the thermocouple well is to measure the surface temperature as accurately as possible without taking up too much volume. The thermocouples used are type J, which typically have an error of ± 0.5 °C. The thermocouple wires, when together, have an approximate diameter of 1 mm. The well diameter should be the smallest possible diameter that will have a temperature difference of less than 0.5 °C. A diameter of 1.5 mm is chosen to ensure the thermocouples fit in

Table 3. ANSYS results for temperature difference between thermocouple well and convective surface when well depth is varied.

d [mm]	L - D [mm]	d/(L – D)	T_{TC} [K]	T_{wall} [K]	ΔT [K]
1.5	1	1.500	353.20	353.15	0.05
1.5	1.35	1.111	353.24	353.15	0.09
1.5	1.6	0.938	353.26	353.15	0.11
1.5	1.85	0.811	353.29	353.15	0.14
1.5	2.35	0.638	353.33	353.15	0.19

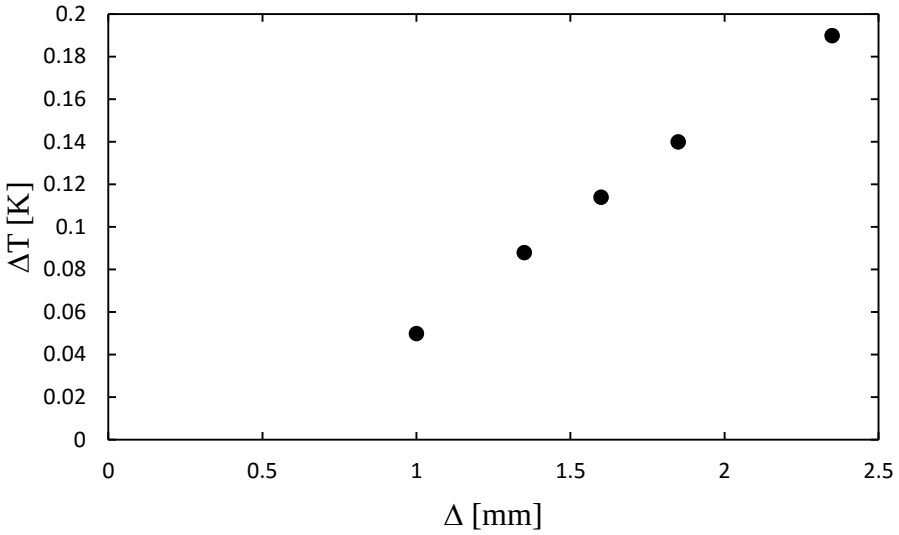

Figure 19. Temperature difference between thermocouple well and convective surface as a function of well depth.

the well and because the difference in temperature is less than the error associated with the thermocouple reading.

Figure 19 shows the difference in area-averaged temperature between the bottom of the thermocouple well and the convective surface when the distance between the two surfaces is varied. As the distance between the two surfaces is increased, the difference in temperature increases. The thermocouples have an error of ± 0.5 ℃. The well depth should be as close to the convective surface as possible so as to prevent surface damage, and it should be chosen so that the temperature difference is less than the error associated with the thermocouple readings. For these two reasons, a thermocouple well depth of

5.35 mm is chosen. This well depth is 1 mm away from the convective surface. The thermally conductive paste is rated for a maximum temperature of 200 °C.

2.6 Boundary Layer Thickness

The boundary layer next to the heated surface must be large enough that the entire droplet can be within in the boundary layer. The boundary layer must also be small enough so that the opposite side of the enclosure has as little effect as possible. Calculating the boundary layer thickness in enclosures is extremely difficult because the simplifying assumptions used when examining external flows do not apply to internal flows. Ostrach (1988) points out that the core region in the center of the enclosure is dependent on the boundary layer because it is contained by the boundary layers. However, the boundary layers themselves are influenced by the core region as well. This coupling of the boundary layers and core region is one of the main difficulties in analyzing flows in enclosures. For this experiment, however, only a rough estimate of the size of the boundary layer will be sufficient so long as the boundary layer thickness is significantly larger than the droplet diameter.

To get an estimate of the boundary layer thickness along the heated plate, an estimate will be obtained from correlations developed for external flows along a vertical flat plate. Sparrow and Gregg (1956) performed an analysis on a laminar free-convection boundary layer along a vertical flat plate with uniform surface heat flux. They performed an integral analysis to determine the boundary layer thickness, the temperature variation along the height of the heated surface, and the local Nusselt number. The expression obtained by Sparrow and Gregg (1956) is,

$$\frac{\delta}{y} = (360)^{1/5} \left[\frac{0.8 + \mathrm{Pr}}{\mathrm{Pr}^2\ \mathrm{Gr}_y}\right]^{1/5} \quad . \tag{14}$$

The boundary layer thicknesses calculated are also likely to be larger than those observed in the experiment. The coupling between the core region and the boundary layers in flow within enclosures causes the boundary layers to be smaller than in external flows. The boundary layer thickness calculated using the equation obtained by Sparrow

Table 4. Boundary layer thickness for varying heights along heater.

H [mm]	δ [mm]
203	2.03
101.5	1.77
50.75	1.54

Table 5. Maximum velocity for varying maximum temperatures of the heater wall.

Maximum Wall Temperature [°C]	u_{max} [cm/s]
56	10.97
60	11.87
65	12.97
75	15.09

and Gregg is great enough so that it is safe to assume the entirely droplet will be within the boundary layer.

Table 4 shows the boundary layer thickness for different heights along the heated surface for $Ra_H = 4.42 \times 10^{12}$. All thermophysical properties are evaluated at the film temperature.

The maximum velocities to be expected are calculated using an approximation due to Gebhart (1961).

$$u_{max} = \sqrt{g\frac{H}{2}\,\beta\,(T_{wall} - T_b)} \tag{15}$$

Using this equation, the maximum velocities for each maximum wall temperature are shown in Table 5.

Also of importance is the amount of time required for the boundary layer to develop along the heated surface. This study looks at the effect of the volume fraction of emulsion and droplet diameter on the heat transfer coefficients in a strong buoyant boundary layer. Thus, it is not a study on the transient behavior, but rather the steady state behavior. The time required for the boundary layer to develop is used as a

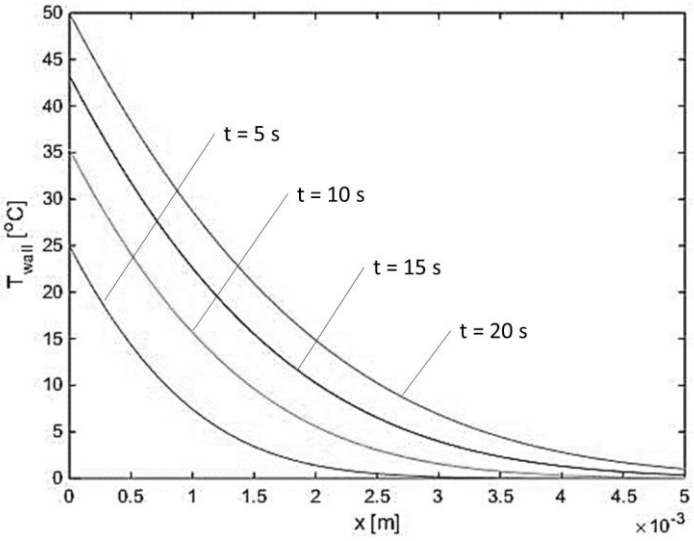

Figure 20. Diffusion layer thickness with respect to distance away from the heated surface and time for $Ra_H = 1.816\times10^{12}$.

minimum time required before steady state can be considered achieved. In addition, the temperatures are monitored to ensure they have reached steady state values as well.

The amount of time required for the boundary layer to develop is estimated by calculating the diffusion layer thickness with respect to time. Because the diffusion layer is dominated by heat conduction, the heat conduction solution can be used to estimate the thickness with respect to time. This solution is well-documented and can be found in numerous heat conduction textbooks. The equation for temperature with respect to the space and time variables is,

$$T(x,t) = \frac{2\,q_0''}{k}\left[\left(\frac{\alpha t}{\pi}\right)^{1/2} e^{-x^2/4\alpha t} - \frac{x}{2}\,\mathrm{erfc}\left(\frac{x}{\sqrt{4\alpha t}}\right)\right] \quad . \tag{16}$$

In natural convection flow, the momentum and thermal boundary layers are the same thickness.

Figure 20 shows the temperature profile with respect to space and time for $Ra_H = 1.816 \times 10^{12}$. As time increases, the diffusion layer thickness increases in the direction normal to the heated surface. At t = 5 s, the diffusion layer is approximately 3 mm

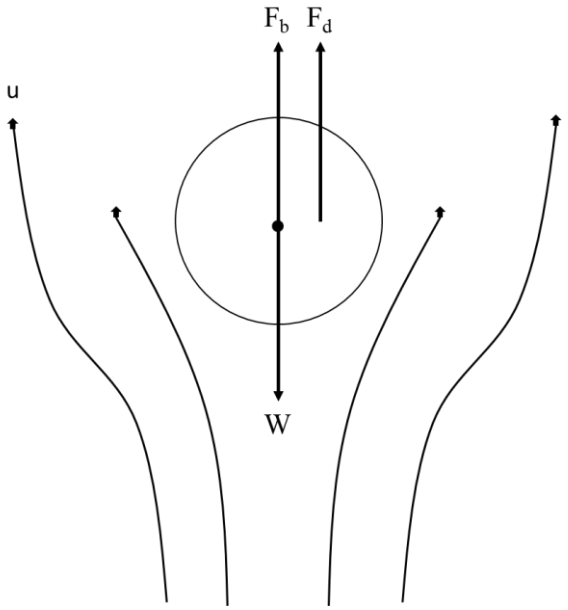

Figure 21. Free-body diagram of FC-72 droplet.

thick, which is almost equivalent to the expected steady-state boundary layer thickness.

2.7 Droplet Dynamics

An estimate of the maximum allowable difference in density between the FC-72 droplet and water is obtained. The FC-72 has a density that is ~1.6 times that of water. In free standing water, the droplets will sink. However, if the velocity generated in the boundary layer is great enough, the drag and buoyancy force can overcome the force due to gravity on a single droplet.

A free body diagram of the droplet is shown in Figure 21. The drag force is approximated using Stoke's drag. Stoke's drag states that the drag force on a small sphere moving through a viscous fluid is,

$$F_d = 6\pi\mu Ru \quad . \tag{17}$$

The assumptions for Stoke's drag are laminar flow, spherical particles, homogenous material, smooth surfaces, and that particles do not interfere with each other.

Table 6. Maximum allowable density ratio for a FC-72 droplet to rise in the boundary layer due to drag.

R [mm]	T_{wall} [°C]	u_{max} [cm/s]	ρ_d / ρ_f
0.1	75	15.09	4.836
0.2	75	15.09	1.959
0.25	75	15.09	1.426
0.3	75	15.09	1.614
0.4	75	15.09	1.24
0.5	75	15.09	1.153
0.6	75	15.09	1.107
0.7	75	15.09	1.078
0.8	75	15.09	1.06
0.9	75	15.09	1.047
1	75	15.09	1.038

The analysis is looking for the maximum allowable density ratio that will allow for the droplet to rise rather than sink. This point is characterized by where the droplet velocity is zero. The velocity of the fluid moving past the droplet is estimated using the maximum velocity present in the boundary layer, which was calculated earlier using boundary layer theory. Summing up the forces in the y-direction and solving for the density ratio, $\frac{\rho_d}{\rho_f}$, the solution becomes,

$$\frac{\rho_d}{\rho_f} = \frac{9\nu_f u}{2gR^2} + 1 \quad . \tag{18}$$

Table 6 shows the maximum allowable density ratio between FC-72 and water for various droplet radii.

If the droplet radius is greater than 0.25 mm, the density of the droplet is too large for the droplet to rise in the boundary layer. It is important to note that this analysis does not account for property changes within the boundary layer. The density of FC-72 is known to decrease when exposed to temperatures higher than room temperature.

Therefore, this is a rough estimate of the allowable density ratio for a rising droplet of FC-72 in water.

Also of importance is an estimate of the amount of energy required to boil a FC-72 droplet. This includes the energy required to raise the temperature of the droplet from room temperature up to its boiling point as well as the energy required to vaporize the droplet.

$$Q_{total} = Q_{sensible} + Q_{latent} \tag{19}$$

The sensible and latent portions of the required energy can be expressed,

$$Q_{total} = mC_p\Delta T + mL_v \tag{20}$$

For a droplet with d_d = 1.3 mm, the required energy to boil it is estimated to be 65.98 J. All thermophysical properties are evaluated at the film temperature and assumed to be constant. The heat flux on the heat transfer surface is 30 kW/m^2 at the highest power setting used in the experiments. Assuming that 10% of the total energy produced by the heated surface goes into vaporizing a single droplet, it would take ~5.7 s for the droplet to vaporize.

2.8 Experimental Plan

There are two experiments of interest to this study. The first uses a dilute emulsion as the working fluid to study the effect of varying the dispersed component percentage of the mixture based on volume. The second uses water as the working fluid, and small droplets of the dispersed component are injected into the boundary layer along the heated surface.

Previous research in the field has looked at the effect of varying volume percentage of the dispersed component on the heat transfer coefficient. However, these studies have all looked at this effect in pool boiling. This study aims to examine this effect in a strong buoyant boundary layer and to determine whether or not the effect is similar or different compared to the previous studies.

One of the aspects of boiling in dilute emulsions that remains unsolved is the way in which the dispersed phase begins to boil. To gain an insight into how this process takes place, the second experiment will use advanced optical equipment to examine a droplet as it rises or falls through the boundary layer. The primary interest is to determine where in the boundary layer the droplet boils and whether or not the droplet needs to come into direct contact with the heated surface to initiate the boiling process.

FC-72 is used as the dispersed component for all experiments in this study. Emulsions are prepared with volume percentages of 0.1, 0.2, 0.5, and 1% for the FC-72. These percentages are the same percentages used by Roesle (2013) in his study and make for good comparisons to pool boiling data. A maximum volume percentage of 1% is chosen because previous studies by Bulanov et al. (1996) have shown that for volume percentages greater than ~1%, there is no effect on the heat transfer coefficient.

Emulsions are prepared in the same way used in Roesle's (2013) study. Distilled water is first degassed by boiling and is then cooled to 25 °C for the experiment. The water then passes through a filter that removes particles 0.22 μm and larger before it is mixed with the FC-72 in a separate container. A gear pump is then used to circulate the mixture. Because FC-72 is denser than water, it tends to settle in large globules on the bottom of the container. The gear pump pulls in the mixture from the bottom of the container, and then pushes it through a partially open ball valve. When the fluid hits the wall of the ball valve it causes the FC-72 to break up in to very fine droplets. The fluid exits the ball valve at the top of the container. The gear pump is run for 15 min to ensure that the entire mixture has circulated through the ball valve multiple times. Each batch is used immediately after preparation and no surfactants are added.

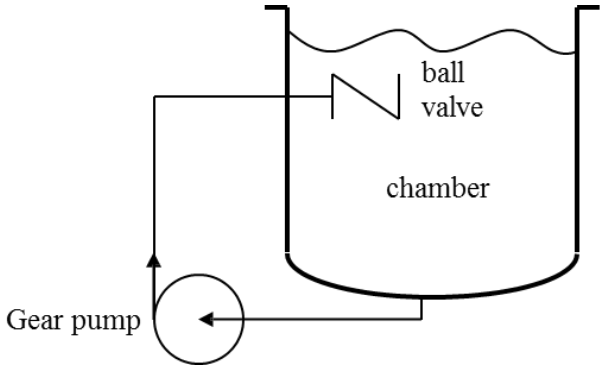

Figure 22. Apparatus for preparation of the emulsion

Table 7. Thermophysical properties for various power levels.

T_{film} [°C]	$\nu \times 10^7$ [m^2/s]	ρ_f [kg/m^3]	$\beta \times 10^4$ [1/K]	k_f [W/m-K]	Pr	C_p [J/kg-K]	Ra_H $\times 10^{-12}$
42.5	6.3	991.2	4.0	0.621	4.2	4.18	1.82
45	6.02	990.2	4.2	0.624	4.0	4.18	2.31
50	5.54	988	4.6	0.631	3.6	4.18	3.09
52.5	5.32	986.9	4.7	0.633	3.5	4.18	4.42

For the second experiment, droplets of FC-72 are injected into the boundary layer near the heated surface. Two different situations are observed. The first is an individual droplet of FC-72 injected in the boundary layer in contact with the heated surface using a pipette. The second is multiple FC-72 droplets injected through the use of a syringe pump. The optical equipment is setup on a rail system that allows for easy-adjustment of the components. The acrylic enclosure is held up using four threaded rods. Holes are placed in the base of the apparatus for the threaded rods and the height of the enclosure is adjusted by turning the nuts on the threaded rods. This allows for easy vertical adjustment so that images can be captured at various heights within the boundary layer. The pipette injects droplets with d_d = ~1.3 mm, while the syringe pump injects a continuous stream of droplets with 0.5 mm $\leq d_d \leq$ 1 mm through a 25 Ga needle.

For the heat transfer experiments, data is taken at four different power levels and thus, four different Rayleigh numbers. Each power level has a different set of thermophysical property values. Table 7 outlines the thermophysical property values for each power level.

3. Data Reduction

Figure 23 and Figure 24 show a schematic and picture of the overall experimental setup. The Agilent Data Logger is used to record the thermocouple readings and the voltage being supplied to the heater by the voltage regulator. The voltage regulator plugs directly into the laboratory outlet and supplies voltage on a percentage basis. The camera and laser are used to take holographic images of the emulsion near the heated surface. Cold water is supplied directly from the laboratory and fed through the cooling coil to keep the bulk temperature of the fluid from rising significantly during the experiment.

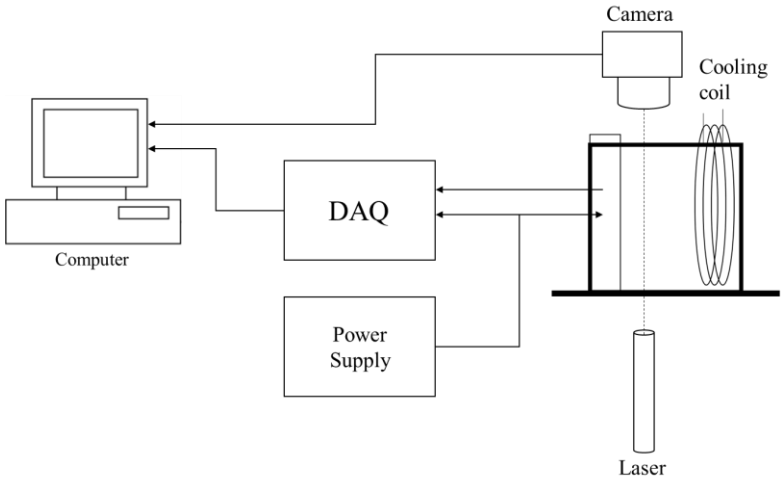

Figure 23. Schematic of overall experimental setup

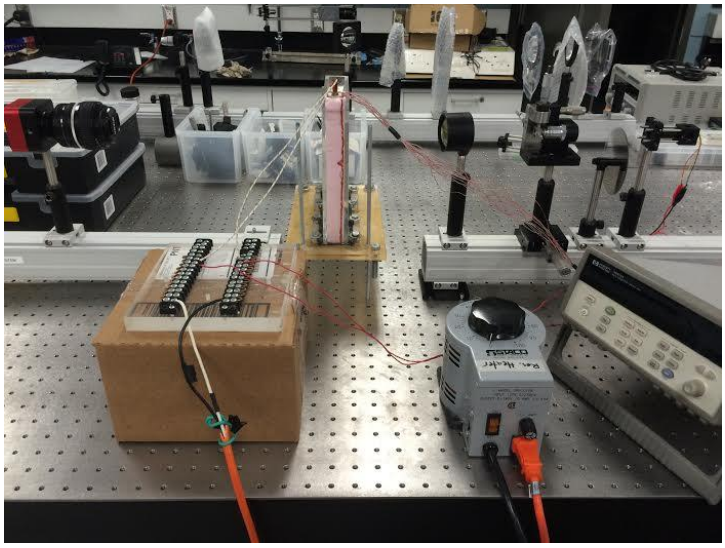

Figure 24. Photograph of optical setup and apparatus.

3.1 Calculation of Heat Transfer Coefficients

Each experimental run lasts 10 min. The temperatures for each thermocouple and the voltage drop across the heater are averaged over the 10 min duration to obtain one data point. The local heat transfer coefficient is then calculated for each thermocouple embedded in the heater and averaged over the length to determine the average heat transfer coefficient, and thus the average Nusselt number. There are twelve thermocouples embedded in the copper plate. For each thermocouple, the local heat transfer coefficient is,

$$h = \frac{q''}{(T_{TC} - T_{\infty})} \quad . \tag{21}$$

Once the local heat transfer coefficient is calculated for all 12 thermocouples, the arithmetic average is taken to determine the average Nusselt number by,

$$\overline{Nu}_H = \frac{\bar{h}\, H}{k} \quad . \tag{22}$$

This procedure is carried out at every time step throughout the duration of each experimental run. To obtain a single data point and the corresponding standard deviation for each Rayleigh number, temperature data is analyzed to determine when steady state operating conditions are reached for each run. When the thermocouple temperature data is observed to no longer increase by more than 1 °C over a time period of 1 min, it is assumed that steady state operating conditions have been reached. From this point forward, the numerical average of each quantity at each time step is taken. This approach creates a single data point for each run that can then be easily plotted.

3.2 Uncertainty Analysis

The overall uncertainty in the measurements must be taken into account to determine the accuracy of the experiment. During the tests conducted, the wall temperature, bulk temperature of the fluid, and the voltage drop across the cartridge heater are measured. The resistance of the heater and voltage drop across the heater are measured to determine the power being produced by the heater. The uncertainty in the power produced by the cartridge heater is supplied by the manufacturer. Table 8 shows

Table 8. Measurement uncertainties

Quantity	Uncertainty
Δv	± 1 V
R_h	± 3%
T_{wall}	± 0.5 °C
T_b	± 0.5 °C
H	± 0.03 in.
W	± 0.008 in.
k	± 2%

each of the measured quantities and their corresponding uncertainty. The equation for the heat transfer coefficient is,

$$h = \frac{q''}{T_{wall} - T_b} = \frac{\Delta v^2 / R_h}{HW(T_{wall} - T_b)} \quad . \tag{23}$$

The uncertainty in the temperature difference between the wall and the fluid bulk is,

$$U_{\Delta T} = \sqrt{\left(U_{T_{wall}}\right)^2 + \left(U_{T_b}\right)^2} = 3.11\ ^\circ C \quad . \tag{24}$$

The uncertainty in the length of the copper plate is ± 0.25 in. and the uncertainty in the width is ± 0.008 in. Thus, the uncertainty in the area of the heater is,

$$\frac{U_A}{A} = \sqrt{\left(\frac{U_W}{W}\right)^2 + \left(\frac{U_H}{H}\right)^2} = 0.011 \quad . \tag{25}$$

The uncertainty for the heat transfer coefficient is calculated by Eqn. (26). The temperature difference between the wall and the bulk varies according to 31 °C ≤ ΔT ≤ 50 °C. The smallest temperature difference is used because that will yield a worst-case estimate of the uncertainty in the heat transfer measurements. The voltage readings vary

according to 58 VAC ≤ Δv ≤ 79 VAC. Again, the lowest voltage reading is used to yield the largest possible uncertainty.

$$\frac{U_h}{h} = \sqrt{2\left(\frac{U_{\Delta v}}{\Delta v}\right)^2 + \left(\frac{U_{R_h}}{R_h}\right)^2 + \left(\frac{U_A}{A}\right)^2 + \left(\frac{U_{\Delta T}}{\Delta T}\right)^2} \tag{26}$$

The calculated uncertainty in the heat transfer coefficient is ± 9.4%.

The uncertainty in the heat transfer coefficient and the length of the heater are used to determine the uncertainty in the Nusselt number.

$$\frac{U_{\overline{Nu}_H}}{\overline{Nu}_H} = \sqrt{\left(\frac{U_h}{h}\right)^2 + \left(\frac{U_H}{H}\right)^2 + \left(\frac{U_k}{k}\right)^2} \tag{27}$$

Therefore, the total uncertainty in the average Nusselt number is ± 9.6%.

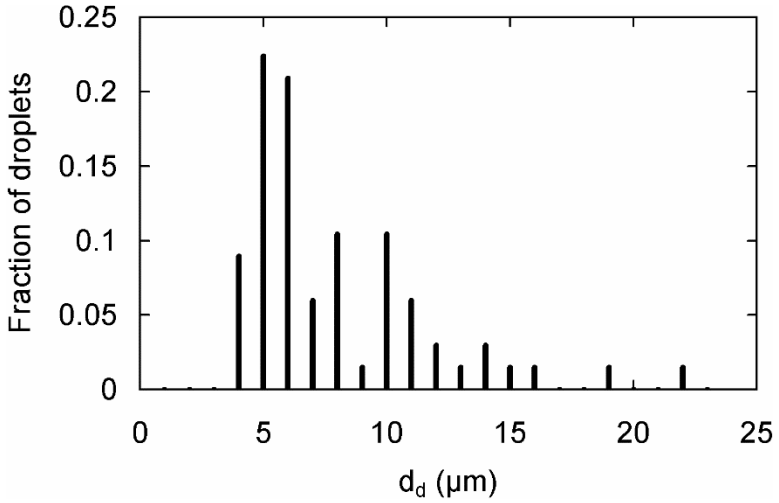

Figure 25. Histogram of droplet diameter for emulsion (Roesle and Kulacki 2013).

4. Results and Discussion

4.1 Measured Heat Transfer Coefficients

4.1.1 Water

The first set of experimental runs used distilled water with no FC-72 added. These experimental runs provide a base-line for comparison with the results obtained for emulsions as well as demonstrating that the apparatus behaves as expected. Emulsions are prepared as described in section 2.8. This process produces FC-droplets with 4 μm ≤ $d_d \leq 22$ μm and give an average droplet diameter of 8 μm (Figure 25). The average diameter and distribution of the droplet diameter does not change dramatically as the volume fraction, ε, is changed (Roesle and Kulacki 2013).

The correlation proposed by Bejan (2004) for a constant heat flux side wall is,

$$\overline{\mathrm{Nu}}_{\mathrm{H}} = 0.34\ \mathrm{Ra}_{\mathrm{H}}^{2/9} \left(\frac{\mathrm{H}}{\mathrm{S}}\right)^{1/9} \quad . \tag{28}$$

This correlation is valid for $\mathrm{Ra}_{\mathrm{H}} > 10^9$.

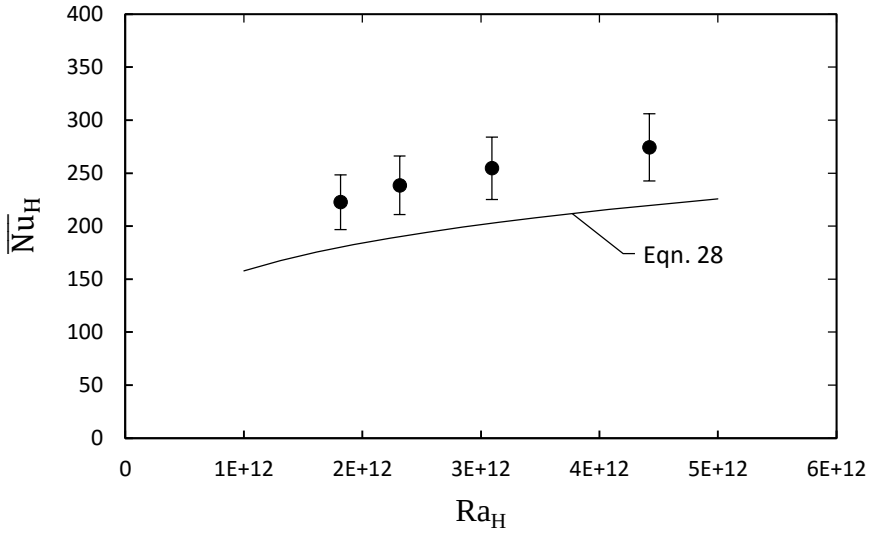

Figure 26. Average Nusselt number as a function of Rayleigh number along with Eqn. (28).

Figure 26 shows the average Nusselt number with respect to the Rayleigh number. Both correlations along with the experimental data are included. The experimental data yields an average Nusselt number that is slightly higher than that of Eqn. (28), which represents the constant heat flux boundary condition. Even though the data shows Nusselt numbers that are slightly higher than that of Eqn. (28), the data follows the trend exhibited by Eqn. (28) very well. The error bars in Figure 26 represent the uncertainty in the average Nusselt number.

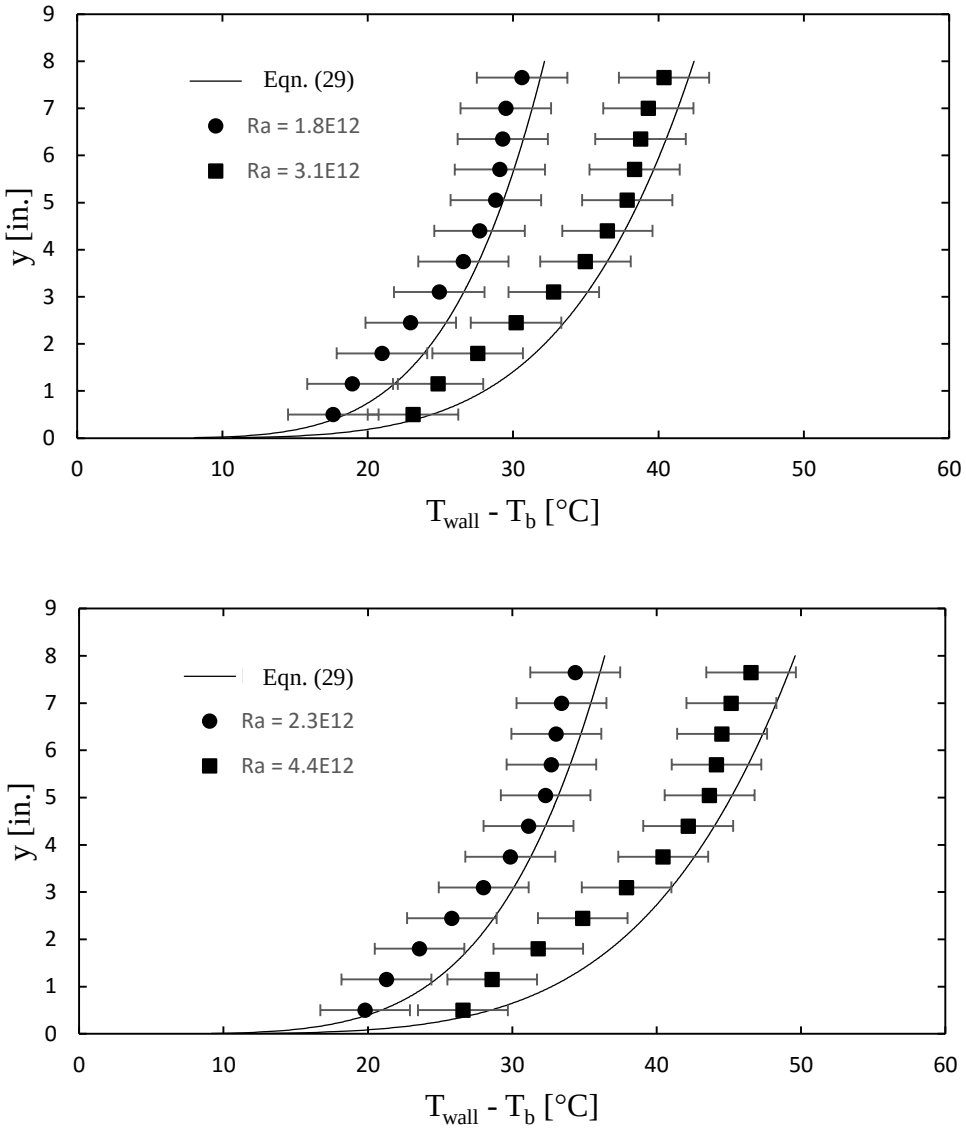

Figure 27. Temperature difference between heated wall and bulk compared to the integral solution, Eqn. (29).

Figure 27 shows the difference between the measured wall temperature and the bulk temperature as a function of vertical distance up the heater. As the Rayleigh number increases, the temperature difference between the lowest and highest thermocouples also increases. At the lowest Rayleigh number, the temperature difference is approximately 10 °C. Whereas, at the highest Rayleigh number, the temperature difference between the lowest and highest thermocouple is almost 20 °C. There is a rapid increase in temperature

from the bottom of the heater up to approximately half the overall height of the heater. This occurs because the boundary layer thickness increases the fastest between these two heights. Above half the height of the heater, the boundary layer thickness increases, but at a much slower rate. The data is compared to the integral analysis performed by Sparrow and Gregg (1956). The correlation is,

$$T_{wall} - T_b = 1.622 \frac{q''y}{k} \left[\frac{0.8 + Pr}{Pr^2 \, Gr_y}\right]^{1/5} \quad . \tag{29}$$

The solution determined by Sparrow and Gregg (1956) is for laminar natural convection form a vertical surface with uniform heat flux. Bejan (2004) states that for fluids of the air-water Prandtl number range ($0.7 \leq Pr \leq 10$), the transition to turbulence occurs in the vicinity of $Ra_H \sim 10^{13}$. As can be seen in Figure 27, the temperature data fit very well to Eqn. (29) and further verify the uniform wall heat flux boundary condition.

The duration of each experimental run is 10 min. Figure 28 through Figure 31 show the bulk temperature profile throughout the duration of each experimental run for water. There are three thermocouples that are placed in the center of the acrylic enclosure. The thermocouples are placed at varying heights of 7.6 cm, 10.2 cm, and 12.7 cm from the bottom of the enclosure. The bulk temperature never changes by more than 1.5 °C during a 10 min run. This is well within the uncertainty of the thermocouple measurements.

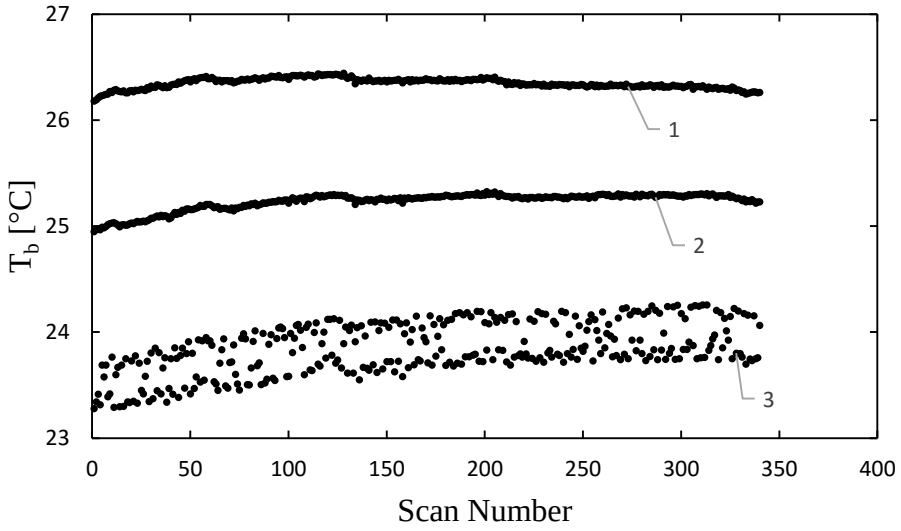

Figure 28. Temperature profiles for the bulk thermocouples at heights of (1) 12.7 cm, (2) 10.2 cm, and (3) 7.6 cm. $Ra_H = 1.82\times10^{12}$.

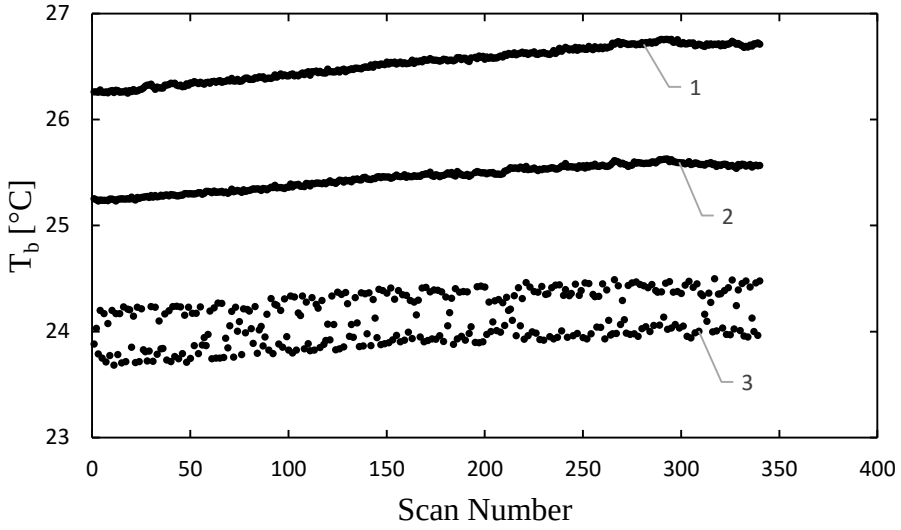

Figure 29. Temperature profiles for the bulk thermocouples at heights of (1) 12.7 cm, (2) 10.2 cm, and (3) 7.6 cm. $Ra_H = 2.31\times10^{12}$.

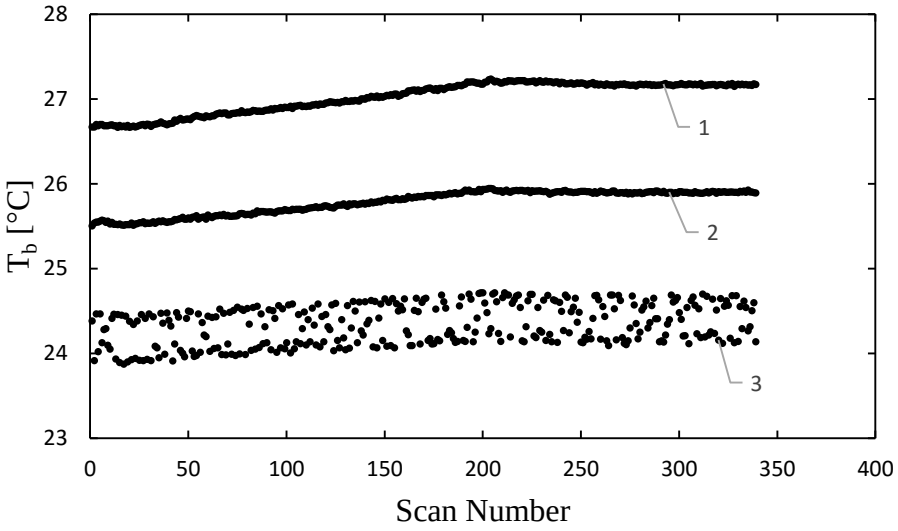

Figure 30. Temperature profiles for the bulk thermocouples at heights of (1) 12.7 cm, (2) 10.2 cm, and (3) 7.6 cm. $Ra_H = 3.09\times10^{12}$.

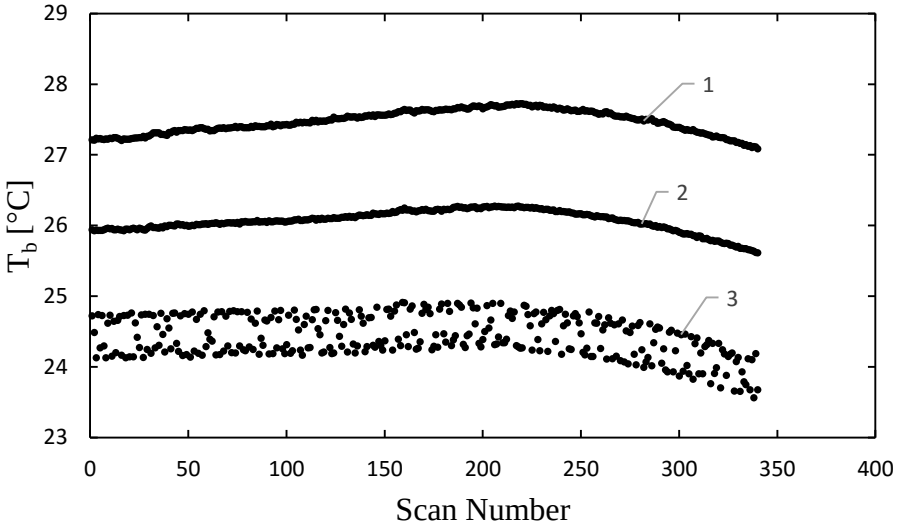

Figure 31. Temperature profiles for the bulk thermocouples at heights of (1) 12.7 cm, (2) 10.2 cm, and (3) 7.6 cm. $Ra_H = 4.42\times10^{12}$.

Table 9. Experimental runs carried out for heat transfer results.

	ε				
$Ra_H \times 10^{-12}$	0%	0.1%	0.2%	0.5%	1%
1.82	Experimental runs				
2.31					
3.09					
4.42					

4.1.2 FC-72 in Water Emulsions

The average Nusselt numbers for FC-72 in water emulsions are shown in Figure 32. Due to mechanical and fluid limitations, the Rayleigh number is not increased further beyond 4.42×10^{12}.

Figure 32 shows the average Nusselt number for FC-72 in water emulsions and normalizes them with the average Nusselt number seen in the pure water tests. Data was gathered for four different Rayleigh numbers and 0, 0.1, 0.2, 0.5, and 1% volume fractions of FC-72. Previous studies by Bulanov et al. (1986) have shown that for volume fractions greater than 1%, there is no effect on the heat transfer coefficient. Table 9 outlines the experimental tests that were conducted.

To the naked eye, all emulsions prepared for heat transfer tests were opaque. Images could not be obtained because the opaqueness did not allow for a laser to pass through to obtain holographic images. Figure 33 shows a picture of an emulsion with $\varepsilon = 0.5\%$. The thermocouples in the center of the enclosure are difficult to see due to the fogginess caused by the emulsion.

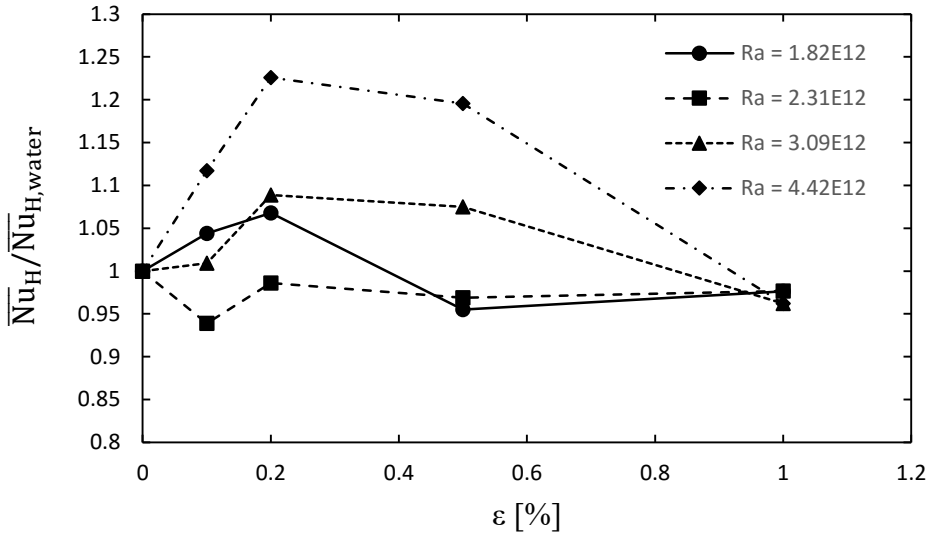

Figure 32. Average Nusselt number for FC-72 in water emulsions at varying volume fractions and Rayleigh numbers.

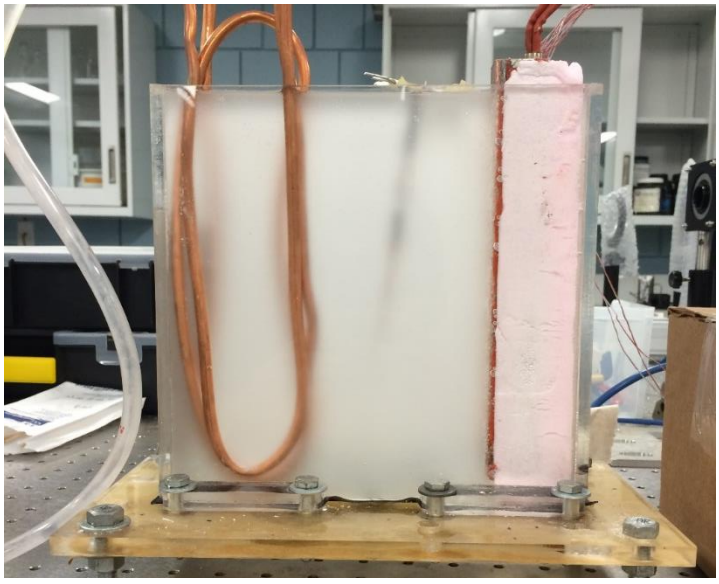

Figure 33. FC-72 in water emulsion. $\varepsilon = 0.5\%$. $Ra_H = 2.31\times10^{12}$.

No significant increase in the average Nusselt number based on volume percentage of FC-72 for the two lowest Rayleigh number cases. When $Ra_H = 4.42\times10^{12}$, there is a slight increase in the average Nusselt number up to $\varepsilon = 0.2\%$. When $\varepsilon > 0.2\%$, a decrease is seen in the average Nusselt number. At the same Ra_H and $\varepsilon = 0.5\%$, there is an increase in the average Nusselt number compared to that of water, about 20%.

However, this is less than when $\varepsilon = 0.2\%$. The uncertainty in the average Nusselt is ± 11.7%. At $Ra_H \geq 3.09\times10^{12}$, the increase seen in the average Nusselt number is beyond that of the uncertainty limits for $\varepsilon = 0.2\%$ and 0.5%.

During all experimental tests, vapor bubbles formed along the heated surface. There is no evidence to suggest that these bubbles are vaporized FC-72, as this would have led to an increase in the average Nusselt number. Also, the bubbles appear on the heated surface at the lowest Ra_H numbers when the temperature of the heated surface is below that of the saturation temperature of FC-72. A more likely cause is the re-absorption of atmospheric gases during emulsification and handling. The process of emulsification is long, and thus gives ample time after boiling for atmospheric gases to be re-absorbed. These atmospheric gases appear to be responsible for the bubbles observed on the heated surface.

Previous studies by Bulanov et al. (1984, 2006) and Roesle (2013) have shown that a large degree of superheat is required to achieve boiling of the dispersed component in dilute emulsions. Roesle did not see boiling of FC-72 until the wire temperature was ~90 °C, an overshoot of at least 30 °C. Due to mechanical and fluid limitations, the maximum surface temperature reached in the present investigation was ~75 °C, an overshoot of ~20 °C. Roesle (2013) study used a thin horizontal wire and looked at pool boiling heat transfer. A large degree of overshoot was expected because droplets are only near the heated wire for a short amount of time. In the present experiments, an 8 in. vertical flat plate was used. An FC-72 droplet in the boundary layer would be next to the heated surface during its entire ascent along the surface. It was expected that given the significant increase in the amount of time a droplet spends next to the heated surface, less superheat would be required to initiate boiling of the dispersed component. However, based on the fact that no significant increase was seen in the Nusselt number, it is believed that FC-72 droplets did not boil during the tests. It is likely then that a larger degree of superheat is needed in this configuration to initiate boiling of the FC-72, and therefore see a significant increase in the Nusselt number.

4.2 Visualization

4.2.1 Individual Droplets of FC-72

Optical holography was used to capture images of the individual droplets of FC-72 falling and rising in the boundary layer. The heater was allowed to reach steady-state temperatures before droplets of FC-72 were injected. After each droplet was injected, 10 to 20 s passed before another droplet was injected to allow the flow to re-stabilize. The optical equipment takes images that can later be analyzed to determine distances. For each power level and thus each Rayleigh number, a video was taken for the duration of the 10 min test. From these videos, individual frames were used to produce the images in this thesis. It was not possible to obtain images for emulsions where $\varepsilon \geq 0.05\%$. The amount of droplets created in these emulsions was too great, thus making the emulsion too opaque for visualization.

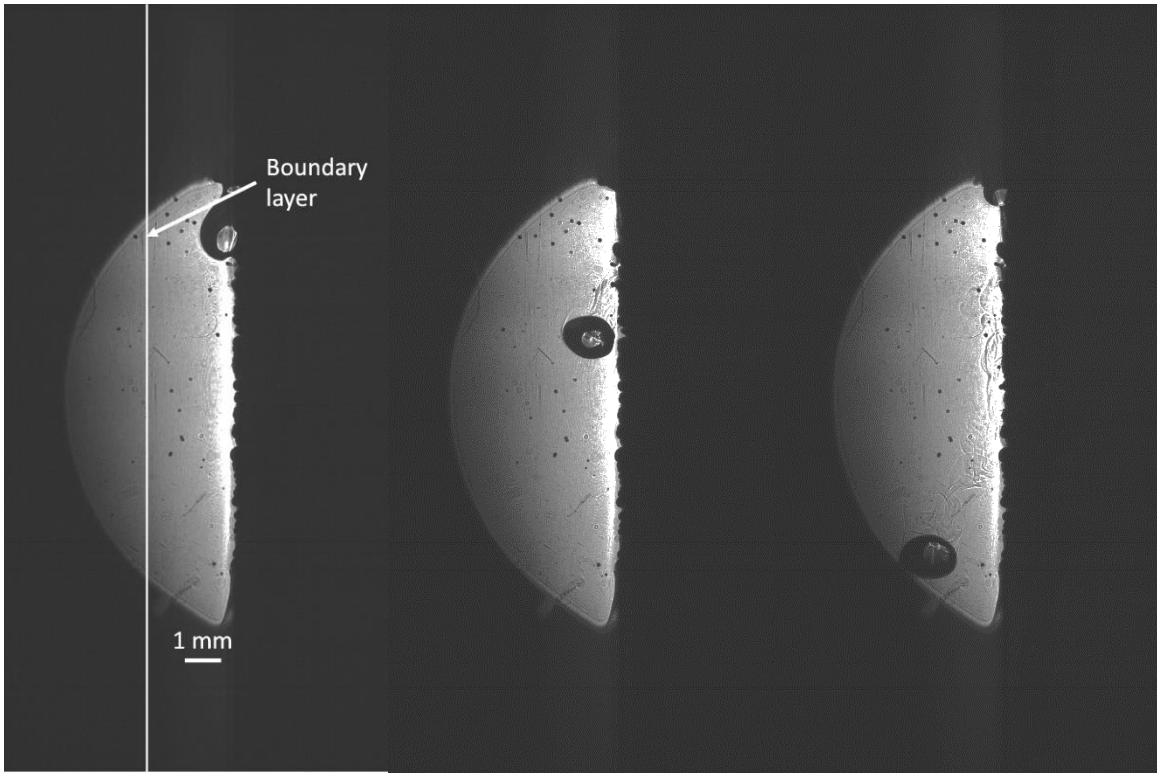

(a) (b) (c)

Figure 34. FC-72 droplet falling in the boundary layer; y = 6.25 in.; $Ra_y = 6.61\times10^{11}$; $Ra_H = 1.82\times10^{12}$; $q'' = 16.8$ kW/m^2; $\delta = 2.30$ mm; $u_{max} = 10.97$ cm/s; $d_d = 1.3$ mm.

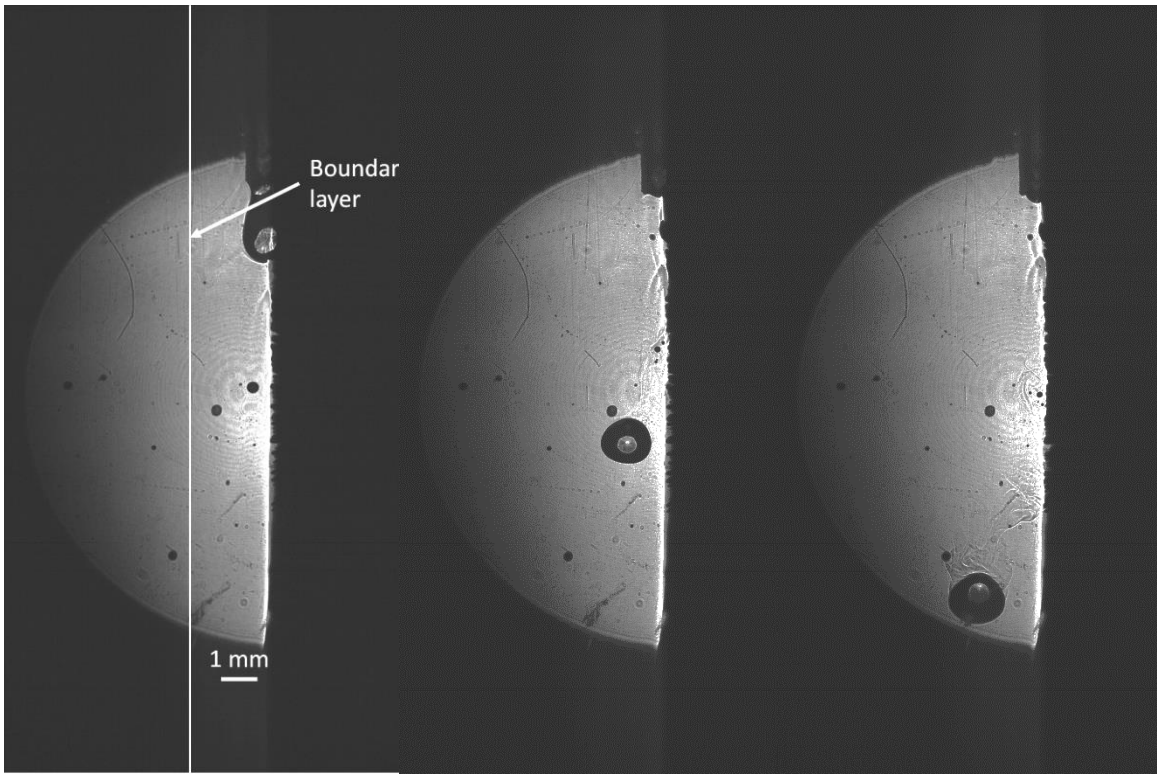

(a) (b) (c)

Figure 35. FC-72 droplet falling in the boundary layer; y = 6.25 in.; $Ra_y = 8.58\times10^{11}$; $Ra_H = 2.31\times10^{11}$; $q'' = 20.3$ kW/m^2; $\delta = 2.19$ mm; $u_{max} = 11.87$ cm/s; $d_d = 1.3$ mm.

Figure 34 shows a 1.3 mm diameter droplet of FC-72 falling in the boundary layer. The droplet was injected adjacent to the heated surface at a height of approximately 6.5 in. using a pipette. Figure 34 (a) shows the droplet as it is about to be released from the pipette in contact with the heated surface. Figure 34 (b) shows the droplet just after release from the pipette. The droplet is already moving away from the heated surface at this point in time. Figure 34 (c) shows the droplet even farther away from the heated surface as it is about to leave frame of view. At this point, the center of the droplet is 2 mm away from the surface. Vapor bubbles are present along the heated surface. These bubbles are atmospheric gases that were most likely re-absorbed during emulsification and handling.

Figure 35 shows a 1.3 mm diameter FC-72 droplet falling in the boundary layer. Figure 35 (a) shows the droplet just as it is separating from the pipette next to the heated surface. As the droplet falls through the boundary layer, it moves farther away from the

heated surface. Figure 35 (c) shows the droplet when the center of the droplet is 1.8 mm away from the heated surface. In Figure 35 (b) and (c), the fluid above the droplet is slightly disturbed after the droplet has passed through the frame of view. The fluid recovers rather quickly (approximately 10 s later) due to its laminar nature.

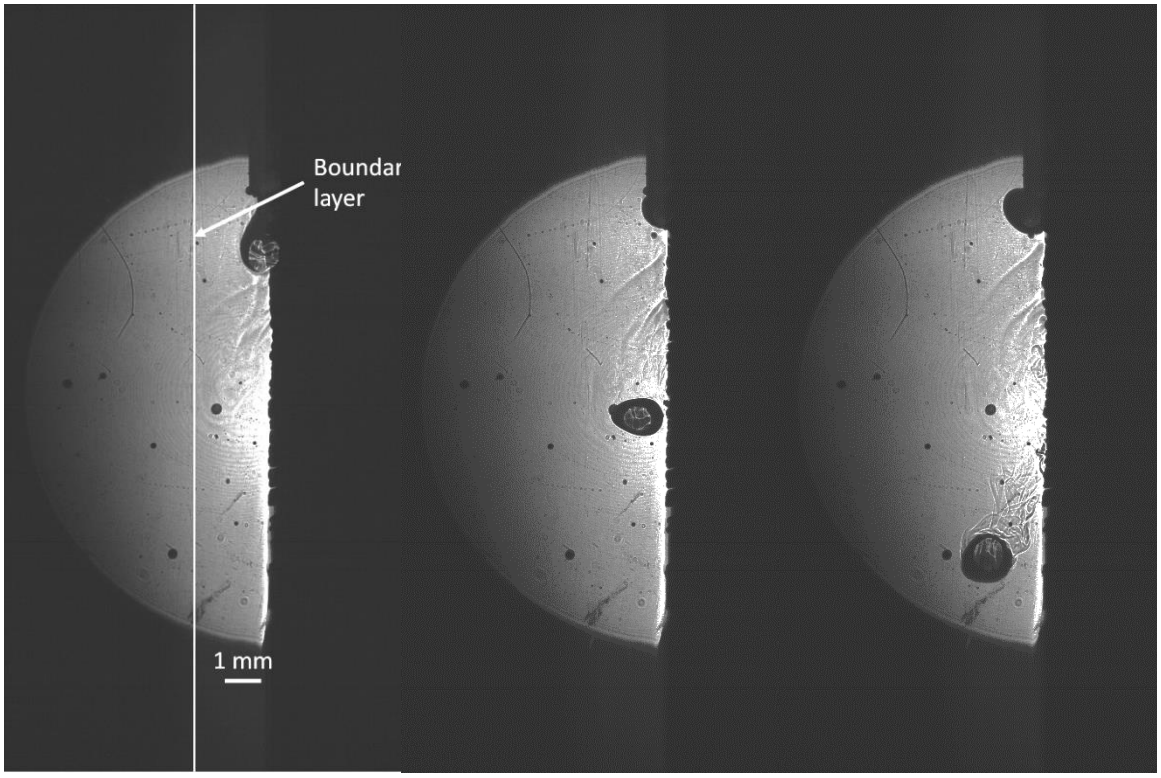

(a) (b) (c)

Figure 36. FC-72 droplet falling in the boundary layer; y = 6.25 in.; $Ra_y = 1.14\times10^{11}$; $Ra_H = 3.09\times10^{12}$; $q'' = 24.6$ kW/m^2; $\delta = 2.07$ mm; $u_{max} = 12.97$ cm/s; $d_d = 1.375$ mm.

Figure 36 shows a 1.375 mm diameter FC-72 droplet falling in the boundary layer. Figure 36 (a) shows the droplet just as it is separating from the pipette. The droplet is in contact with the heated surface and still exhibits a round shape. In Figure 36 (b), the droplet has begun to deform slightly. The height of the droplet is smaller and the width is 1.432 mm. At this Rayleigh number, the velocity of the fluid in the boundary layer is faster, causing more drag, and thus deforming the droplet. Figure 36 (c) shows the droplet 1.5 mm away from the heated surface just before it leaves the frame of view. The disturbance caused by the droplet as it falls through the boundary layer is visible and more chaotic than the disturbance seen at the lower Rayleigh numbers.

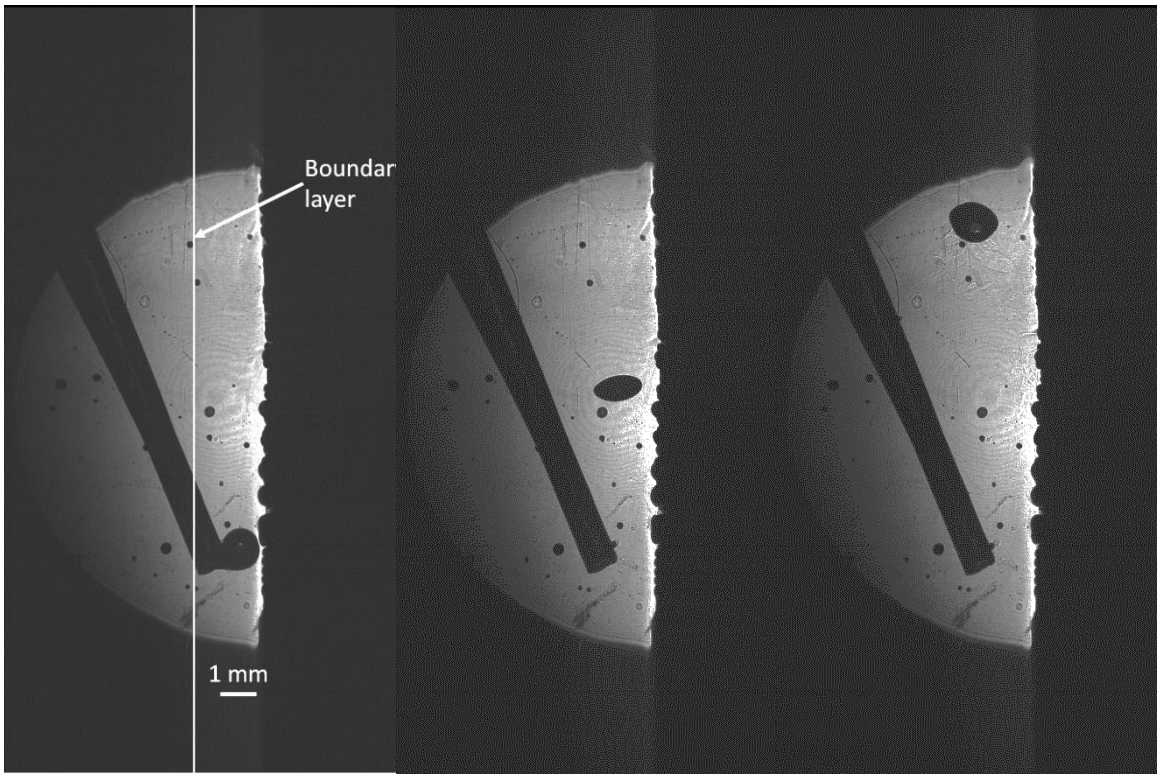

(a) (b) (c)

Figure 37. FC-72 droplet rising in the boundary layer; y = 6.25 in.; $Ra_y = 1.63\times10^{11}$; $Ra_H = 4.42\times10^{12}$; $q'' = 30.4$ kW/m^2; $\delta = 1.937$ mm; $u_{max} = 15.09$ cm/s; $d_d = 1.3$ mm.

Figure 37 shows a FC-72 droplet rising through the boundary layer. At the highest Rayleigh number tested, the fluid velocity is large enough to create enough drag to cause the droplet to rise. Figure 37 (a) shows the droplet as it is being released from the pipette. In Figure 37 (b), the droplet has deformed and has a height of 0.72 mm by a width of 1.3 mm. Figure 37 (c) shows the droplet 1.8 mm away from the heated surface just before leaving the frame of view. No disturbance to the flow caused by the droplet's wake is observed in these images. This is most likely due to the droplet rising rather than falling with viscous effects of the fluid quickly mitigating any disturbance.

The FC-72 droplets fell for $Ra_H \leq 3.09\times10^{12}$. At $Ra_H = 4.42\times10^{12}$, the droplets rose to the surface of the enclosure. As the Rayleigh number is increased, the fluid velocity in the boundary layer increases, thus creating more drag on the spherical droplet.

At all four Rayleigh numbers, the droplets fell or rose very quickly and moved farther away from the heated surface. A likely cause for this is the Magnus effect. The

velocity profile in the boundary layer causes the large droplets to spin as they fall or rise. This spinning motion creates a horizontal force that pushes the droplets away from the heated surface and outside the boundary layer.

The height of the heated surface in the images captured by the optical equipment is 14 mm. The total height of the heated surface is 203 mm. In less than 10% of the total height of the heated surface, the droplet at all Rayleigh numbers was nearly outside the estimated boundary layer. This suggests that the droplet does not spend nearly enough time in the boundary layer to initiate the boiling process.

Vapor bubbles were observed on the heated surface at all Rayleigh numbers. No FC-72 was emulsified in the water for these tests. It was only injected through the use of a pipette. These vapor bubbles are atmospheric gases that were re-absorbed into the water while the water was allowed to cool and during transfer.

4.2.2 FC-72 Droplet to Droplet Interaction

This section discusses images of multiple FC-72 droplets in the boundary layer and the interactions between these droplets. The emulsions themselves were too opaque, and thus holography could not capture images of individual droplets. A syringe pump was used to inject a continuous stream of small FC-72 droplets (0.5 mm – 1 mm) into the boundary layer at a rate of 495.8 mL/hr. The FC-72 was injected directly into the boundary layer through a 25 Ga needle. This allowed for the ability to capture images with small droplets without making the overall solution too opaque. Videos were taken at $Ra_H = 1.82 \times 10^{12}$, 2.31×10^{12}, 3.09×10^{12}, and 4.42×10^{12}. For each Rayleigh number, the heater was given ample time to reach steady-state. Once the heater reached steady-state temperatures, videos of approximately one minute in duration were recorded. The camera captures images with a resolution of 2 μm/px at a frame rate of ~330 s^{-1}.

Figure 38 shows multiple FC-72 droplets falling in the boundary layer next to the heated surface at $Ra_H = 1.82 \times 10^{12}$. In Figure 38 (a), the boundary layer is marked by the white line. The lighter areas in the middle of the droplets are caused by the laser. The droplet acts as a lens as the laser passes through it, which causes a difference in the diffraction pattern. In all three images, there are smaller, lighter circles. These circles

are caused by small particles that mix with the fluid during handling and transfer between containers. As opposed to the single droplet case, these droplets do not move away from the heated surface as they fall. All the droplets fell in a relatively vertical path. The Magnus effect is proportional to the square of the droplet diameter. The diameter of the droplets observed during these tests are less than half the diameter of the droplets seen during the individual droplet tests. Thus, the horizontal forces imparted on the droplets in the multi-droplet tests are less than a fourth of the forces that would be seen on the larger droplets.

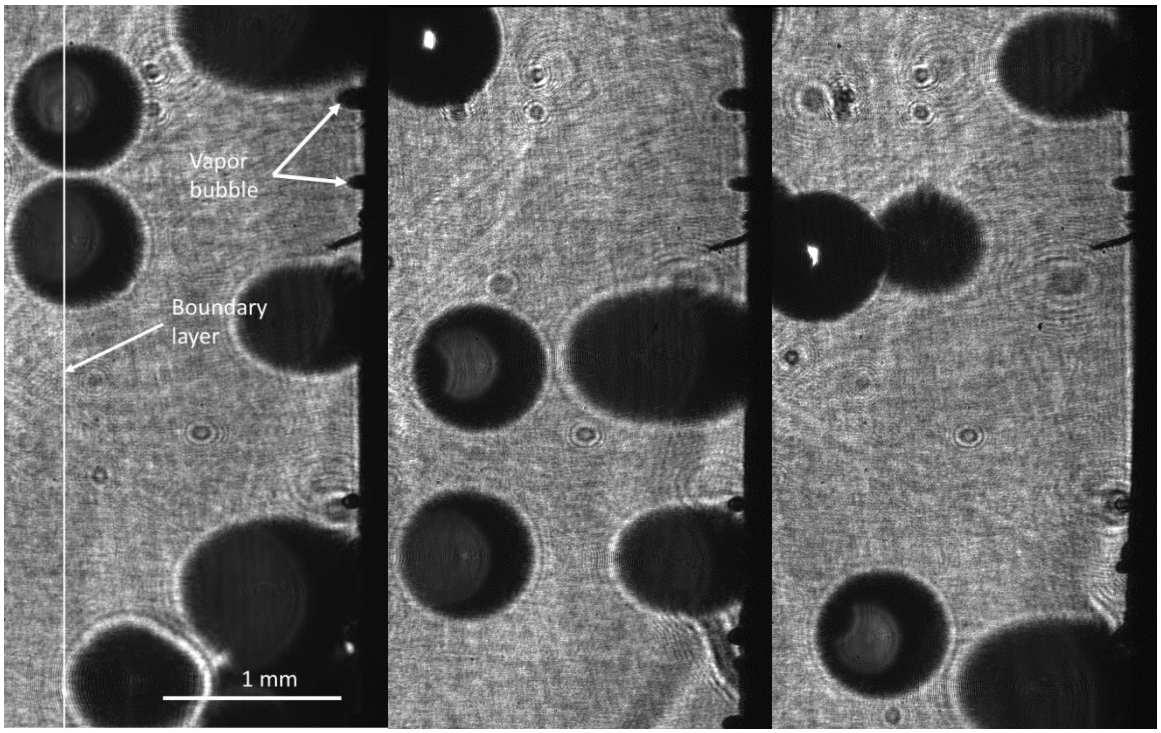

(a) (b) (c)

Figure 38. Multiple FC-72 droplets in boundary layer. y = 2.25 in.; $Ra_y = 1.11\times10^{10}$; $Ra_H = 1.82\times10^{12}$; $q'' = 16.8$ kW/m^2; $\delta = 2.30$ mm; $u_{max} = 10.97$ cm/s.

Figure 39 shows multiple droplets of FC-72 falling in the boundary layer at a height of 2.25 in. on the heated surface. The heated surface is along the right edge of the frame. As the temperature of the heated surface increases, the fluid in the immediate vicinity of the surface increases in temperature. This causes a change in the refraction index. This change in the refraction causes the heated surface to appear bent and also causes the loss of sharpness in the image.

It was observed during these tests that when the bubbles along the heated surface were wiped away from the surface, the surface temperature decreased by more than 10 °C within minutes. A likely source of these bubbles is the degree to which the distilled water is degassed. The distilled water is boiled before each test, and then allowed to cool to 25 °C. After the FC-72 is added, the solution is emulsified through the use of a gear pump for 15 min. Throughout the entire process of preparing the emulsion and transferring the fluids, it is possible that the water re-absorbed atmospheric gases. These

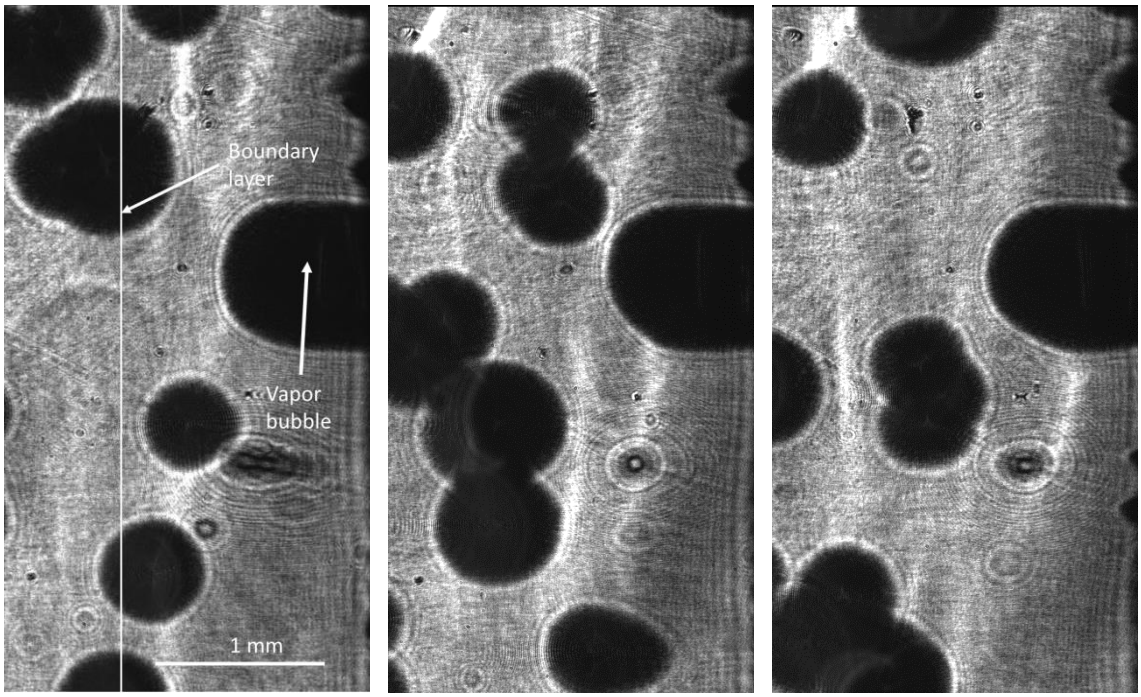

(a) (b) (c)

Figure 39. Multiple FC-72 droplets in boundary layer. y = 2.25 in.; $Ra_y = 2.73\times10^{10}$; $Ra_H = 4.42\times10^{12}$; $q'' = 30.4$ kW/m^2; $\delta = 1.937$ mm; $u_{max} = 15.09$ cm/s.

atmospheric gases are responsible for the large and small bubbles that form along the heated surface.

5. Conclusions

5.1 Current Study

Previous work by Bulanov et al. as well as Roesle have shown an enhancement in the heat transfer coefficient when boiling of the dispersed phase in a dilute emulsion occurs. These studies have provided both experimental and numerical data as well as visual observations to gain an insight into the process and mechanism by which the dispersed phase in a dilute emulsion boils. This study was performed to expand upon these results and look at boiling of dilute emulsions where strong buoyant forces are present.

Experiments were carried out with dilute emulsions of FC-72 in water and a heated vertical flat plate. FC-72 in water emulsions were analyzed previously in Roesle's (2010) experiments and showed an increase in the heat transfer coefficient when the FC-72 boiled. However, Roesle's experiments used a thin copper wire as a heat source, which produced much smaller Rayleigh numbers than in this study. Lunde (2011) carried out experiments with a thin horizontal strip of metal. The goal of this study was to look at the effect on the heat transfer coefficient at higher Rayleigh numbers, where the buoyancy forces are much stronger than the viscous forces.

The data suggests that mixing caused by the FC-72 droplets within the emulsion are responsible for the increase in the average Nusselt number. Holographic images were obtained for two different situations: 1) individual FC-72 droplets in the boundary layer near the heated surface, and 2) multiple FC-72 droplets in the boundary layer near the heated surface. These images show disturbances in the fluid caused by the wake of the FC-72 droplet as it either falls or rises in the boundary layer. These disturbances effectively mix the fluid and increase the heat transfer in a fashion similar to that of eddies in turbulent flow. Individual droplets with large diameters (d_d = 1.3 mm) tend to move away from the heated surface as they fall or rise due to the Magnus effect.

The Magnus effect was observed when individual droplets of FC-72 were injected directly into the boundary layer next to the heated surface. The horizontal distance between the droplet and the heated surface was measured from the images obtained during the experiment. These distances were used to calculate the horizontal acceleration

of the droplet, which was then used to determine the horizontal forces acting on the droplet and the angular velocity. The highest acceleration, force, and angular velocity were observed at the lowest Rayleigh number. Details on the analysis and numerical values are in Appendix D.

Individual droplets of FC-72 were injected into the boundary layer along the heated surface using a pipette. The droplets varied slightly in diameter, but were on average 1.3 mm. At the three lowest Rayleigh numbers, the droplets fell and moved away from the heated surface as they fell. At the highest Rayleigh number, the droplet rose in the boundary layer and again moved away from the heated surface as it rose. It is suspected that individual droplets do not have enough time in the boundary layer to absorb enough energy to vaporize in this configuration. It is necessary in future experiments to determine if higher temperatures can cause boiling of the dispersed component at these high Rayleigh numbers.

There is no evidence suggesting that the FC-72 droplets vaporize during any of the experimental tests. If FC-72 droplets vaporized during the heat transfer tests, vapor would have been observed along the upper edges of the enclosure or along the fluid surface. In addition, vaporization of the FC-72 droplets was not observed during any of the droplet injection tests.

The highest surface temperatures reached in the current experiments were ~20 °C above the saturation temperature of FC-72 and were kept lower than the saturation temperature of water. Boiling of the dispersed component was not observed in any of the experiments conducted, suggesting that a higher degree of superheat is required in this configuration to initiate the boiling process.

5.2 Future Work

The purpose of this study was to look at the effect of boiling of dilute emulsions in a configuration that exhibits strong buoyancy forces. In these experiments, no boiling of the dispersed phase component was observed due to mechanical and fluid limitations. In future studies, the apparatus could be modified so as to observe higher surface temperatures. It is possible that a higher degree of superheat is needed for the droplets to

boil in this configuration due to the small amount of time that the droplets were observed next to the heated surface.

Also of interest is the study of different geometries that exhibit strong buoyancy forces as well. Cylinders are the next logical step given their simplistic geometry. However, many other geometric configurations such as spheres would be worth studying. Other possible configurations such as channels could produce different results. It is likely that channels would lead to a larger amount of time in temperatures higher than the dispersed phase boiling point, thus accelerating the initiation of the boiling process.

Previous studies have looked at the addition of particles and surfactants in both pool and flow boiling. It is necessary to determine whether the same effects seen in those experiments are seen in experiments involving strong buoyancy forces.

Also of interest is what happens in the turbulent regime. Almost all studies on boiling of dilute emulsions to date have limited their experiments to the laminar regime. In single component flow, heat transfer is known to be greater when turbulence is present due to the large amount of mixing that occurs. It is necessary to see whether or not boiling of the disperse phase would occur when large amounts of mixing are present in the flow that tend to carry away energy much quicker than laminar flow.

Finally, a numerical study would serve to validate the experimental results obtained in this study. While some work has been done in the numerical sector with regards to boiling of dilute emulsions, much remains to be discovered regarding the process and mechanism by which the dispersed phase component boils.

6. References

Bejan, A., 2004, *Convection Heat Transfer*, Wiley, Hoboken, NJ.

Bulanov, N.V., Skripov, V.P., and Khmyl'nin, V.A., 1984, "Heat transfer to emulsion with superheating of its disperse phase." *Journal of Engineering Physics* 46: 1-3.

Bulanov, N.V., Skripov, V.P., and Khmylnik, V.A., 1993, "Heat transfer to emulsion with a low-boiling disperse phase." *Heat Transfer Research* 25: 786-789.

Bulanov, N.V., Skripov, V.P., Gasanov, B.M., and Baidakov, V.G., 1996, "Boiling of emulsions with a low-boiling dispersed phase. *Heat Transfer Research* 27: 312-315.

Bulanov, N.V., 2001, "An analysis of the heat flux density under conditions of boiling internal phase of emulsion." *High Temp.* 39: 462-469.

Bulanov, N.V., and Gasanov, B.M., 2005, "Experimental setup for studying the chain activation of low-temperature boiling sites in superheated liquid droplets." *Colloid Journal* 67: 531-536.

Bulanov, N.V., and Gasanov, B.M., 2006, "Characteristic features of the boiling of emulsions having a low-boiling dispersed phase." *Journal of Engineering Physics and Thermophysics* 79: 1130-1133.

Bulanov, N. V., Gasanov, B. M., and Turchaninova, E. A., 2006, "Results of Experimental Investigation of Heat Transfer with Emulsions with Low-boiling Disperse Phase." *High Temperature* 44(2): 267-82.

Bulanov, N.V., and Gasanov, B.M., 2007, "Special features of boiling of emulsions with a low-boiling dispersed phase." *Heat Transfer Research* 38: 259-273.

Bulanov, N.V., and Gasanov, B.M., 2008, "Peculiarities of boiling of emulsions with a low-boiling disperse phase." *International Journal of Heat and Mass Transfer* 51: 1628-1632.

Catton, I., 1978, "Natural Convection in Enclosures." *Proceedings of the Sixth International Heat Transfer Conference* 6: 13-31.

Churchill, S. W., and Chu, H.H.S., 1975, "Correlating Equations for Laminar and Turbulent Free Convection from a Vertical Plate." *International Journal of Heat and Mass Transfer* 18(11): 1323-329.

Chu, H.H.S., Churchill, S.W. and Patterson, C.V.S., 1976, "The Effect of Heater Size, Location, Aspect Ratio, and Boundary Conditions on Two-Dimensional, Laminar, Natural Convection in Rectangular Channels." *Journal of Heat Transfer* 98(2): 194-201.

De Vahl Davis, G., 1968, “Laminar Natural Convection in an Enclosed Rectangular Cavity.” *International Journal of Heat and Mass Transfer* 11(11): 1675-1693.

Gebhart, B., 1971, *Heat Transfer*, New York, McGraw-Hill.

Ghiaasiaan, S.M.. 2011, *Convective Heat and Mass Transfer*, Cambridge, Cambridge University Press.

Gill, A. E., 1966, "The Boundary-layer Regime for Convection in a Rectangular Cavity." *Journal of Fluid Mechanics* 26(03): 515.

Goldstein, R.J., and Eckert E.R.G., 1960, "The Steady and Transient Free Convection Boundary Layer on a Uniformly Heated Vertical Plate." *International Journal of Heat and Mass Transfer* 1(2-3): 208-18.

Hahn, D.W., and Özişik M.N., 2012, *Heat Conduction*, 3rd ed. Wiley, Hoboken, NJ.

Holman, J. P., 1976, *Heat Transfer*, McGraw-Hill, New York.

Hu, S., and Kinter, R. C., 1955, "The Fall of Single Liquid Drops through Water." *AIChE Journal AIChE J.* 1(1): 42-48.

Ishii, M., and Zuber, N., 1979, "Drag Coefficient and Relative Velocity in Bubbly, Droplet or Particulate Flows." *AIChE Journal* 25(5): 843-55.

Jaluria, Y., 1980, *Natural Convection: Heat and Mass Transfer*, Pergamon, Oxford.

Krishna, P. M., Venkateswarlu, D., and Narasimhamurty, G. S. R., 1959, "Fall of Liquid Drops in Water. Terminal Velocities." *Journal of Chemical & Engineering Data* 4(4): 336-40.

Mori, Y. H., Inui, E., and Komotori, K., 1978, "Pool Boiling Heat Transfer to Emulsions." *J. Heat Transfer* 100(4): 613.

Oosthuizen, P. H., and Kalendar, A.Y., 2013, *Natural Convective Heat Transfer from Narrow Plates*. Springer, New York.

Ostrach, S., 1988, “Natural Convection in Enclosures.” *Journal of Heat Transfer* 110: 1175-1190.

Roesle, M. L. and Kulacki, F. A., 2013, *Boiling Heat Transfer in Dilute Emulsions*. Springer, New York.

Roesle, M. L., and Kulacki, F.A., 2010, "Boiling of Dilute Emulsions—Toward a New Modeling Framework." *Industrial & Engineering Chemistry Research* 49(11): 5188-196.

Sparrow, E.M. and Gregg, J.L., 1956, "Laminar free convection from a vertical flat plate with uniform heat flux." *Transaction ASME* 78: 435-440.

Turan, O., Poole, R. J., and Chakraborty, N., 2013, "Influences of Boundary Conditions on Laminar Natural Convection of Bingham Fluids in Rectangular Enclosures With Differentially Heated Side Walls." *Heat Transfer Engineering* 35(9): 822-49.

Vliet, G. C., and Liu, C. K., 1969, "An Experimental Study of Turbulent Natural Convection Boundary Layers." *Journal of Heat Transfer* 91(4): 517.

Vliet, G. C., and Ross, D. C., 1975, "Turbulent Natural Convection on Upward and Downward Facing Inclined Constant Heat Flux Surfaces." *Journal of Heat Transfer* 97(4): 549.

Appendix A. Experimental Design

This appendix shows a detailed analysis of the 1-dimensional transient heat conduction problem for the copper plate.

The heater for this study is designed to produce a constant heat flux to the enclosed fluid. The design consists of an electric heater attached to a 1/4 in. thick copper plate. The first portion of the analysis uses a one-dimensional, transient formulation of the heat conduction equation to get a rough estimate of the heat flux required to produce the temperatures required to initiate boiling of the dispersed component in the emulsion and to determine the amount of time required to reach steady state. The governing equation and the boundary conditions are listed below. It is assumed that all thermophysical properties are constant in the analysis.

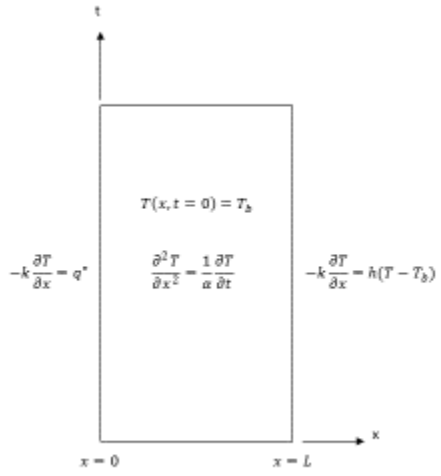

When the temperature is shifted as $\theta = T(x,t) - T_b$, the governing equations and boundary conditions are,

$$\frac{\partial^2 \theta}{\partial x^2} = \frac{1}{\alpha}\frac{\partial \theta}{\partial t}$$
$$@\ x = 0; \quad -k\frac{\partial \theta}{\partial x} = q'' \tag{30}$$

$$@\ x = L; \quad -k\frac{\partial\theta}{\partial x} = h(\theta)$$

$$\theta(x, t = 0) = 0$$

The solution to this problem is obtained through the superposition method shown below.

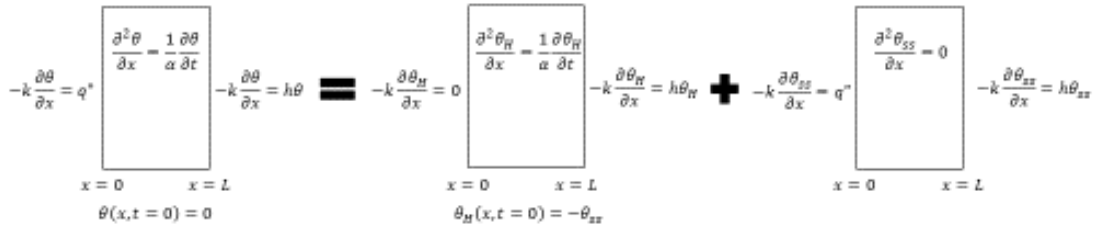

Figure 40. Superposition method for solution to one-dimensional heat conduction problem.

$$\theta(x, t) = \theta_H(x, t) + \theta_{ss}(x) \tag{31}$$

The homogenous problem, $\theta_H(x, t)$, takes the homogenous boundary conditions and the non-homogenous initial condition. The steady-state problem, $\theta_{ss}(x)$, takes the non-homogenous boundary condition.

$$\frac{\partial^2\theta_{ss}}{\partial x^2} = 0$$

$$@\ x = 0; \quad -k\frac{\partial\theta_{ss}}{\partial x} = q'' \tag{32}$$

$$@\ x = L; \quad -k\frac{\partial\theta_{ss}}{\partial x} = h\ (\theta_{ss})$$

The general solution to the governing equation is $\theta_{ss}(x) = C_1 x + C_2$. The boundary condition at x = 0 yields

$$-k\frac{\partial\theta}{\partial x} = -k\ C_1 = q''$$

$$C_1 = -\frac{q''}{k} \tag{33}$$

The boundary condition at x = L gives

$$-k\,C_1 = h\,(C_1 L + C_2)$$
$$hC_2 = -k\left(-\frac{q''}{k}\right) - hL\left(\frac{-q''}{k}\right) \tag{34}$$
$$C_2 = \frac{q''}{kh}(k + hL)$$

Hence, the solution to the steady-state problem is

$$\theta_{ss}(x) = q''\left(\frac{1}{h} + \frac{L - x}{k}\right) \tag{35}$$

The formulation for the homogenous problem is shown below.

$$\frac{\partial^2 \theta_H}{\partial x^2} = \frac{1}{\alpha}\frac{\partial \theta_H}{\partial t}$$
$$@\ x = 0; \quad -k\frac{\partial \theta_H}{\partial x} = 0 \tag{36}$$
$$@\ x = L; \quad -k\frac{\partial \theta_H}{\partial x} = h\,(\theta_H)$$
$$\theta_H(x, t = 0) = -\theta_{ss}(x)$$

Since both boundary conditions are homogenous and the initial condition is non-homogenous, the separation of variables technique can be applied.

$$\text{let } \theta_H(x, t) = X(x)\Gamma(t) \tag{37}$$

$$\frac{1}{X}\frac{\partial^2 X}{\partial x} = \frac{1}{\alpha\,\Gamma}\frac{\partial \Gamma}{\partial t} = -\lambda^2 \tag{38}$$

The introduction of the separation constant, λ^2, yields two equations which can be solved using the boundary conditions in equation .

$$\Gamma(t) = C_3 e^{-\alpha\lambda^2 t}$$
$$X(x) = C_4 \cos(\lambda x) + C_5 \sin(\lambda x) \tag{39}$$

First, the homogenous boundary conditions in the x-direction will be used to determine the general solution for X(x) and to determine the eigenfunction.

$$-k\frac{\partial X}{\partial x} = -k[-C_4\lambda \sin(\lambda x) + C_5\lambda \cos(\lambda x)] \tag{40}$$

When evaluated at x = 0,

$$-kC_5\lambda \cos(\lambda * 0) = 0 \tag{41}$$

Therefore, $C_5 = 0$ and the general solution for the x-direction is

$$X(x) = C_4 \cos(\lambda x) \tag{42}$$

The boundary condition at x = L yields

$$\lambda_n \tan(\lambda_n L) = \frac{h}{k} \tag{43}$$

Eqn. (43) can be solved numerically to determine the eigenvalues, λ_n.

Now that the eigenvalues are known and the general solutions for both variables are known, the general solution to the homogenous problem is

$$\theta_H(x,t) = \sum_{n=1}^{\infty} C_n \cos(\lambda_n x)\, e^{\alpha \lambda_n^2 t} \tag{44}$$

The initial condition is now used to determine the constant, C_n.

$$-\theta_{ss}(x) = \sum_{n=1}^{\infty} C_n \cos(\lambda_n x) \tag{45}$$

Multiplying both sides by $\int_{x=0}^{L} \cos(\lambda_n x)\, dx$ and solving for C_n yields

$$C_n = \frac{\int_{x=0}^{L} -\theta_{ss}(x) \cos(\lambda_n x)\, dx}{\int_{x=0}^{L} \cos^2(\lambda_n x) dx} \tag{46}$$

The denominator in Eqn. (46) is the norm of the eigenfunction and is tabulated in heat conduction texts.

$$1/N(\lambda_n) = 2\frac{\lambda_n^2 + K^2}{L(\lambda_n^2 + K^2) + K} \tag{47}$$

Where K = h / k

Using Eqn. (47) and solving the integral in the numerator of Eqn. (41) yields

$$C_n = \frac{-\frac{q''L}{k\lambda_n}\sin(\lambda_n L) - \frac{q''}{h\lambda_n}\sin(\lambda_n L) + \frac{q''}{k}\left(\frac{1}{\lambda_n^2}\cos(\lambda_n L) + \frac{L}{\lambda_n}\sin(\lambda_n L)\right) - \frac{q''}{k\lambda_n^2}}{N(\lambda_n)} \tag{48}$$

The complete solution is

$$T(x,t) = \sum_{n=1}^{\infty} C_n \cos(\lambda_n x)\, e^{-\alpha \lambda_n^2 t} + q''\left(\frac{1}{h} + \frac{L-x}{k}\right) + T_b \tag{49}$$

$$C_n = \frac{-\frac{q''L}{k\lambda_n}\sin(\lambda_n L) - \frac{q''}{h\lambda_n}\sin(\lambda_n L) + \frac{q''}{k}\left(\frac{1}{\lambda_n^2}\cos(\lambda_n L) + \frac{L}{\lambda_n}\sin(\lambda_n L)\right) - \frac{q''}{k\lambda_n^2}}{N(\lambda_n)} \tag{50}$$

$$\frac{1}{N(\lambda_n)} = 2\frac{\lambda_n^2 + K^2}{L(\lambda_n^2 + K^2) + K} \tag{51}$$

$$\lambda_n \tan(\lambda_n L) = K\,; \quad K = \frac{h}{k} \tag{52}$$

The steady-state temperature distribution, Eqn. (35), can be used in conjunction with the correlation proposed by Bejan (2004) to determine the heat flux and heat transfer coefficient for a given wall temperature. The correlation proposed by Bejan (2004) for rectangular enclosures with constant wall heat flux is shown below.

$$\overline{Nu}_H = \frac{\bar{h}\,H}{k_f} = 0.34\,Ra_H^{2/9}\left(\frac{H}{S}\right)^{1/9} \tag{53}$$

When Eqns. (53) and (35) are both solved for h and equated to each other, the result is

$$0.34\frac{k_f}{H}\,Ra_H^{2/9}\left(\frac{H}{S}\right)^{1/9} = \frac{q''}{T_{wall} - T_b} \tag{54}$$

Eqn. (54) takes any desired wall temperature and will yield the heat flux required to obtain that temperature at steady-state. All thermophysical properties of the fluid are assumed constant and evaluated at the film temperature,

$$T_{film} = \frac{T_{wall} + T_b}{2}\ . \tag{55}$$

Appendix B. Apparatus Drawings

This appendix contains detailed drawings of the components used to make the test enclosure components and the heater configuration. The test enclosure is made out of clear acrylic. Two endplates, two side plates, the base, and four flanges are assembled as shown in Figure 9. The heater configuration is assembled using a sealant, and then an epoxy to ensure no leakage of water between the heater and the insulation surrounding it.

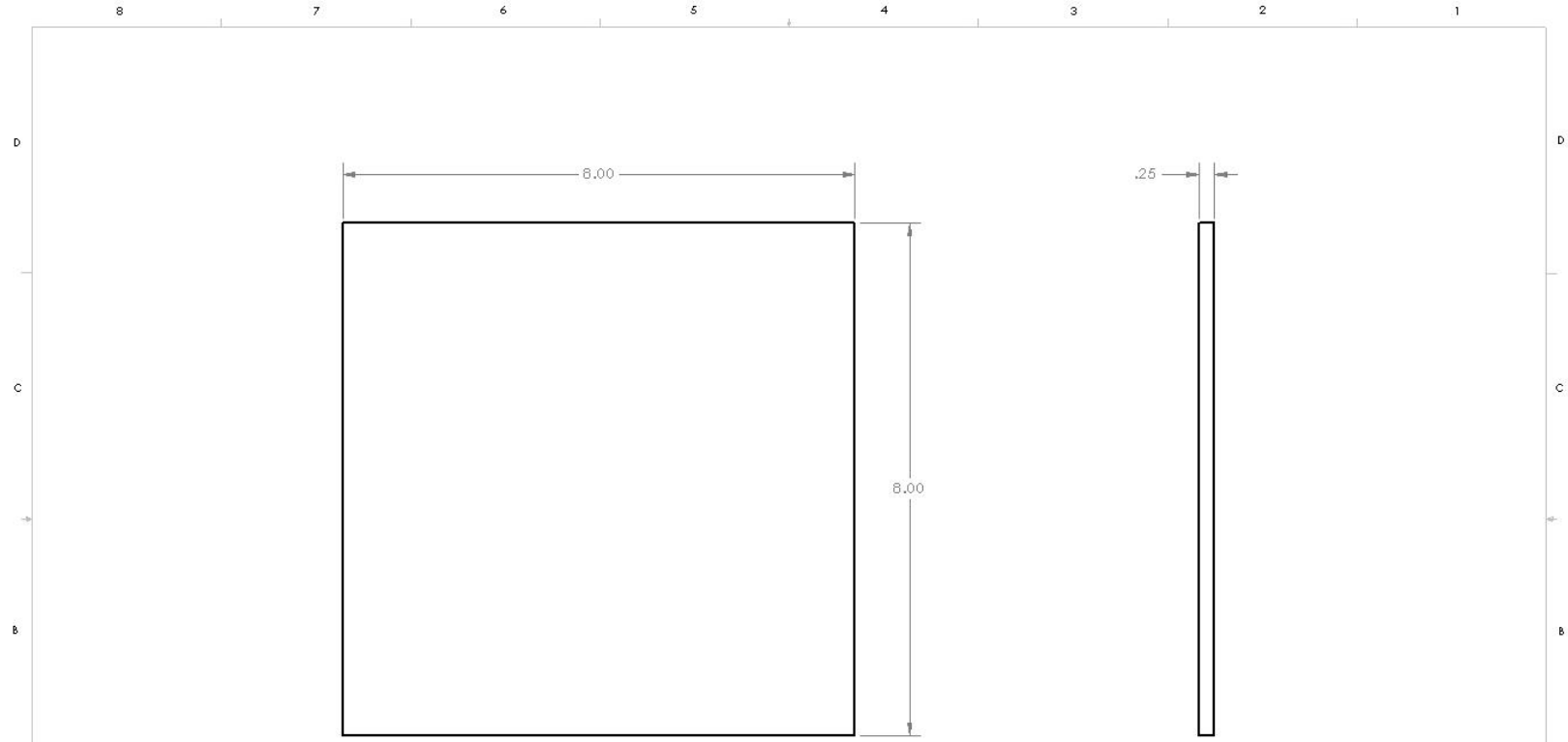

		UNLESS OTHERWISE SPECIFIED:		NAME	DATE
		DIMENSIONS ARE IN INCHES TOLERANCES: FRACTIONAL ± ANGULAR: MACH ± BEND ± TWO PLACE DECIMAL ± THREE PLACE DECIMAL ±	DRAWN		
			CHECKED		
			ENG APPR.		
			MFG APPR.		
		INTERPRET GEOMETRIC TOLERANCING PER:	Q.A.		
		MATERIAL	COMMENTS:		
NEXT ASSY	USED ON	FINISH			
APPLICATION		DO NOT SCALE DRAWING			

TITLE:

SIZE B | DWG. NO. side plate | REV

SCALE: 1:2 | WEIGHT: | SHEET 1 OF 1

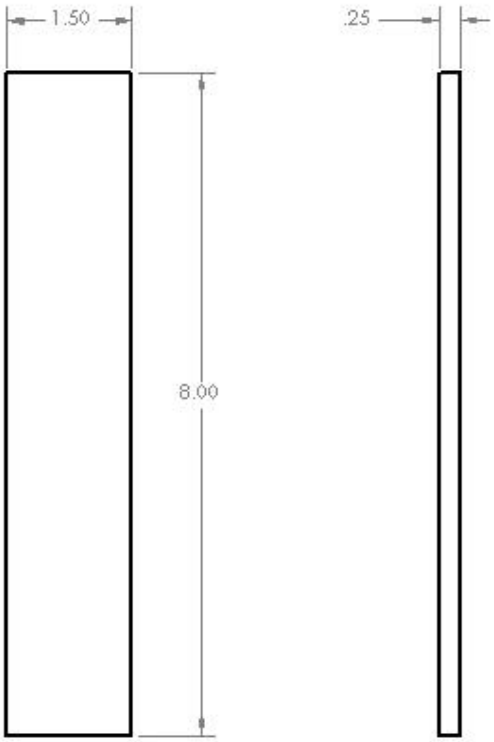

		DIMENSIONS ARE IN INCHES		MACH	BEND
		TOLERANCES:	DRAWN		
		FRACTIONAL ±	CHECKED		
		ANGULAR: MACH ± BEND ±	MFG APPR.		
		TWO PLACE DECIMAL ±			
		THREE PLACE DECIMAL ±	Q.A.		
		NAME	COMMENTS		
		DATE			
NEXT ASSY	USED ON				
APPLICATION		DO NOT SCALE DRAWING			

PROPRIETARY AND CONFIDENTIAL
THE INFORMATION CONTAINED IN THIS DRAWING IS THE SOLE PROPERTY OF <INSERT CO. NAME HERE>. ANY REPRODUCTION IN PART OR AS A WHOLE WITHOUT THE WRITTEN PERMISSION OF <INSERT CO. NAME HERE> IS PROHIBITED.

SIZE A	DWG. NO. end plate	REV.
SCALE:	WEIGHT:	SHEET 1 OF 1

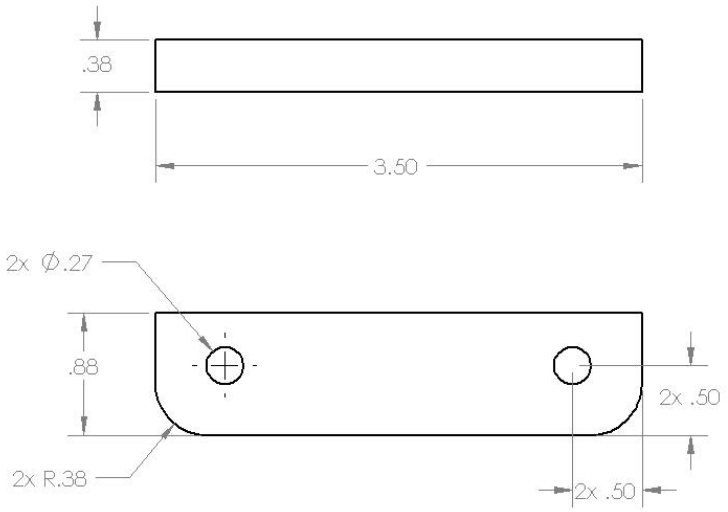

		DIMENSIONS ARE IN INCHES TOLERANCES: FRACTIONAL ± ANGULAR: MACH ± BEND ± TWO PLACE DECIMAL ± THREE PLACE DECIMAL ±		NAME	DATE
			DRAWN		
			CHECKED		
			ENG APPR.		
			MFG APPR.		
		MATERIAL	Q.A.		

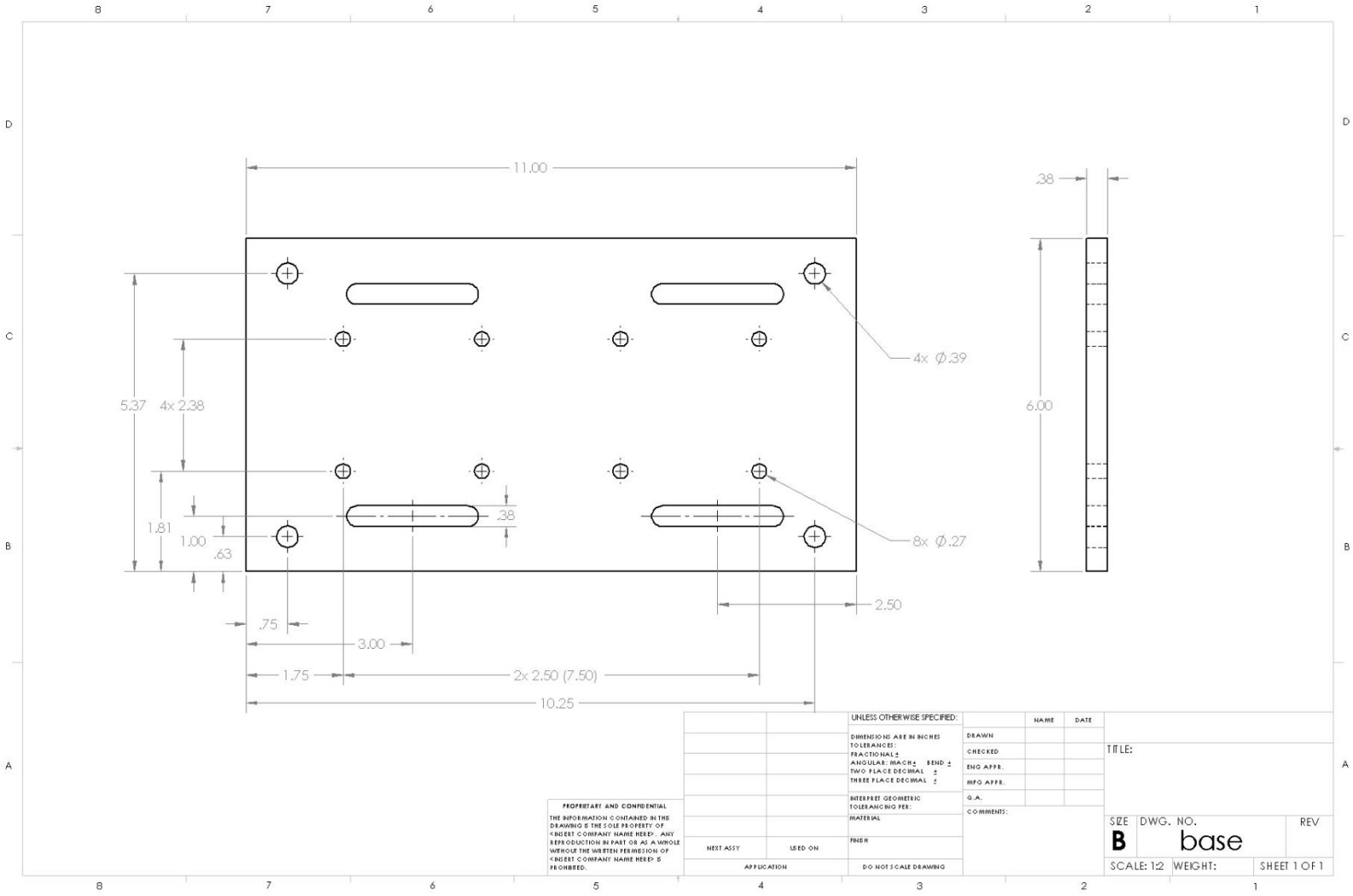

		UNLESS OTHERWISE SPECIFIED:		NAME	DATE
		DIMENSIONS ARE IN INCHES TOLERANCES: FRACTIONAL ± ANGULAR: MACH ± BEND ± TWO PLACE DECIMAL ± THREE PLACE DECIMAL ±	DRAWN		
			CHECKED		
			ENG APPR.		
			MFG APPR.		
		INTERPRET GEOMETRIC TOLERANCING PER:	Q.A.		
		MATERIAL	COMMENTS:		
NEXT ASSY	USED ON	FINISH			
APPLICATION		DO NOT SCALE DRAWING			

TITLE:

SIZE	DWG. NO.	REV
B	base	
SCALE: 1:2	WEIGHT:	SHEET 1 OF 1

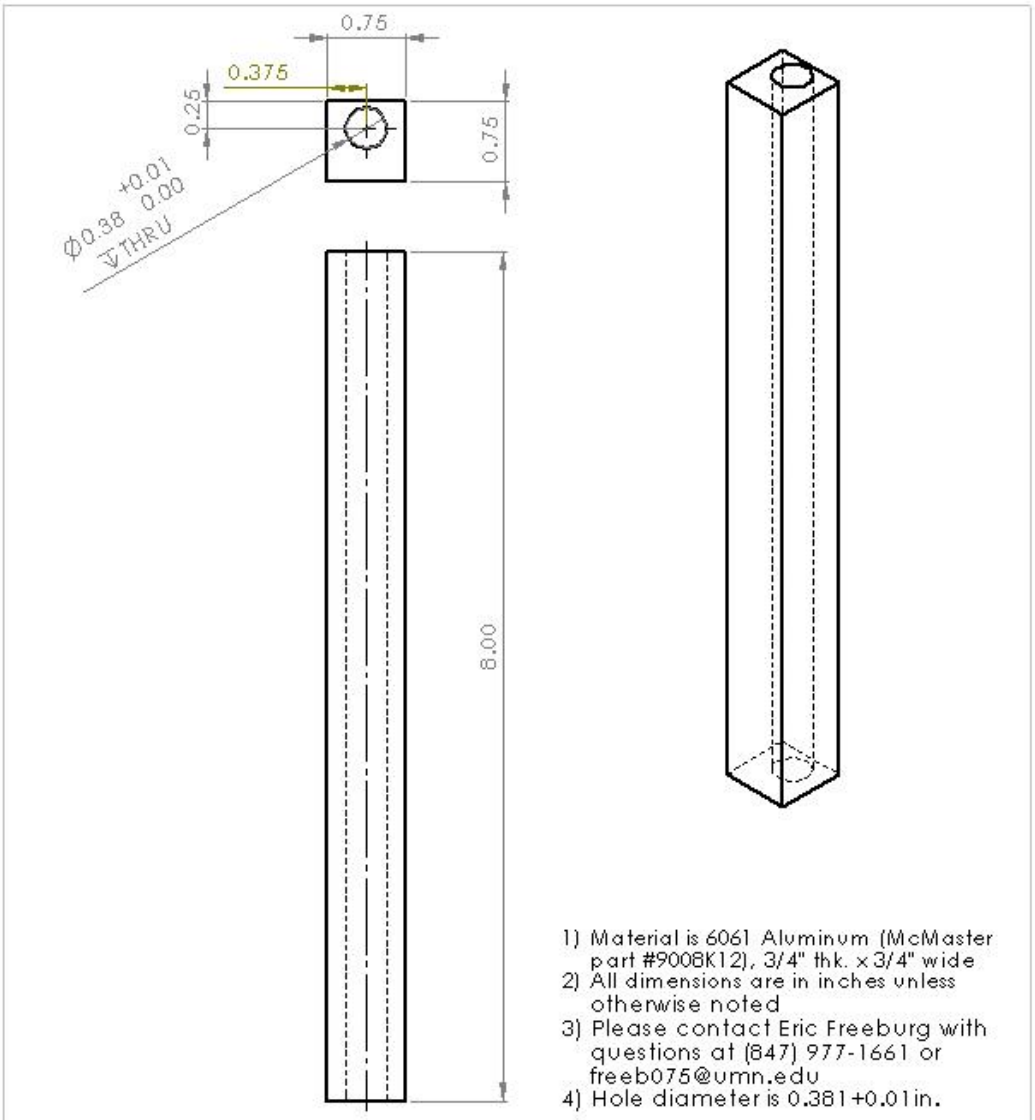

1) Material is 6061 Aluminum (McMaster part #9008K12), 3/4" thk. x 3/4" wide
2) All dimensions are in inches unless otherwise noted
3) Please contact Eric Freeburg with questions at (847) 977-1661 or freeb075@umn.edu
4) Hole diameter is 0.381+0.01in.

		DIMENSIONS ARE IN INCHES TOLERANCES: FRACTIONAL ANGULAR: MACH ± BEND ± TWO PLACE DECIMAL ± THREE PLACE DECIMAL ±		NAME	DATE
			DRAWN		
			CHECKED		
			ENG APPR		
			MFG APPR		
			Q.A		
			COMMENTS:		
PROPRIETARY AND CONFIDENTIAL THE INFORMATION CONTAINED IN THE DRAWING IS THE SOLE PROPERTY OF <ENTER COMPANY NAME HERE>. ANY REPRODUCTION IN PART OR AS A WHOLE WITHOUT THE WRITTEN PERMISSION OF <ENTER COMPANY NAME HERE> IS PROHIBITED.		MATERIAL			
	NEXT ASSY	USED ON	FINISH		
	APPLICATION		DO NOT SCALE DRAWING		

SIZE A | DWG. NO. aluminum | REV

SCALE: WEIGHT: SHEET 1 OF 1

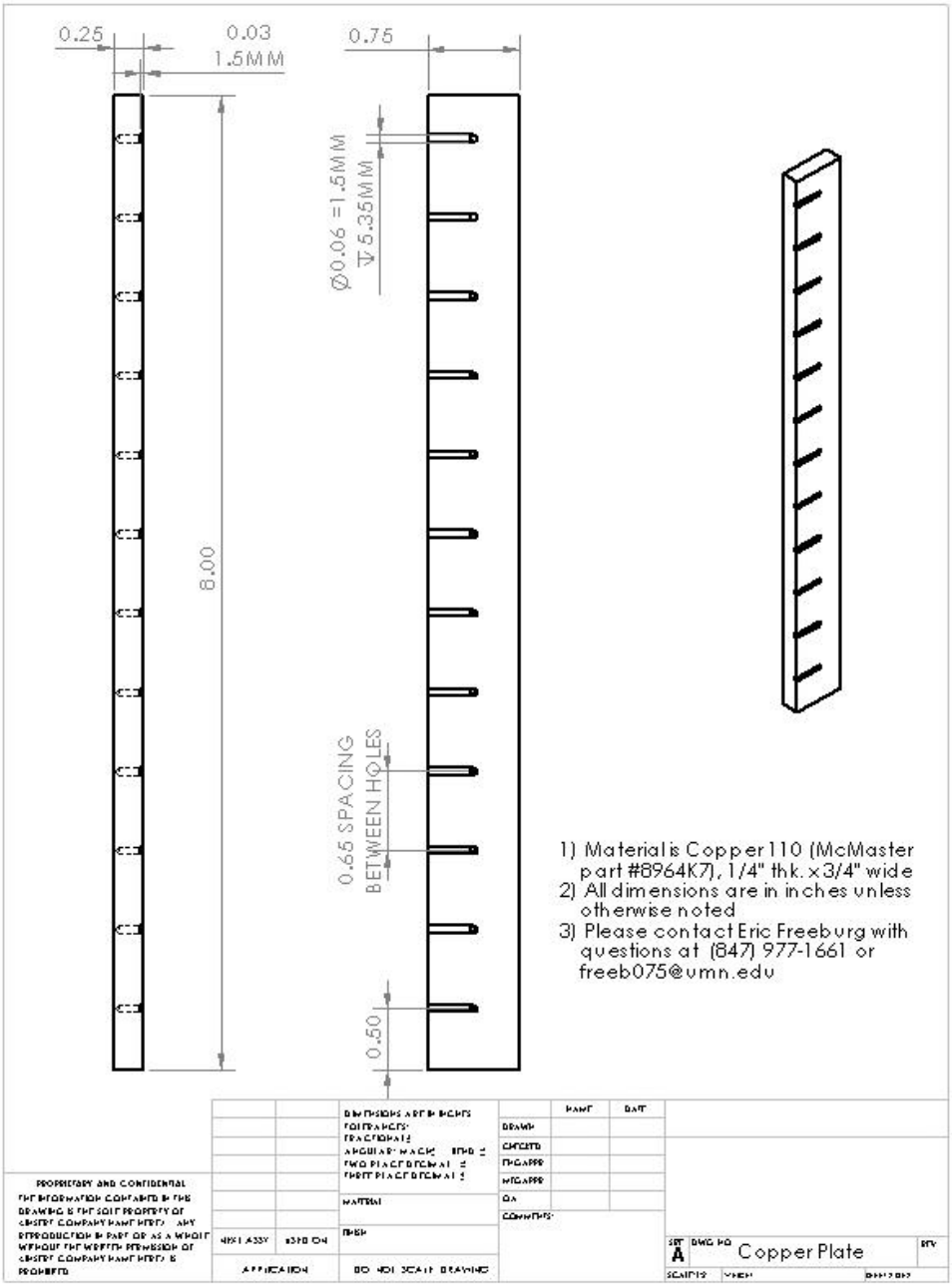
0.25
0.03
1.5MM
0.75
Ø0.06 =1.5MM
↧5.35MM
8.00
0.65 SPACING
BETWEEN HOLES
0.50
1) Material is Copper110 (McMaster part #8964K7), 1/4" thk. x 3/4" wide
2) All dimensions are in inches unless otherwise noted
3) Please contact Eric Freeburg with questions at (847) 977-1661 or freeb075@umn.edu
PROPRIETARY AND CONFIDENTIAL
DRAWN
CHECKED
ENG APPR
MFG APPR
QA
COMMENTS:
MATERIAL
FINISH
APPLICATION
DO NOT SCALE DRAWING
SIZE
A
DWG NO
Copper Plate
REV

Appendix C. Holographic Images

This section contains holographic images obtained during the experimental tests where individual FC-72 droplets were injected into the boundary layer using a pipette and where multiple FC-72 droplets were injected into the boundary layer using a syringe pump. For the individual droplet tests, the camera resolution was 30 μm/px and the frame rate was 60 s^{-1}. For the multiple droplet tests, the resolution of the camera was 2μm/px and the frame rate was 338.2 s^{-1}.

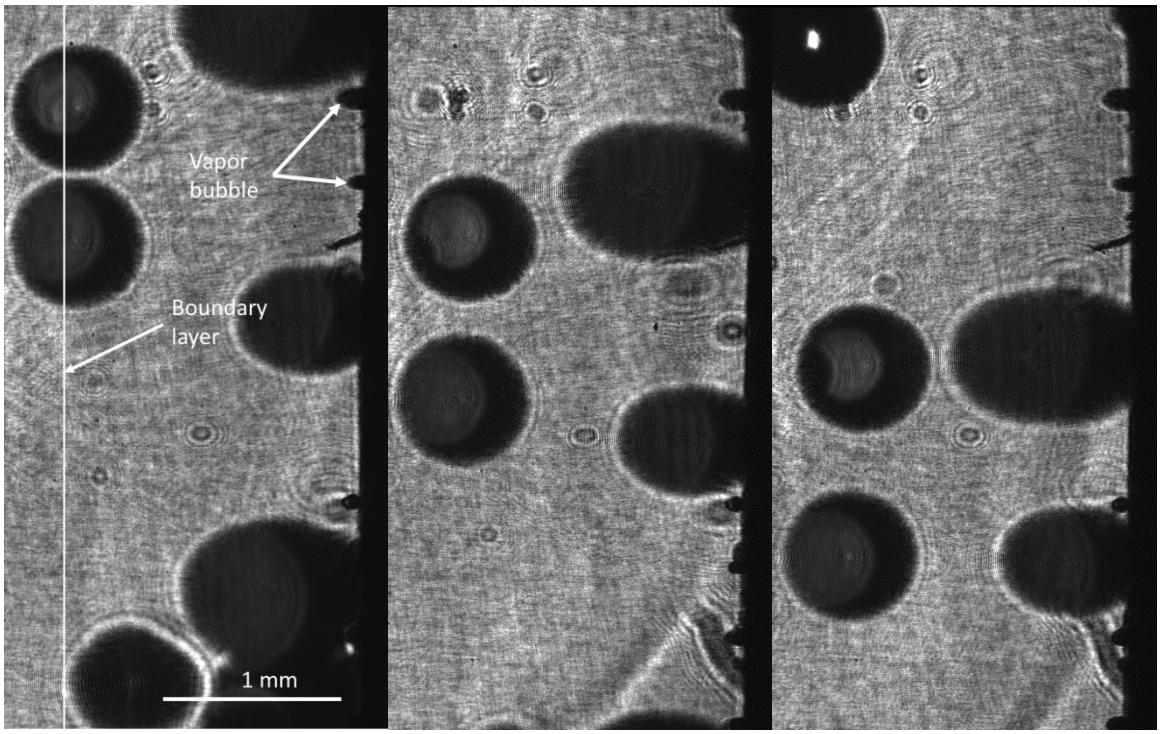

(a) (b) (c)

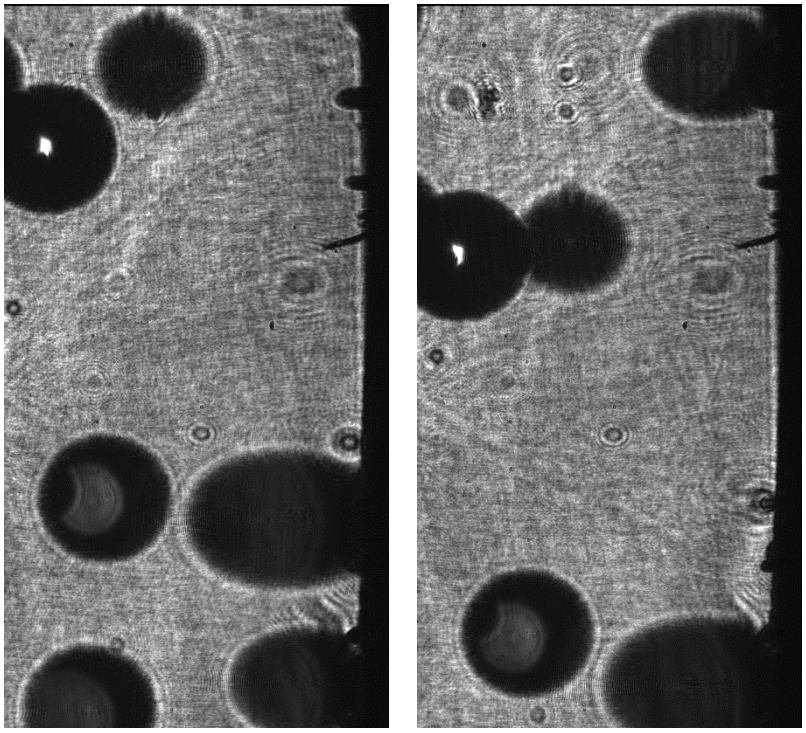

(d) (e)

Figure 41. Multiple FC-72 droplets in boundary layer. y = 2.25 in.; $Ra_y = 1.11\times10^{10}$; $Ra_H = 1.82\times10^{12}$; $q'' = 16.8$ kW/m^2; $\delta = 1.878$ mm; $u_{max} = 10.97$ cm/s; $\Delta t = 0.044$ s.

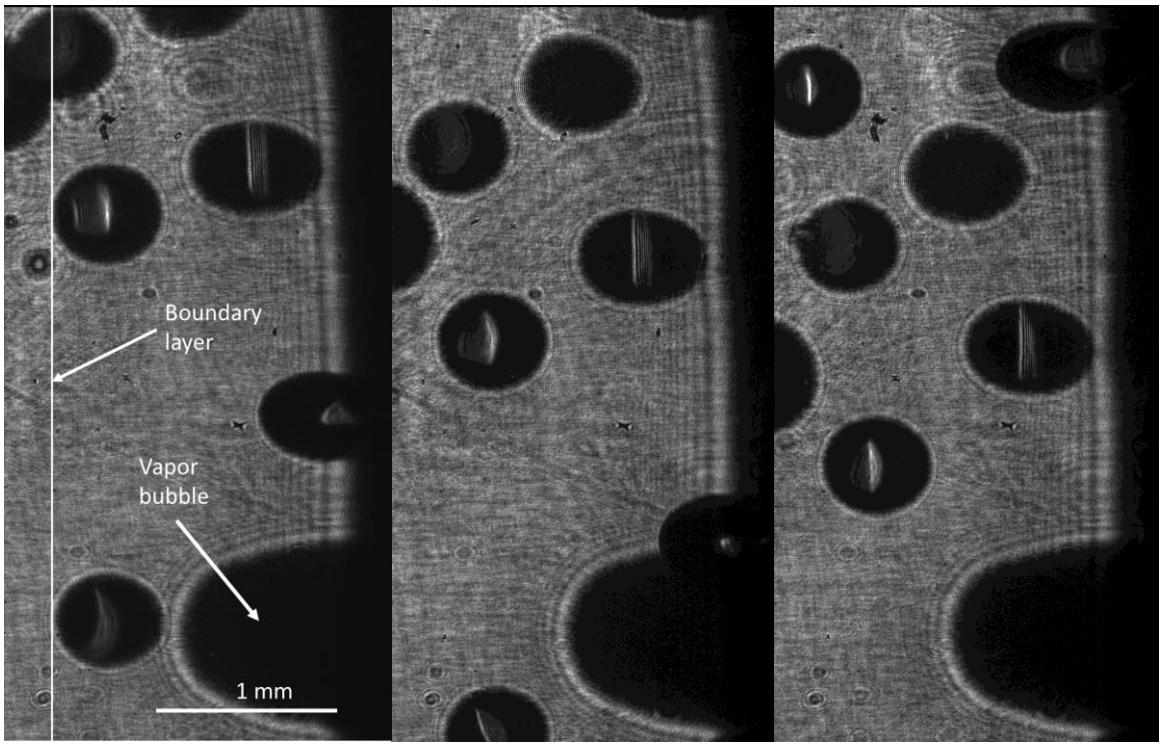

(a) (b) (c)

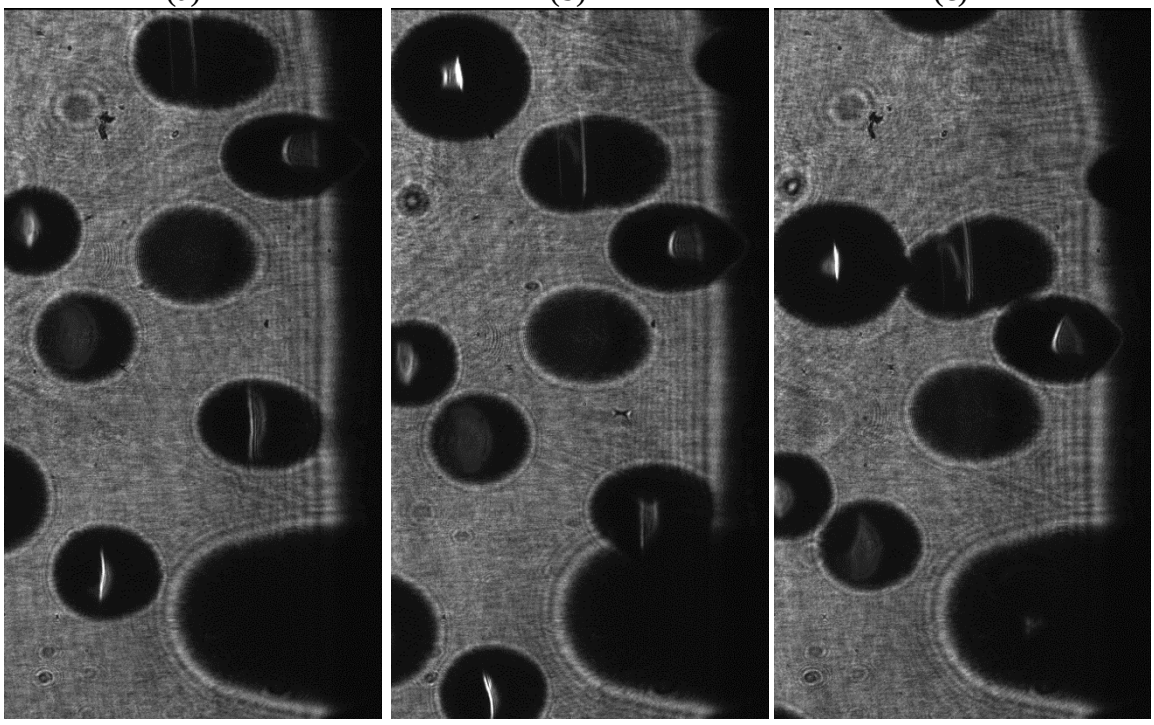

(d) (e) (f)

Figure 42. Multiple FC-72 droplets in boundary layer. y = 2.25 in.; $Ra_y = 1.44\times10^{10}$; $Ra_H = 2.31\times10^{12}$; $q'' = 20.3$ kW/m^2; $\delta = 1.785$ mm; $u_{max} = 11.87$ cm/s; $\Delta t = 0.053$ s.

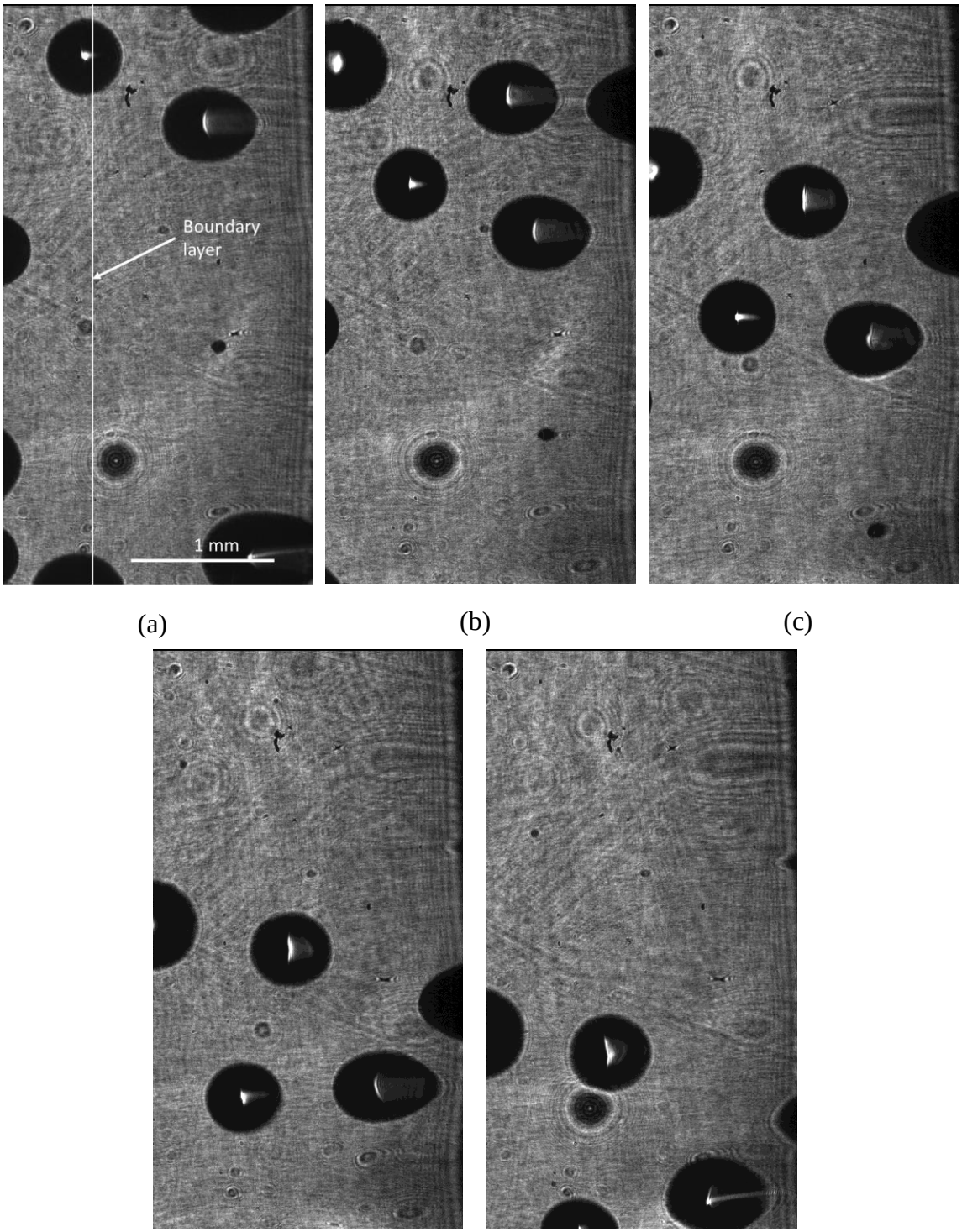

Figure 43. Multiple FC-72 droplets in boundary layer. y = 2.25 in.; $Ra_y = 1.91\times10^{10}$; $Ra_H = 3.09\times10^{12}$; q″ = 24.6 kW/m2; δ = 1.689 mm; u_{max} = 12.97 cm/s; Δt = 0.044 s.

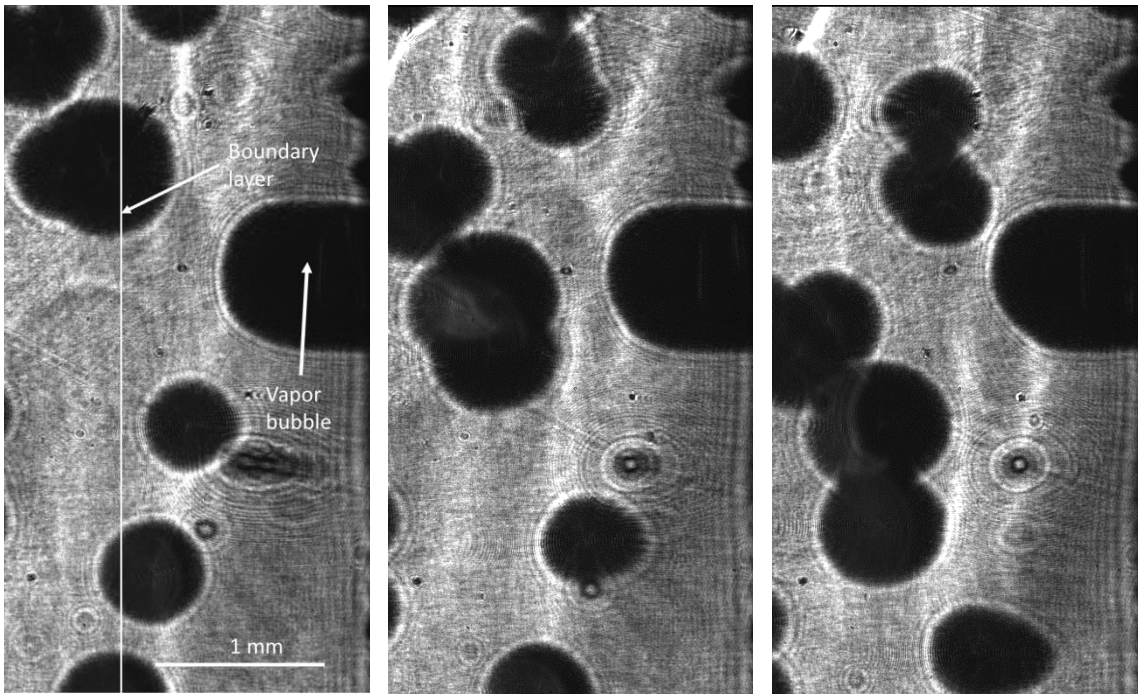

(a) (b) (c)

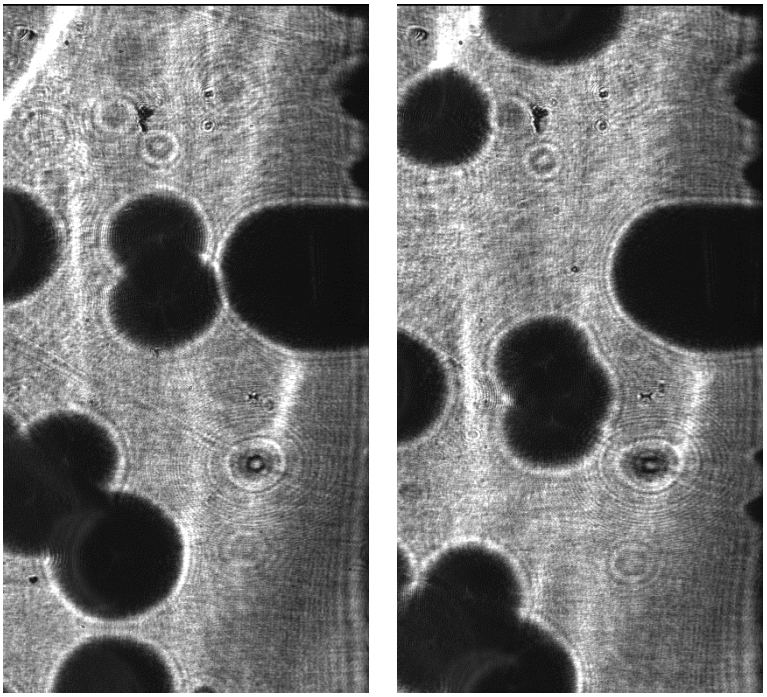

(d) (e)

Figure 44. Multiple FC-72 droplets in boundary layer. y = 2.25 in.; $Ra_y = 2.73\times10^{10}$; $Ra_H = 4.42\times10^{12}$; q″ = 30.4 kW/m2; δ = 1.579 mm; u_{max} = 15.09 cm/s; Δt = 0.044 s.

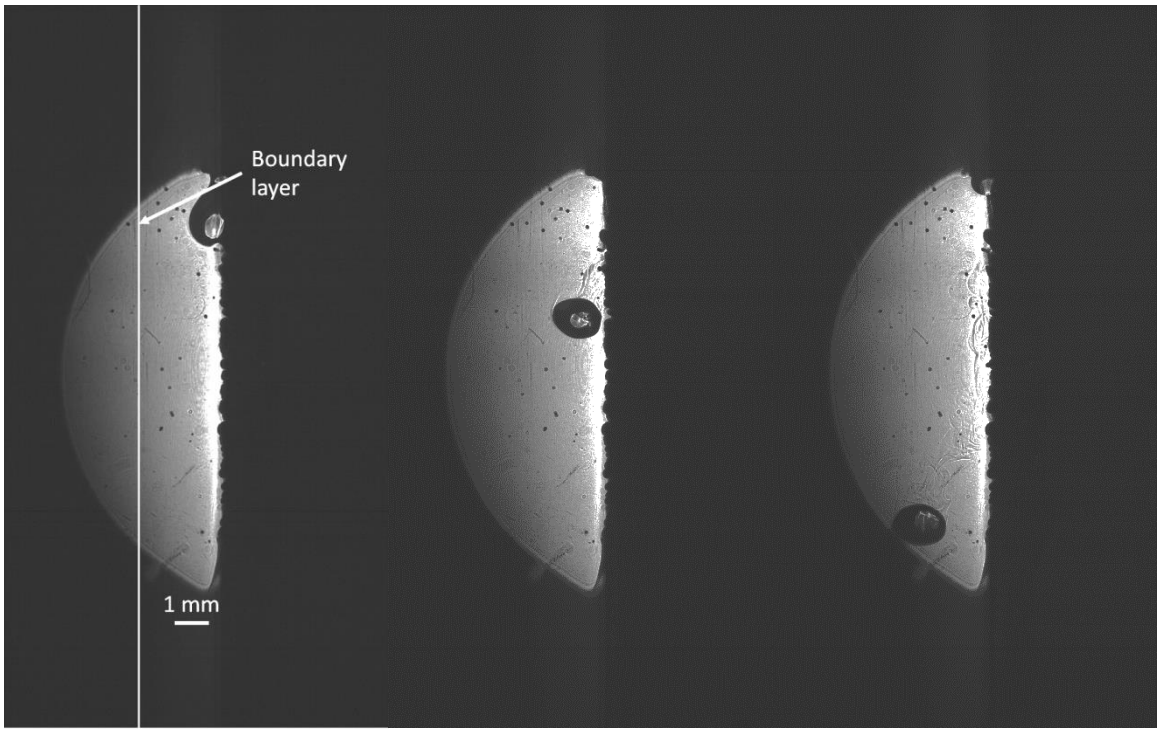

(a) (b) (c)

Figure 45. FC-72 droplet in the boundary layer; y = 6.25 in.; $Ra_y = 6.61\times10^{11}$; $Ra_H = 1.82\times10^{12}$; $q'' = 16.8$ kW/m^2; $\delta = 2.30$ mm; $u_{max} = 10.97$ cm/s; $d_d = 1.3$ mm; $\Delta t = 0.08$ s.

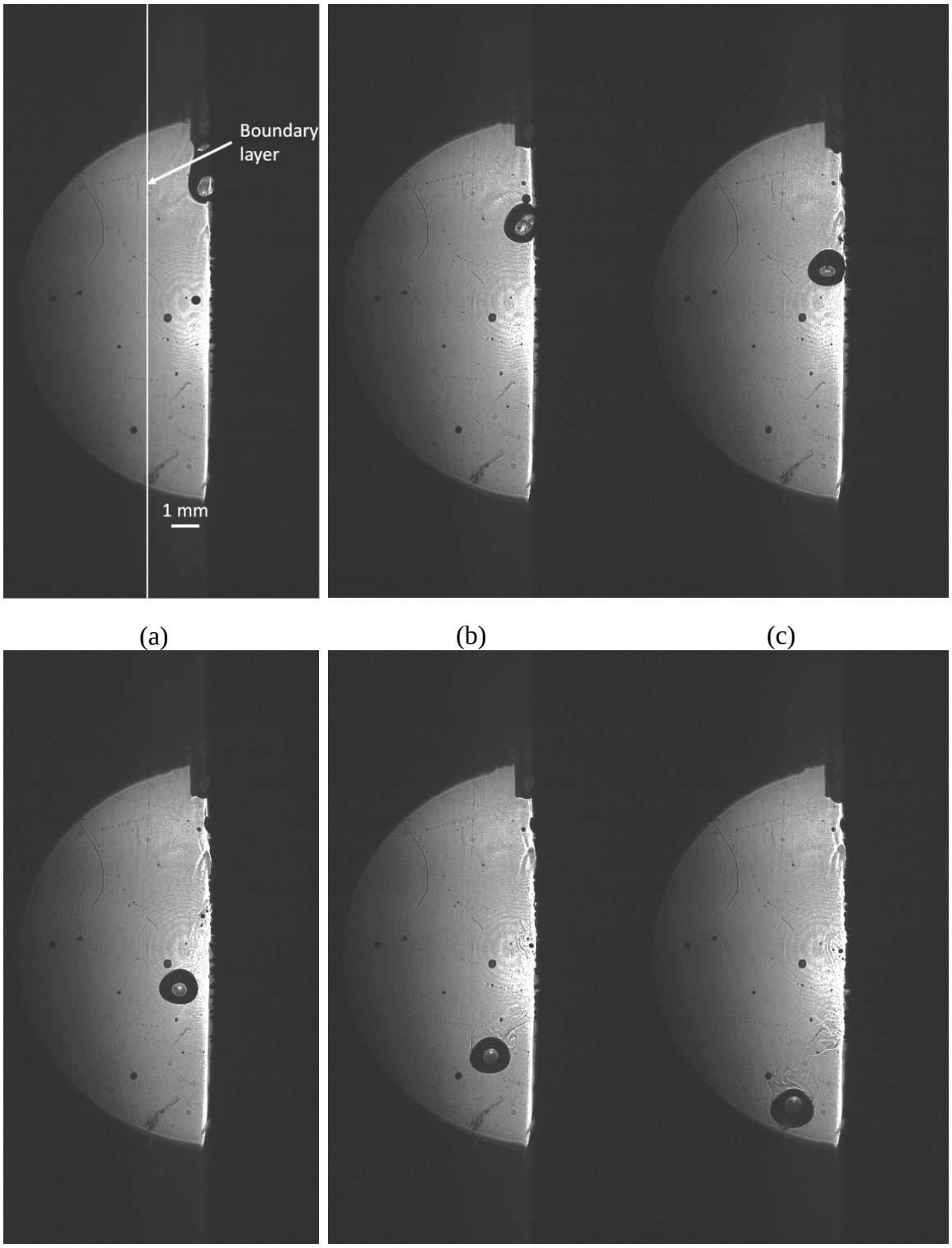

Figure 46. FC-72 droplet in the boundary layer; y = 6.25 in.; $Ra_y = 8.58\times10^{11}$;$Ra_H = 2.31\times10^{12}$; $q'' = 20.3$ kW/m^2; $\delta = 2.19$ mm; $u_{max} = 11.87$ cm/s; $d_d = 1.3$ mm; $\Delta t = 0.10$ s.

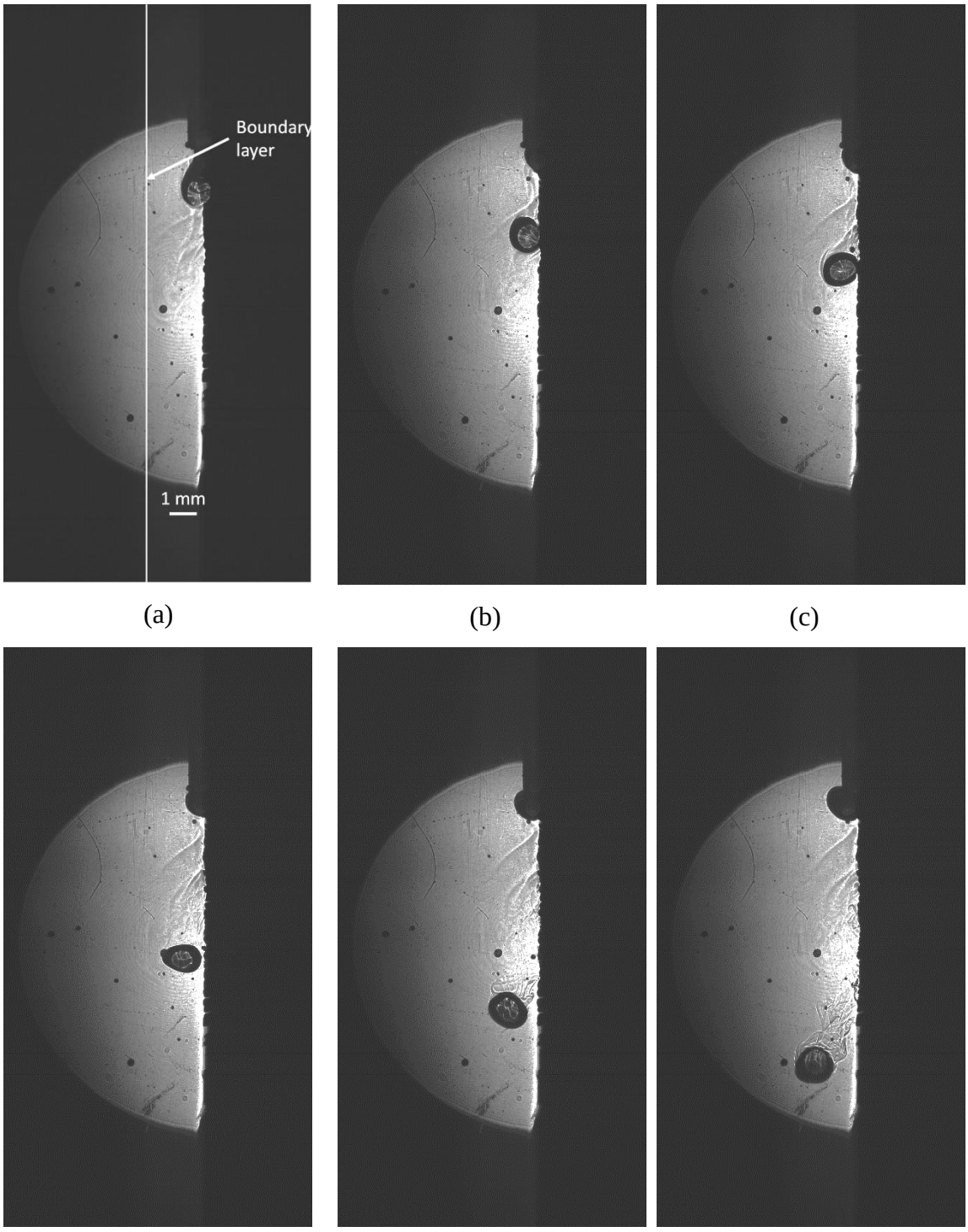

Figure 47. FC-72 droplet in the boundary layer; y = 6.25 in.; $Ra_y = 1.14\times10^{12}$;$Ra_H = 3.09\times10^{12}$; $q'' = 24.6$ kW/m^2; $\delta = 2.07$ mm; $u_{max} = 12.97$ cm/s; $d_d = 1.3$ mm; $\Delta t = 0.10$ s.

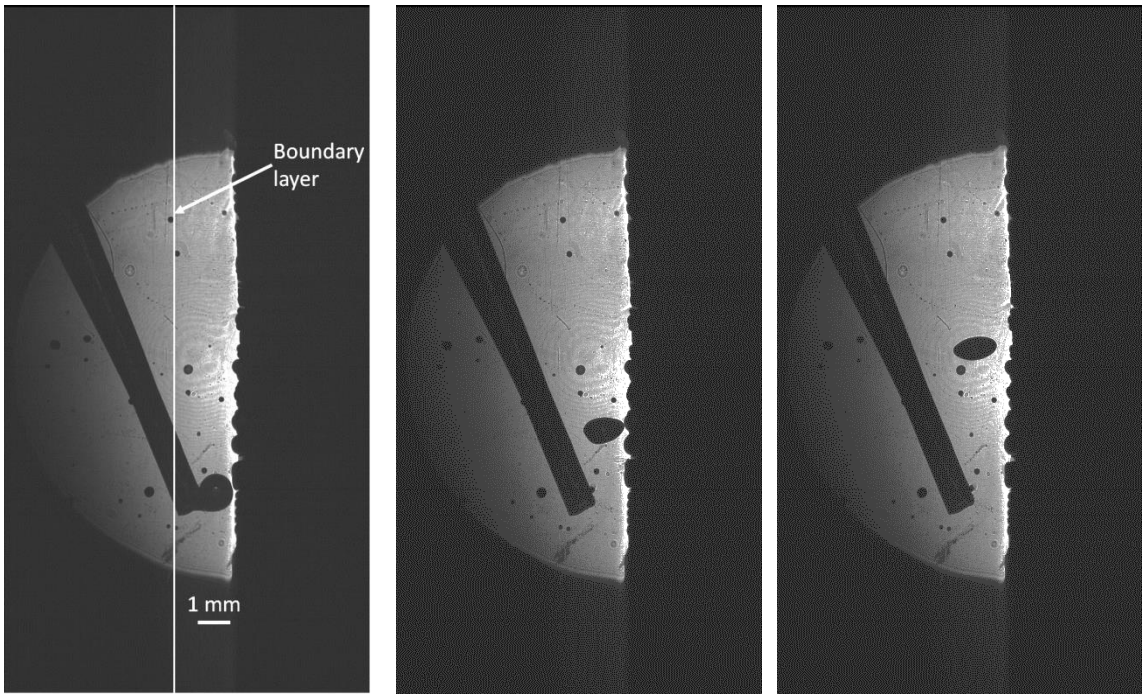

(a) (b) (c)

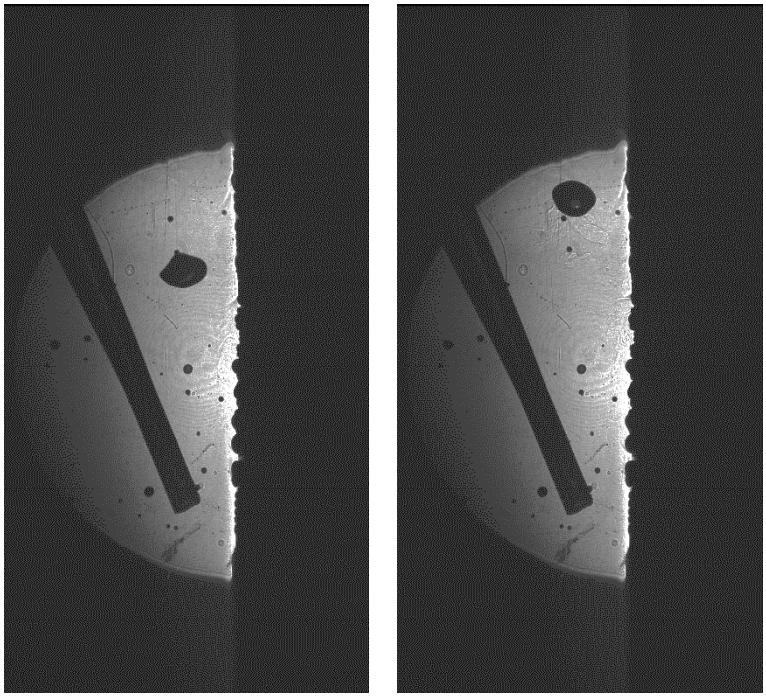

(d) (e)

Figure 48. FC-72 droplet in the boundary layer; y = 6.25 in.; $Ra_y = 1.63\times10^{12}$;$Ra_H = 4.42\times10^{12}$; $q'' = 30.4$ kW/m^2; $\delta = 1.937$ mm; $u_{max} = 15.09$ cm/s; $d_d = 1.3$ mm; $\Delta t = 0.08$ s.

Appendix D. Magnus Effect

The Magnus effect consists of the Kutta-Joukowski lift force, which is responsible for the lateral movement of spinning objects in velocity fields. An estimate of the horizontal forces acting on the FC-72 droplet in the boundary layer can be obtained from

$$\frac{F}{d_d} = \rho_f \, u_{avg} \, G \quad , \tag{56}$$

where $G = (2\pi R)^2 \omega$, is the vortex strength on the spinning droplet.

Using the holographic images obtained, the horizontal velocity and acceleration are calculated by measuring the horizontal distance the droplet is away from the heated surface. The acceleration is then used along with the mass to calculate the horizontal force acting on the droplet. Using Eqn. (56), the vortex strength can then be calculated, which is then used to calculate the angular velocity of the droplet. Table 10 shows the horizontal acceleration, force, and angular velocity due to the Magnus effect. Quantities were determined based on distance measurements obtained from the individual droplet images.

Table 10. Horizontal acceleration, force, and angular velocity of droplet due to Magnus effect.

$Ra_H \times 10^{-12}$	a [m/s^2]	$F \times 10^{-7}$ [N]	ω [rad/s]
1.8	1.125	13.8	1.173
2.3	0.36	4.438	0.348
3.1	0.36	4.449	0.320
4.4	0.09	1.116	0.069

Appendix E. Optical Equipment

This appendix contains a photograph of the optical equipment and the apparatus. Each component of the optical setup is identified. The Schneider lens is missing from the photograph. The Schneider lens is used to magnify the image and is mounted to the rail between the camera and the apparatus.

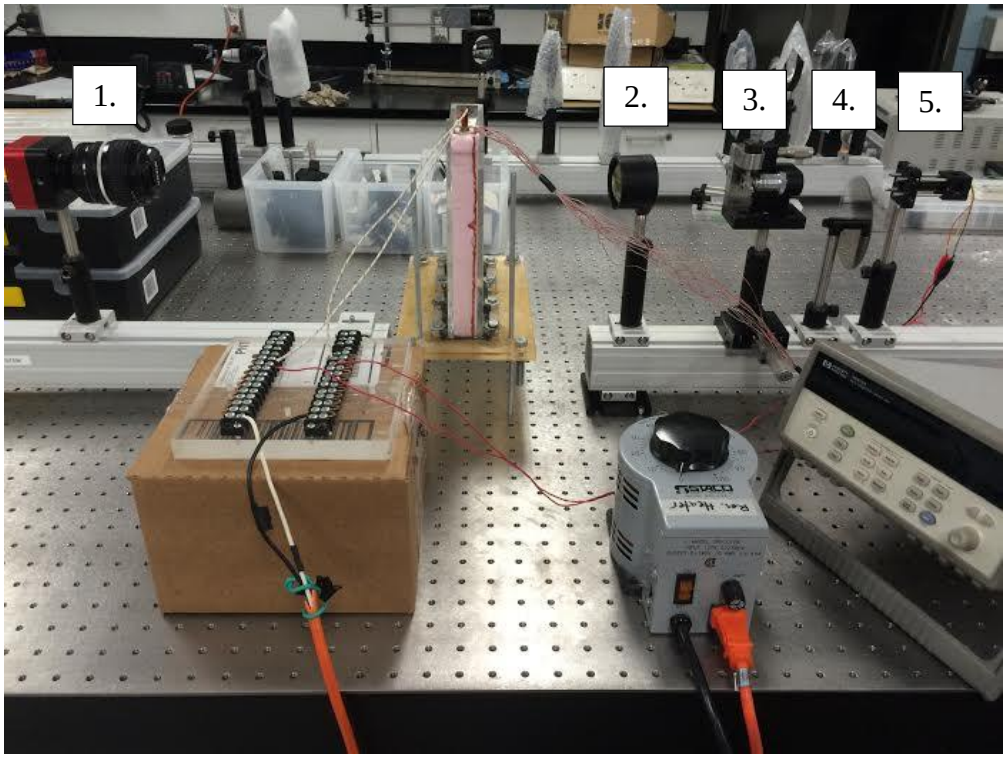

Figure 49. Optical rail and components.

1. Camera
2. Collimating lens
3. Spatial filter
4. Neutral density filter
5. Laser